INVESTIGATION OF COMPRESSIBLE-FLUID FLOW THROUGH A CASCADE OF BLUNT-NOSED PROFILES

By

WALTER ASCHER

Bachelor of Science

Tulane University

New Orleans, Louisiana

1949

Submitted to the Faculty of the Graduate School of

the Oklahoma Agricultural and Mechanical College

in Partial Fulfillment of the Requirements

for the Degree of

MASTER OF SCIENCE

1953

INVESTIGATION OF COMPRESSIBLE-FLUID FLOW

THROUGH A CASCADE OF BLUNT-NOSED PROFILES

WALTER ASCHER

MASTER OF SCIENCE

1953

THESIS AND ABSTRACT APPROVED:

Ladislaus J. Fila

Thesis Adviser

C. M. Leonard

Faculty Representative

D. C. McIntosh

Dean of the Graduate School

ACKNOWLEDGMENT

The author feels grateful and indebted to Professor Rollo E. Venn and the School of Mechanical Engineering for granting him the Graduate Fellowship which enabled him to carry forward his education.

Sincere thanks are due Professor Carroll M. Leonard for carefully reading the entire thesis and offering much valuable criticism.

The author owes deepest thanks to Professor Ladislaus J. Fila under whose direction this thesis was written, and without whose encouragement this work never would have been completed.

For their help and great patience throughout school the author is very grateful to his parents.

TABLE OF CONTENTS

LIST OF TABLES

LIST OF ILLUSTRATIONS

LIST OF SYMBOLS AND ABBREVIATIONS

Many of the symbols in the text are composites of those defined below; that is, one symbol may serve as subscript for another. The meaning of these combinations is always clear. For example, $F_{\Delta \mathcal{M}_x}$ is a composite of F, $\Delta \mathcal{M}$, and x. The definition of the composite is

Force (F) due to change in momentum ($\Delta \mathcal{M}$) in the x-direction (x).

LATIN CAPITALS

A	station area, sq. in.,
$A, B, \ldots,$	center pattern subregion, also point on wave,
$\bar{A}, \bar{B}, \ldots,$	center pattern subregion, also point on wave,
A_x	component of control surface segment A parallel to x-axis, sq. in., ($A_x = 0$ sq. in.),
A_y	component of control surface segment A parallel to y-axis, sq. in.,
D	sphere diameter, inches,
F	force, lbs,
$\bar{F}$	force, lbs,
K_s	curvature of attached nose shock, $\frac{1}{\text{in.}}$,
K_w	curvature of ogive portion of wall, $\frac{1}{\text{in.}}$,
M	Mach number,
M_i	Mach wave,
N_j	normal to characteristic curve,
O	hodograph origin point,
OWL	oblique wave originating at lower channel wall entrance,
OWU	oblique wave originating at upper channel wall entrance,
P	static pressure, psia,

P_j	end point of vector on hodograph corresponding to w_i , whenever $i = j$,
P_s	stagnation pressure, psia,
R	Rankine,
R_w	radius of curvature of the ogive portion of the wall, inches,
R_s	radius of curvature of attached nose shock, inches,
T	ambient temperature, degrees Rankine,
T_s	stagnation temperature, degrees Rankine,
V	flow velocity, fps,
V_n	velocity component normal to control surface, fps,
V_x	velocity component along x-axis, fps,
V_y	velocity component along y-axis, fps,

LATIN LOWER CASE

a	velocity of sound in air, fps,
$a, a_1, a_2, \ldots$	constants,
c	chord,
$\bar{c}$	compression characteristic resulting from combination of c_{25} and c_{20} ,
$\tilde{c}$	compression characteristic resulting from combination of $\bar{c}$ and c_{15} ,
$\check{c}$	compression characteristic resulting from combination of c_{35} and c_{30} ,
$\breve{c}$	balancing compression characteristic,
c_ϕ	compression characteristic corresponding to ϕ ,
d	distance from "shoulder circle" center to normal shock point on detached wave, inches,
$\breve{e}$	balancing expansion characteristic,
e_ϕ	expansion characteristic corresponding to ϕ ,

e_{20c}	continuation of e_{20} ,
e_{25c}	continuation of e_{25} ,
e_{25L}	e_{25} of lower wall,
e_{25Lc}	continuation of e_{25L} ,
e_{25U}	e_{25} of upper wall,
e_{25Uc}	continuation of e_{25U} ,
f ( )	function of quantity enclosed in parentheses,
i	exit station number,
i, j	1, 2, . . . ,
m	polynomial in M,
n_1	outward normal to channel-entrance control surface,
n_2	outward normal to channel-exit control surface,
owc_{ℓ}	continuation of lower portion of detached nose wave,
owc_{u}	continuation of upper portion of detached nose wave,
s	stagnation condition,
w_i	flow velocity, fps,
x	chord station abscissa, per cent of chord, also reference to x-axis, x-direction,
y	y-axis, y-direction,
y_c	mean-line ordinate measured from chord, per cent of chord,

LATIN SCRIPT CAPITALS

$\mathscr{I}$, $\mathscr{J}$, $\mathscr{L}$, $\mathscr{M}$,	dummy pattern subregions,
$\mathscr{M}$	momentum, lbs (144),
$\mathscr{P}$	force due static pressure, lbs,
$\mathscr{R}$	any center pattern subregion,

GREEK CAPITALS

Δ	change in, or difference between,

$\Delta \mathfrak{M}$	change of momentum, lbs (144),
θ_s	deflection angle, degrees,
$\theta_{s,crit}$	wedge angle of maximum magnitude for attached shock, degrees,
θ_w or $\theta_{w,(\ )}$	wave angle, degrees,
$\bar{\theta}_w$ or $\bar{\theta}_{w,(\ )}$	local wave angle with respect to free-stream flow direction, degrees,
Σ	summation indicator,
Σc	compression wave resulting from combination of $\tilde{c}$ and c_{10},
Σc_c	continuation of Σc,
ϕ	expansion angle of Prandtl-Meyer relation, degrees,

GREEK LOWER CASE

α	angle between local flow direction and outward normal to control surface, degrees,
α, β	dummy characteristics,
γ	ratio of specific heats of gas,
γ_{s0}	weight density of air at Standard Sea Level, lbs/cf,
δ	detach distance, inches, also flow deflection through wave, degrees,
$\bar{\delta}$	local flow direction with respect to free-stream direction, degrees,
ζ	substitute wave for owc_ℓ and e_{25Lc},
$\bar{\vartheta}_\ell$	$\bar{\delta}$ corresponding to ϕ = 0 degrees along lower channel wall, degrees,
$\bar{\vartheta}_u$	$\bar{\delta}$ corresponding to ϕ = 0 degrees along upper channel wall, degrees,
λ	substitute wave for owc_ℓ, e_{20c}, and Σc_c,
ν	substitute wave for owc_u and e_{25c},
ξ	substitute wave for owc_u and e_{25Uc},
ρ	mass density of air, slugs/cf,

ρ_{s0}	mass density of still air at Standard Sea Level, slugs/cf,
χ	substitute wave for $\breve{c}$ and ζ ,

ARABIC NUMERALS

1, 2, . . . ,	points along wall,
$\bar{1}$, $\bar{2}$, . . . ,	points along wall,
3, 5, 20, . . . ,	subscripts indicating value of ϕ preceding wave segment,
0	subscript referring to Standard Sea Level conditions,
(1), (2), (3),	segments of characteristic 1,

ABBREVIATIONS

$\equiv$	is identical to,
$>$	is greater than,
$<$	is less than,
$\ll$	is much less than,
$\doteq$	is very nearly equal to,
$\uparrow$, $\downarrow$	upward and downward direction tendencies,
'	prime, superscript on P, P_s , ρ, ρ_s , and BNC referring to fictitious distribution of channel-exit quantities,
BNC	blunt-nosed profile channel,
BNC'	blunt-nosed profile channel with fictitious channel-exit distribution,
cf	cubic foot,
fps	feet per second,
lbs	pounds,
NACA	National Advisory Committee for Aeronautics,
psi	pounds per square inch,
psia	pounds per square inch, absolute,

R	Report,
SNC	sharp-nosed profile channel,
sec.	seconds,
sq. in.	square inches,
TM	Technical Memorandum,
TN	Technical Note .

PREFACE

In the analysis of turbomachinery, it is very necessary to know flow behavior in certain velocity ranges. Airfoil and cascade theories already have provided solutions of the flow problem for incompressible fluids. The development of cascade theory for compressible fluids carries with it a great number of difficulties. One of the unsolved problems is that of the behavior of a cascade of blunt-nosed profiles in a mixed compressible-fluid flow. When a flow is initially supersonic, a detached, curved shock wave forms in front of each profile. Behind the wave, there exists a region of subsonic velocities bordered by the shock curve and the nose of the profile. Further downstream, the flow becomes supersonic again.

The method of successive approximations frequently is productive of useful results. This, then, is the first approximation of the solution of the flow of a compressible fluid through a cascade of blunt-nosed profiles. As such, it carries the properties of a guidepost, but not those of a map. The rigorous development of the theory is hampered by tremendous mathematical difficulties. Proof of the existence of a solution is given by Bergman[1] for the irrotational case. Frankl demonstrates the uniqueness of the solution for an isolated cone with detached nose shock.[2] Neither of the given theorems applies directly to the problem. Thus far, no analytical

---

1 Stefan Bergman, "On Supersonic and Partially Supersonic Flows," NACA, TN 1096 (December, 1946).

2 F. Frankl, "On the Problem of Chaplygin for Mixed Sub- and Supersonic Flows," NACA, TM 1155 (June, 1947).

results have been discovered. Under these conditions, the author feels justified in accomplishing his ends by non-rigorous means.

CHAPTER I

INTRODUCTION

The solution of mixed compressible-fluid flow through a straight cascade of blunt-nosed profiles is of practical importance in furthering the design theory of axial-flow turbomachinery. The development of compressible-fluid flow theory is step-by-step; starting with the simplest flow configurations, and continuing to slightly more complicated ones. This approach is the soundest one, for the theory thereby is assured of a solid foundation. Necessity and lack of time often force the engineer to attack a more advanced problem for which some of the foundations stones are missing. Necessarily, many assumptions must be made; some of which cannot be justified solidly. Retaining rigor is next to impossible, and the method of successive approximations becomes the chief tool. Individual solutions of this type serve as direction indicators in the development of the general theory, and as starting points in the evolution of particular-case theories. Thus in this study, a two-dimensional analysis is made of the flow between two adjacent turbomachine blades. The summation of all flows through all blades will produce the required results for one turbomachine wheel.

Full advantage is made of a step-by-step solution. Since the analysis depends heavily on the geometry of the flow, and since the inequalities used in reasoning often change directions with only slight changes in local values of flow variables, conjecture on expected results is quite difficult. Later research may solve the entire range of veloci-

ties for a given cascade. At that time, a solution to the general prob-
lem should have more encouraging probability than it does now.

CHAPTER II

ANTECEDENT INVESTIGATIONS

Since momentum theory in its old form, applied to turbomachines, fails to produce results in certain velocity ranges, it is necessary to apply cascade theory, and to develop it further. The general theory of incompressible-fluid flow through straight cascades is already far advanced.[1] In the region of compressible subsonic potential flow, Costello,[2] using the method outlined by Lin[3] produces a cascade design. More precise, more tedious, and entirely different is the method presented by Wang.[4] Although it is given for an isolated body only, it seems adaptable to cascade flow. Pure supersonic flow about blunt-nosed objects is not possible physically.

Very little is known about the problem under consideration, that of mixed compressible-fluid flow about a blunt body. The work of

---

1 A unified treatment is given in F. Weinig, Die Strömung um die Schaufeln von Turbomaschinen.

2 George R. Costello, "Method of Designing Cascade Blades with Prescribed Velocity Distributions in Compressible Potential Flows," NACA, R 978 (1950).

3 C. C. Lin, "On an Extension of the von Kármán-Tsien Method to Two-Dimensional Subsonic Flows with Circulation around Closed Profiles," Quarterly of Applied Mathematics, IV (October, 1946), 291-297.

4 Chi-Teh Wang, "Variational Method in the Theory of Compressible Fluid," Journal of the Aeronautical Sciences, XV (November, 1948), 675-685; also errata, XVI (February, 1949), 125 f.

Dugundji[5] is quite misleading when applied to the two-dimensional case. The only other pertinent writing is that of Busemann.[6] His survey of known experimental and theoretical results is sparse. However, he introduces the concept of "shoulder circle," a very useful tool which is explained later.

---

5 John Dugundji, "An Investigation of the Detached Shock in Front of a Body of Revolution," Journal of the Aeronautical Sciences, IV (December, 1948), 699-705.

6 Adolf Busemann, "A Review of Analytical Methods for the Treatment of Flows with Detached Shocks," NACA, TN 1858 (April, 1949).

CHAPTER III

STATEMENT OF PROBLEM

The determination of the thrust- and torque-reactions of a straight cascade of blunt-nosed profiles to the flow of air with an entrance Mach number of 1.7 is the chief purpose of this investigation. The same problem is to be solved for a straight cascade of sharp-nosed profiles, the element of which corresponds very closely in shape and position to the element of the blunt-nosed profile cascade. The results of the two problems are to be compared with each other, and analyzed.

CHAPTER IV

ANALYSIS AND COMPUTATIONS

A Cascade of Modified NACA Profiles

1 Profile and Channel Layout

Entrance Mach number and profile configuration are chosen such that channel theory may be employed in the two-dimensional analysis of the flow between two adjacent blades. The NACA 63-206 airfoil is the basic profile selected. To produce turning of the flow, the profile is modified to increase the camber. Actual chord length, or bucket width equals 2 inches, and the layout scale ratio chosen is 10 to 1. The construction follows. NACA Mean Line 63 is plotted from the data of Table 4-1. The

Table 4-1

NACA Mean Line 63[1]			
x (per cent c)	y_c (per cent c)	x (per cent c)	y_c (per cent c)
0	0	30	6.000
1.25	0.489	40	5.878
2.5	0.958	50	5.510
5.0	1.833	60	4.898
7.5	2.625	70	4.041
10	3.333	80	2.939
15	4.500	90	1.592
20	5.333	95	0.827
25	5.833	100	0

x's are the chord (c) station abscissae, and the y_c's are the mean line ordinates, measured from the chord. A tangent is drawn to the mean line at the leading edge, or at station 0. The slope of the leading-edge

---

1 Ira H. Abbott and Albert E. von Doenhoff, Theory of Wing Sections, p. 384.

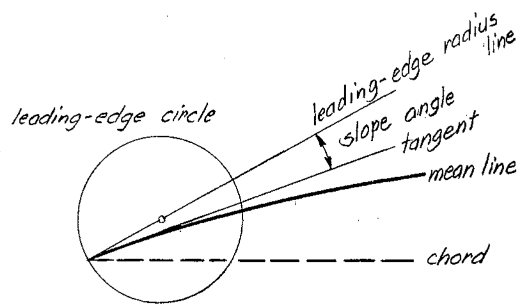

Figure 4-1

Construction of
Leading-Edge Circle

radius line is laid out with respect to this tangent, and the leading-edge circle drawn as shown in Figure 4-1. Values of slope and radius are given at the end of Table 4-2, page 8. Upper and lower surfaces are then laid out, using the data for NACA 63-206. The new stations are plotted along the original chord. A point corresponding to each station is located along the mean line by finding the mean line intercept of a line drawn perpendicular to the chord at each chord station. The station ordinates are laid off at right angles to the mean line; above or below, as required. The layout procedure is indicated in Figure 4-2.

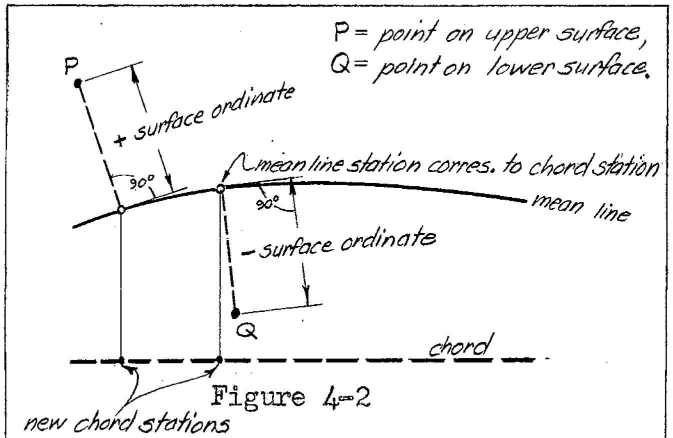

Figure 4-2

Layout of Profile Surfaces

Two blades are arranged to form the walls of the channel under

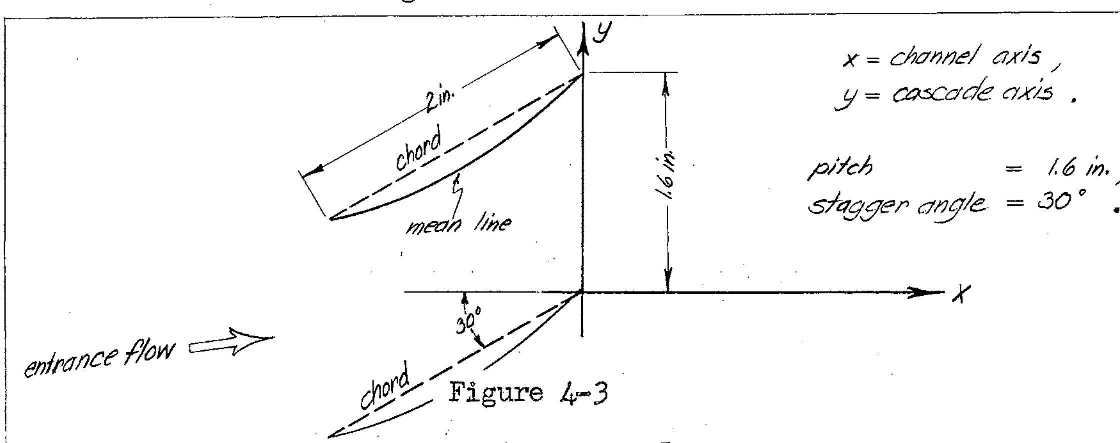

Figure 4-3

Channel Reference System

Table 4-2

NACA 63-206 Wing Section Data[2]			
Upper Surface		Lower Surface	
Station	Ordinate	Station	Ordinate
0	0	0	0
.458	.551	.542	- .451
.703	.677	.797	- .537
1.197	.876	1.303	- .662
2.438	1.241	2.562	- .869
4.932	1.776	5.068	-1.144
7.429	2.189	7.571	-1.341
9.930	2.526	10.070	-1.492
14.934	3.058	15.066	-1.712
19.941	3.451	20.059	-1.859
24.950	3.736	25.050	-1.946
29.960	3.926	30.040	-1.982
34.970	4.030	35.030	-1.970
39.981	4.042	40.019	-1.900
44.991	3.972	45.009	-1.782
50.000	3.826	50.000	-1.620
55.008	3.612	54.992	-1.422
60.015	3.338	59.985	-1.196
65.020	3.012	64.980	- .952
70.023	2.642	69.977	- .698
75.023	2.237	74.927	- .447
80.022	1.804	79.978	- .212
85.019	1.356	84.981	- .010
90.013	.900	89.987	.134
95.006	.454	94.994	.178
100.000	0	100.000	0
Leading-edge circle radius: 0.297, slope of leading-edge circle radius line through leading edge: 0.0842.			

analysis. The reference axes are located such that the velocity components along them generally are positive. Figure 4-3 shows the skele-

2 Ibid., p. 415.

ton layout of the channel. The leading edges are at the left, and the mean lines are drawn below the chords. The flow is from left to right.

2 Nose Region

The entrance portion of the stagnation line must be located first in order to define the channel walls upstream, and to locate the optimum direction of approach. The nose of the profile is very nearly symmetric about the leading-edge radius line. If the direction of approach is chosen parallel to this line, the profile presents its slimmest aspect to the incoming stream, and thereby minimizes the region of strong shock of the detached nose wave. Because of the symmetry property, the entrance portion of the stagnation line coincides with a continuation of the leading-edge radius line, and the stagnation point with chord station zero.

The detach distance of the shock from the stagnation point is found next. Only experimental results are available. It must be assumed that the detach distance in front of the profile coincides with that of a sphere in free flight, at the same Mach number. A shadowgraph picture of a sphere is available for a Mach number, M, of 1.8.[3] The quantities obtained by measurement must be corrected to $M = 1.7$. Let

δ = detach distance, inches;

D = sphere diameter, inches.

The scale is arbitrary, since only the ratios are important. To reduce error, the measurements are taken as shown in Figure 4-4. Let m be a

---

3 Hans Wolfgang Liepmann and Allen E. Puckett, Introduction to Aerodynamics of a Compressible Fluid, Fig. 6·13, p. 99.

polynomial in M, and f (M) a function of M. Then, let

$$\delta/D = f\ (M) = a_1 m + a_2 m^2 + a_3 m^3 + \ldots + ,$$

where the a's are constants, and $0 \leqq \delta/D \ll 1$. If $m = M - 1$, and if the power terms, which tend toward zero, are neglected, then

$$\delta/D = a\ (M - 1), \qquad (1).$$

The constant a then can be determined from experimental data.

At $M = 1$, $\delta/D = 0$. Substitution into the last equation produces the identity

$0 = a\ (0) = 0$, yielding no solution for a.

At $M = 1.8$,

$$(\delta/D)_{1.8} = a\ (1.8 - 1).$$

Therefore,

$$a = (\delta/D)_{1.8}(1/0.8).$$

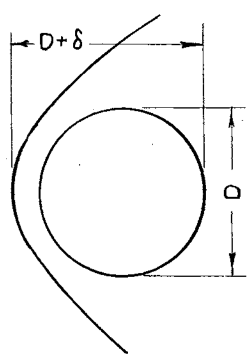

Figure 4-4

Measurement of δ at $M = 1.8$

On the shadowgraph, the measurements are:

$$D = 0.46 \text{ in.},$$

$$D + \delta = 0.54 \text{ in.}$$

Therefore, $\delta = 0.08$ in., and

$$(\delta/D)_{1.8} = 0.08/0.46.$$

$$a = (0.08/0.46)(1/0.8) = 0.2174 .$$

The equation (1) now reads

$$\delta/D = 0.2174(M - 1) .$$

At $M = 1.7$,

$$(\delta/D)_{1.7} = 0.2174(1.7 - 1) = 0.1522 .$$

According to the data at the end of Table 4-2, the diameter of the leadind-edge circle, D, in per cent of c, equals 0.594. The detach distance in per cent of c equals

$$\delta = (\delta/D)_{1.7}(D) = 0.1522(0.594) \quad ,$$
$$\delta = 0.0905 \quad .$$

Next to be found is the shape of the nose shock wave. There exists no analytical relation between the shape of the nose and that of the detached wave. However, the shapes are related indirectly. For this relation, the concept of "shoulder circle" must be introduced.[4] The "shoulder circle" is located as follows: At $M = 1.7$, $\Theta_{s,\ crit}$, the wedge angle of maximum magnitude for attached shock equals 17 degrees, Chart 2-1.[5] The nose region of the profile is redrawn, magnified 125 to 1. On tracing paper, an acute angle equal to 2 $\Theta_{s,\ crit}$ is laid off. The traced angle is superimposed on the nose region until the unique tangency condition shown in Figure 4-5 is obtained. The points of tangency are "shoulder points," and the shoulder circle may be located by drawing normals to the surfaces at the points of tangency, locating the point of intersection of these normals, and, using this as center, drawing a circle through both points of tangency. Because of the approximate symmetry of the nose about the leading-edge radius line,

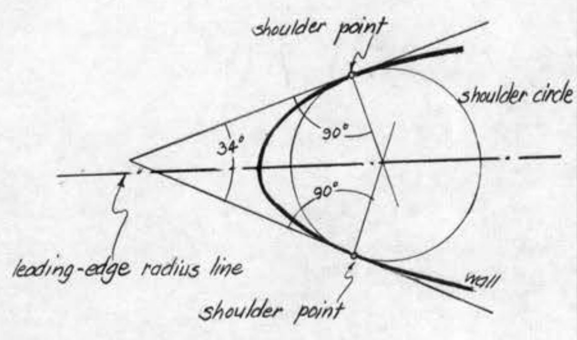

Figure 4-5

Location of "Shoulder Circle"

---

4 Adolf Busemann, op. cit., p. 11.

5 C. L. Dailey and F. C. Wood, Computation Curves for Compressible Fluid Problems.

the center of the shoulder circle falls on that line. The leading edge of an object has little or no influence on the shape of the detached shock. Two sensitive arcs behind and on either side of the leading edge bear the greatest influence. These arcs may be called "shoulders," and it follows that the shoulder circle is the main factor in the definition of the relation between the nose shape and the shape of the detached wave. Thus the curved portion of the nose wave is defined as a circle which is concentric with the shoulder circle, and which has a radius equal to the distance from the stagnation point to the center of the shoulder circle plus the detach distance. The circular portion terminates in a tangent which coincides with a wave angle of 37 degrees. The straight wave portion has a turning strength of 1 degree at a free-stream M of 1.7,[6] which is equivalent to the turning strength of the straight portion of a detached wave with a free-stream M of 1.8, as shown in a shadowgraph.[7] This configuration holds true at least for the length of wave front under consideration.

The locus of the sonic line behind the detached shock is the next item to be found. At the wave, the sonic point falls where the local wave angle equals 61.4 degrees, according to Chart 2.1.[8] This means that immediately downstream of this point $M = 1$. The sonic line is one of the borders of the subsonic region. The sonic point at the wall must be located next. Its locus is given in Figure 4-6, where d is the length of the shock arc radius. The justification for the location of the sonic

---

6 Ibid.

7 Hans Wolfgang Liepmann and Allen E. Puckett, loc. cit.

8 C. L. Dailey and F. C. Wood, op. cit.

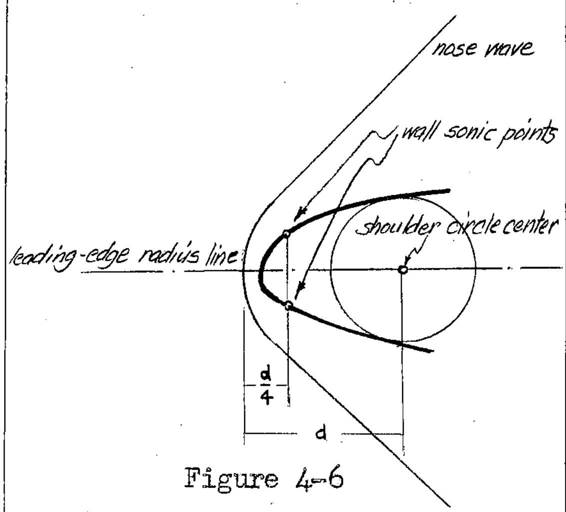

Figure 4-6

Loci of Wall Sonic Points

point at the surface and upstream from the shoulder point is given by Busemann.[9] The direction of the sonic line in the neighborhood of the wall is known to be perpendicular to the wall, since the flow there is parallel to the wall. Since it may be assumed that the sonic line is a simple curve, the outer portion of which is already constructed, it can be concluded that the inner portion is the longer of two segments forming the sonic line. The definition of the locus of the wall sonic point results in a satisfactory proportion between the two segments of the sonic line, as shown in Figure 4-7. The sharp corner of the intersection of the inner and outer segments of the line is removed by drawing a smooth fillet, as shown. The flow is deflected 16.7 degrees away from the wall behind the wave sonic point according to Chart 2-1.[10] The outer segment of the sonic line is perpendicular to this direction. The sonic line has two properties: (1) The Mach number at every point along it equals one, and (2) the flow direction is orthogonal to it at every point along it.

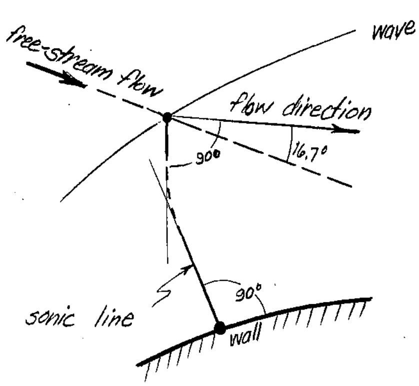

Figure 4-7

Construction of Sonic Line

At the stagnation point, immedi-

---

9 Adolf Busemann, op. cit., p. 12.

10 C. L. Dailey and F. C. Wood, op. cit.

ately behind the normal portion of the nose shock, M ≡ 0. On either side of this point, along the wall, the curvature produces expansion until sonic velocity is reached downstream, at the wall sonic point. Proceeding laterally from the stagnation streamline, the deflection through the curved portion of the nose wave is at first small, then increases, and then decreases after reaching a maximum, as shown in Figure 4-8. However, it is difficult to predict the locus of the streamlines further downstream inside the subsonic zone, since the wall is quite steep with respect to the original flow direction. Because of the increasing-decreasing deflection property, the actual sonic line must be reflexed, as shown in Figure 4-9. The major portion is constructed perpendicular to the wall, which means that some of the subsonic streamlines must be reflexed also. However, to facilitate the analysis, the sonic line of Figure 4-7 is retained.

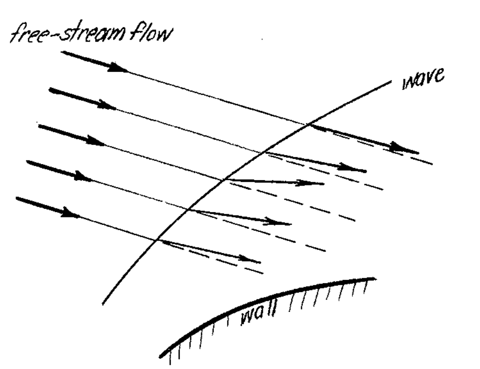

Figure 4-8

Flow Deflection Trends

The curved portion of the nose wave rapidly changes strength from normal shock to very weak oblique shock. A division of the wave into incremental arcs permits the definition of single conditions behind each such portion. Adjacent portions differ sufficiently in flow variables that cross-flows are formed. Static

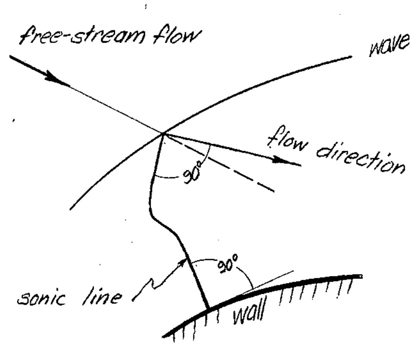

Figure 4-9

Reflexed Sonic Line

pressure-, temperature-, and entropy differences, in other words, are sufficiently large to force a flow across laminae between former stream filaments. After some mixing, the pressures will be matched. The other quantities will be sufficiently different to cause the persistence of shear sheets between adjacent layers. However, since all these adjacent channel flows reach sonic velocity at the sonic line, the shear sheets must disappear at this line. It must be remembered that flows across incremental portions of the sonic line still retain different reservoir conditions.

3 Supersonic Downstream Region

The supersonic portion of the flow pattern is next to be analyzed. A simplification is obtained by the assumption of only two extreme reservoirs; that pertaining to the flow immediately behind the sonic point at the wave, and that pertaining to the wall streamline. Downstream of the wall sonic point, the wall curvature is convex, and the flow is expanding.

The method of characteristics, as given for instance by Liepmann and Puckett,[11] is most advantageous if the flow is prescribed, and the shape of the wall or channel is to be found. If the wall curve already is given exactly, a modification simplifies the work. The new procedure is given below. Essentially, the behavior of the flow is as before.

(1) Construct tangents to the walls at small intervals of arc.

(2) Locate the point corresponding to the tangent direction on characteristic curve.

---

11 Hans Wolfgang Liepmann and Allen E. Puckett, op. cit., Chapter 13.

(3) With superimposed ellipse,[12] read the wave angle corresponding to the tangency point, as illustrated in Figure 4-10.

(4) Construct the Mach wave at the tangency point on the wall such that the wave angle equals the tangency-point Mach angle.

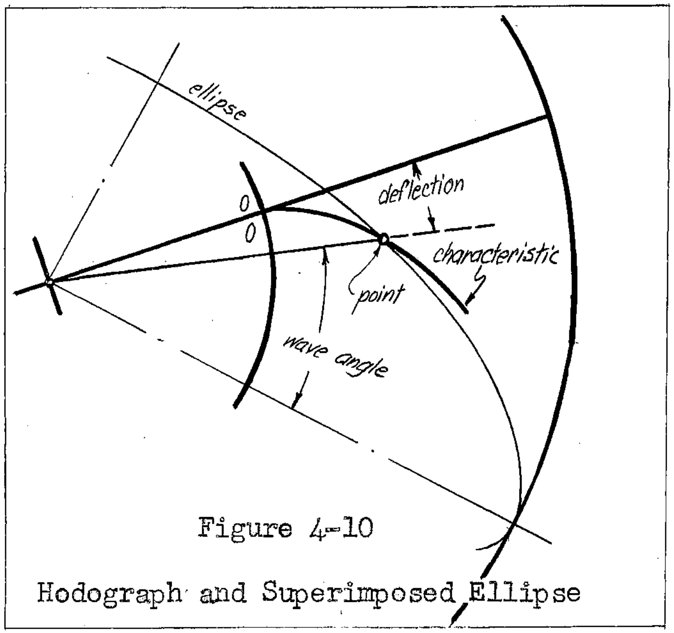

Figure 4-10

Hodograph and Superimposed Ellipse

(5) Assign a turning angle, δ, to the flow as it crosses the wave equal to the angle between successive tangents.

The modified method presented permits the use of the Prandtl-Meyer flow relations, Chart 2-11[13], in the construction of the characteristics. The two methods are thoroughly interchangeable. The application of the characteristics — chart, or hodograph, is independent of the reservoir conditions. This holds true also for the application of the Prandtl-Meyer flow relations. A proof of the last statement is unnecessary, since any sample problem can be solved by either method with identical results. Part of the modified method of characteristics appears in Figure 4-11. The difference between the modification and the original can be seen easily in Figure 4-12. Let

$1, 2, \ldots; \bar{1}, \bar{2}, \ldots,$ = points along wall,

w_i = flow velocity,

M_i = Mach wave,

---

12 Ibid., p. 218.

13 C. L. Dailey and F. C. Wood, op. cit.

N_j = normal to characteristic curve,

P_j = end point of vector on hodograph corresponding to w_i, $i = j$,

$i, j = 1, 2, \ldots$

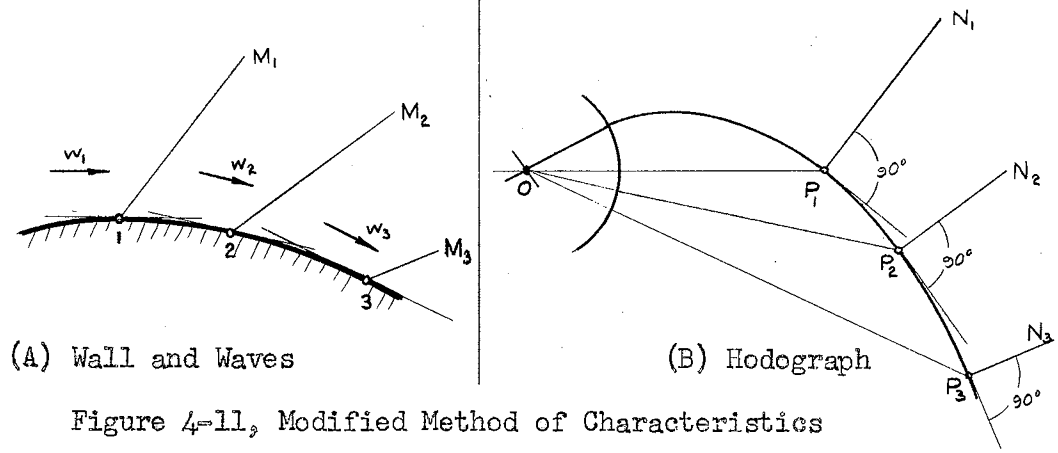

(A) Wall and Waves

(B) Hodograph

Figure 4-11, Modified Method of Characteristics

In Figure 4-11, when $i = j$, $OP_j \parallel w_i$, and $M_i \parallel N_j$.

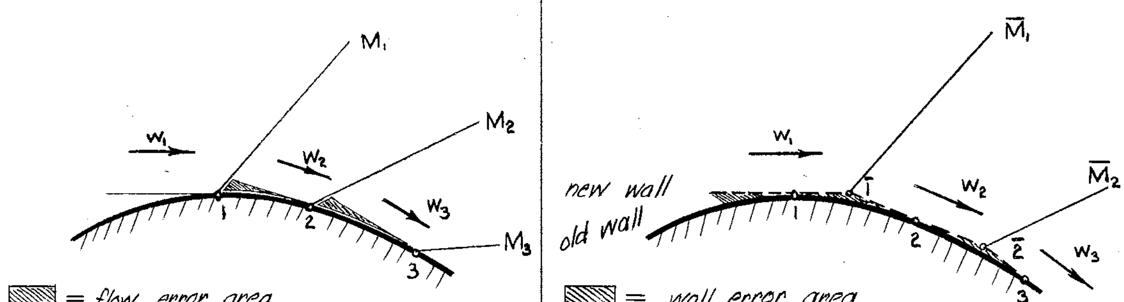

(A) Modified Method

(B) Original Method

Figure 4-12, Comparison of Characteristics Methods

The purpose of the problem is the location of the wave pattern at the channel exit. Any intermediate problem solution not necessary as a step toward the solution is omitted. Hence, the solution which follows often bypasses regions which are unnecessary - and difficult - to solve.

Frequent use is made of a set of curves compiled by Dailey and Wood.[14] On all occasions it is ascertained implicitly that the conditions of the problem correspond to those of the chart used. Usually, no mention is made of the equations the authors employed in the derivations of curve relations. Let

Θ_w = wave angle, degrees;

Θ_s = deflection angle, degrees;

P_s = stagnation pressure, psia;

P = static pressure, psia;

ϕ = expansion angle, degrees, Prandtl-Meyer relation;

T = ambient temperature, degrees Rankine;

T_s = stagnation temperature, degrees Rankine;

γ = ratio of specific heats.

Additional subscripts, usually arabic numerals, refer to points, regions, and interfaces between regions.

Let the flow expand one degree from the condition at the sonic line at the wall. This means that the flow is bent through one degree at the wall. The condition behind the oblique wave corresponding to this is assumed such that the shock wave is decreased in slope by one degree from that at the wave sonic point. At the wave sonic point, $\Theta_w = 61.4$ degrees, Chart 2-1[15]. At point 6, Figure 4-13,

$$\Theta_{w6} = 61.4 - 1 = 60.4 \text{ degrees;}$$

$$\Theta_{s6} = 16.4 \text{ degrees, Chart 2-1}^{15};$$

14 Ibid.

15 Ibid.

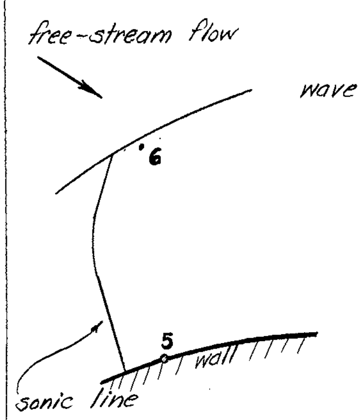

Figure 4-13

One-Degree Expansion

$M_6 = 1.027$, Chart 2-7[16].

$M_5 = 1.08$, Chart 2-11[16];

$\frac{P_{s6}}{P_{s1}} = 0.934$, Chart 2-3[16]; where "1" refers to the upstream free-stream condition.

$\frac{P_{s6}}{P_6} = 1.96$, at $\gamma = 1.40$, Chart 1-1[16];

$\frac{P_{s5}}{P_{s1}} = \frac{P_{s2}}{P_{s1}} = 0.856$, Chart 2-3[16]; since point 2, the nose stagnation point, falls on the same streamline as point 5.

$\frac{P_{s5}}{P_5} = 2.08$, at $\gamma = 1.40$, Chart 1-1[16];

$$\frac{P_{s6}}{P_{s5}} = \frac{P_{s6}}{P_{s1}} \frac{P_{s1}}{P_{s5}} = 0.934 \frac{1}{0.856} = 1.091,$$

$$\frac{P_6}{P_5} = \frac{P_{s6}}{P_{s5}} \frac{\frac{P_{s5}}{P_5}}{\frac{P_{s6}}{P_6}} = 1.091 \frac{2.08}{1.96} = 1.158 \quad .$$

$P_6 > P_5$, or the static pressure at the wave is greater than at the wall.

Past the sonic line, the first characteristic is constructed at 5 degrees of ϕ. The zone between the sonic line and the extension of the portion of the first characteristic originating at the wall shall be called region 1, as shown in Figure 4-14. For the computation of region 1, it is assumed that the border portion of the oblique shock wave is a

---

16 Ibid.

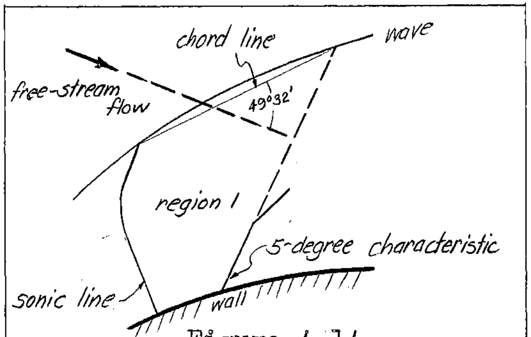

Figure 4-14

Borders of Region 1

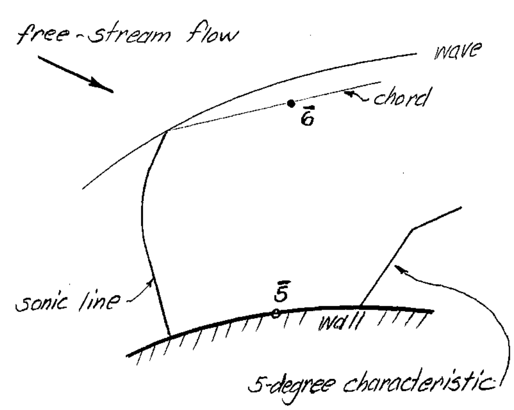

Figure 4-15

Center of Region 1

straight line from the wave sonic point to the point of intersection of the extension of the wall segment of the 5-degree characteristic and the nose wave. The center of region 1 is examined next. As may be seen from Figure 4-15, the wall condition corresponds to a $2\frac{1}{2}$-degree expansion. From a precise drawing, the straight-line portion of the oblique shock has a slope, equal to $\theta_{w\bar{6}}$, of 49° 32'. The remainder or region 1 can be computed next.

$\theta_{s\bar{6}} = 11.5$ degrees, Chart 2-1[17];

$M_{\bar{6}} = 1.285$, Chart 2-7[17];

$\dfrac{P_{s\bar{6}}}{P_{s1}} = 0.982$, Chart 2-3[17];

$\dfrac{P_{s\bar{5}}}{P_{s1}} = \dfrac{P_{s2}}{P_{s1}} = 0.856$, Chart 2-3[17]; since point 2 falls on the same streamline as point $\bar{5}$.

$$\frac{P_{s\bar{6}}}{P_{s\bar{5}}} = \frac{P_{s\bar{6}}}{P_{s1}}\frac{P_{s1}}{P_{s\bar{5}}} = 0.982\,\frac{1}{0.856} = 1.148 ,$$

$M_{\bar{5}} = 1.154$, at $\phi = 2.5$ degrees, Chart 2-11[17];

$\dfrac{P_{s\bar{6}}}{P_{\bar{6}}} = 2.72$, at $\gamma = 1.40$, Chart 1-1[17];

$\dfrac{P_{s\bar{5}}}{P_{\bar{5}}} = 2.29$, at $\gamma = 1.40$, Chart 1-1[17];

17 Ibid.

$$\frac{P_{\bar{6}}}{P_{\bar{5}}} = \frac{P_{s\bar{6}}}{P_{s\bar{5}}} \; \frac{\dfrac{P_{s\bar{5}}}{P_{\bar{5}}}}{\dfrac{P_{s\bar{6}}}{P_{\bar{6}}}} = 1.148\,\frac{2.29}{2.72} = \frac{1}{1.032} \quad .$$

$P_{\bar{6}} < P_{\bar{5}}$, or the static pressure at the wave is less than at the wall.

The pressure difference after one degree of expansion in region 1 necessitates the existence of a compression wave originating at the sonic line, and directed toward the wall. This wave is such that static pressures past the matching wave, immediately past the oblique wave and at the wall, are equalized. It can be shown that the flows in these adjacent zones are very nearly parallel, and that the Mach numbers are different. Therefore, there is a shear sheet between the zones, originating at the sonic line at the same point as the balancing compression wave. The direction of the static-pressure inequality for the greater part of region 1 is that which holds at the condition of 2.5 degrees of expansion from the sonic line. The mid-region condition is used to compute the balancing wave which matches pressures for all of region 1. It is seen that there is a reversal of the static-pressure inequality between the one-degree condition and the mid-region condition, as illustrated in Figure 4-16. There is no necessity for analyzing the indeterminate subregion in order to obtain a satisfactory pattern downstream. That is,

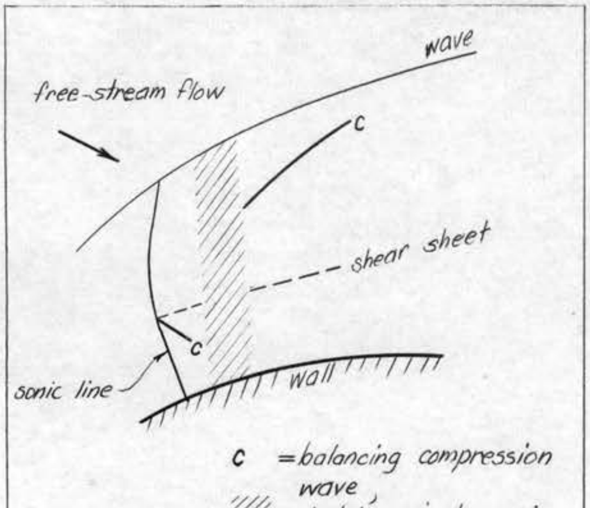

Figure 4-16

Actual Pattern, Region 1

it is safe to assume that the flow behaves as if the compression wave and the shear sheet originated at the midpoint of the sonic line.

$$\theta_{s\bar{6}-\bar{5}} = 0.64 \text{ degrees, Chart } 2\text{-}4^{18} \; ;$$

$$\theta_{w\bar{6}-\bar{5}} = 52.1 \text{ degrees, Chart } 2\text{-}1^{18} \; .$$

Downstream of the balancing shock,

$$M_7 \quad = 1.279, \text{ Chart } 2\text{-}7^{18} \; .$$

Therefore, the shear velocity corresponds to

$M_7 - M_{\bar{5}} = \Delta M_{7-\bar{5}} = 1.279 - 1.154 = 0.125$. Consequently, the shear sheet must be continued.

The balancing compression wave is composed of two segments, each properly directed with respect to the flow direction preceding it. The actual wave, of course, is curved, and the two-segment wave shown in Figure 4-17 is a substitution. A further simplification is the substitution of a single straight wave for the two-segment wave. The direction of the flow preceding this wave is such that $\theta_{w\bar{6}-\bar{5}}$ is the same as before.

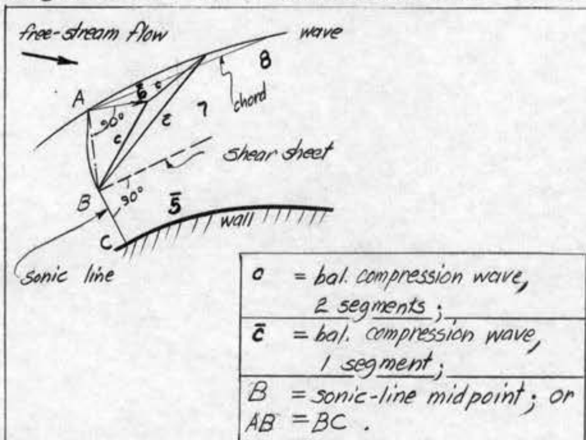

Figure 4-17

Substitute Pattern, Region 1

There is a difference of conditions between subregions 7 and 8. $M_8 = M_{\bar{6}} = 1.285$, since the flow is assumed to cross the chord segment of the oblique wave.

---

18 Ibid.

$$\frac{P_{s7}}{P_{s1}} = \frac{P_{s\bar{6}}}{P_{s1}}, \text{ since } \frac{P_{s\bar{6}}}{P_{s7}} = 1.00, \text{ Chart 2-3}$$ [19].

$$\frac{P_{s7}}{P_{s1}} = 0.982, \text{ Chart 2-3}$$ [19];

$$\frac{P_{s7}}{P_7} = 2.69, \text{ at } \gamma = 1.40, \text{ Chart 1-1}$$ [19];

$$\frac{P_{s8}}{P_8} = \frac{P_{s\bar{6}}}{P_{\bar{6}}} = 2.72, \text{ since } M_8 = M_{\bar{6}} .$$

$$\phi_7 = 5.6 \text{ degrees, and}$$

$$\phi_8 = 5.75 \text{ degrees, Chart 2-11}$$ [19];

$$\Delta\phi_{8-7} = \phi_8 - \phi_7 = 5.75 - 5.6 = 0.15 \text{ degrees,}$$

$$\frac{P_{s7}}{P_{s8}} = 1.00, \text{ since there is no shock wave.}$$

$$\frac{P_7}{P_8} = \frac{P_{s7}}{P_{s8}} \frac{\dfrac{P_{s8}}{P_8}}{\dfrac{P_{s7}}{P_7}} = 1.00 \, \frac{2.72}{2.69} = 1.012 .$$

The expansion wave required to match static pressures of adjacent subregions 7 and 8 originates at the intersection of the interior compression wave and the nose wave, and slopes downstream, toward the wall. This expansion wave is very weak, has negligible turning power, and does not change the Mach number sufficiently to warrant consideration. Therefore, it may be neglected in the first region.

The first five-degree expansion characteristic, called characteristic 1, is located, next. Characteristic 1 is composed of three seg-

---

19 Ibid.

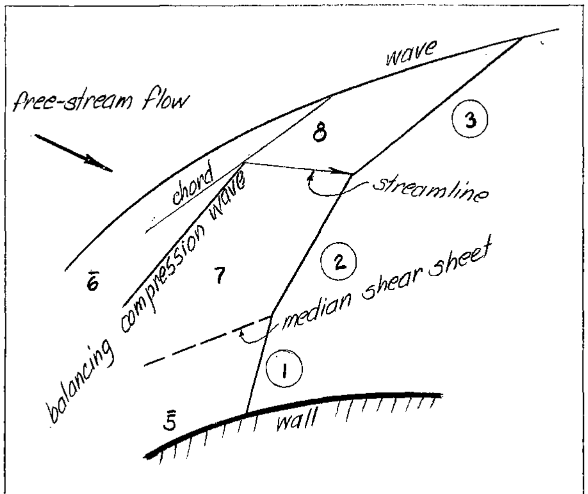

Figure 4-18

Characteristic 1

ments, as shown in Figure 4-18. Segment (1) of characteristic 1 begins at the wall at a point the tangent to which makes an angle of 5 degrees with the wall sonic point tangent. It extends to the median shear sheet, which originates at the midpoint of the sonic line.

$\theta_{w(1)} = 52.7$ degrees, at $\phi = 5$ degrees, Chart 2-11[20]. The condition at segment (2) corresponds to a 2.5-degree expansion from condition 7.

$$\phi_{(2)} = \phi_7 + 2.5 = 5.6 + 2.5 = 9.1 \text{ degrees},$$

$$M_{(2)} = 1.37, \text{ Chart 2-11}^{20};$$

$$\theta_{w(2)} = 46.9 \text{ degrees, Chart 2-11}^{20}.$$

Segment (2) extends from the median shear sheet to the streamline through the nose wave terminus of the interior compression wave. This streamline is also the locus of an extremely weak shear sheet which is neglected, and the direction of which corresponds to the flow downstream of the chord substitute for the curved oblique-wave segment bordering region 1.

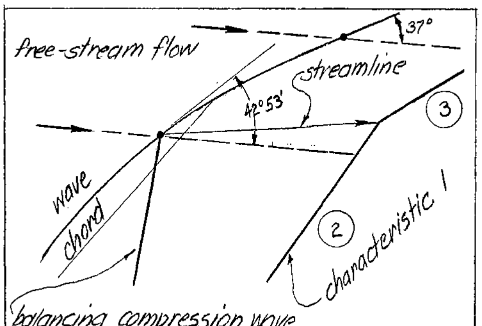

Figure 4-19

Seg. (3) of Characteristic 1

θ_w of the wave portion preceding segment (3) of characteristic 1 is such that $42^\circ 53' \geq \theta_w \geq 37^\circ$. It is assumed that $\theta_{w,\text{ average}} = 40^\circ$, at the wave. The pattern under examination appears in Figure 4-19. Across the portion of the

20 Ibid.

nose wave,

$$\theta_s = 4.1 \text{ degrees, Chart } 2\text{-}1^{21};$$

$$M_{\bar{2}} = 1.55, \text{ Chart } 2\text{-}7^{21}.$$

$$\text{At } M_{\bar{2}},\ \phi_{\bar{2}} = 13.3 \text{ degrees, Chart } 2\text{-}11^{21}.$$

Since the balancing compression wave strikes downstream of the center of the oblique-wave chord, an additional expansion equivalent to a change in ϕ of 2 degrees is assumed to be required to reach the condition immediately ahead of segment (3) of characteristic 1, instead of one equivalent to a change in ϕ of 2.5 degrees. Let

$\Delta\phi_{\bar{2}-(3)}$ = required change in ϕ. Then,

$$\phi_{(3)} = \phi_{\bar{2}} + \Delta\phi_{\bar{2}-(3)} = 13.3 + 2 = 15.3 \text{ degrees,}$$

$$M_{(3)} = 1.616, \text{ Chart } 2\text{-}11^{21};$$

$$\theta_{w\,(3)} = 38.2 \text{ degrees, Chart } 2\text{-}11^{21}.$$

Immediately preceding the wave, the static pressures are such that $P_{(1)} > P_{(2)} > P_{(3)}$, as is demonstrated below.

$$\frac{P_{s(1)}}{P_{(1)}} = 2.61,$$

$$\frac{P_{s(2)}}{P_{(2)}} = 3.05, \text{ and}$$

$$\frac{P_{s(3)}}{P_{(3)}} = 4.35 \text{ at } \gamma = 1.40, \text{ Chart } 1\text{-}1^{21};$$

$$\frac{P_{s(1)}}{P_{s1}} = 0.856, \text{ Chart } 2\text{-}3^{21};$$

$$\frac{P_{s(2)}}{P_{s1}} = \frac{P_{s\bar{6}}}{P_{s1}} = 0.982,$$ since no shock wave exists between $\bar{6}$ and (2).

21 Ibid.

$$\frac{P_{s(1)}}{P_{s(2)}} = \frac{\frac{P_{s(1)}}{P_{s1}}}{\frac{P_{s(2)}}{P_{s1}}} = \frac{0.856}{0.982} = \frac{1}{1.147} \quad ,$$

$$\frac{P_{(2)}}{P_{(1)}} = \frac{P_{s(2)}}{P_{s(1)}} \frac{\frac{P_{s(1)}}{P_{(1)}}}{\frac{P_{s(2)}}{P_{(2)}}} = 1.147 \, \frac{2.61}{3.05} = 0.982 \quad ,$$

or $P_{(1)} > P_{(2)}$.

$\frac{P_{s(3)}}{P_{s1}} = 1.00$, at $\theta_s = 4.1$ degrees, Chart 2-3[22] ;

$$\frac{P_{s(2)}}{P_{s(3)}} = \frac{\frac{P_{s(2)}}{P_{s1}}}{\frac{P_{s(3)}}{P_{s1}}} = \frac{0.982}{1.00} = 0.982 \quad ,$$

$$\frac{P_{(2)}}{P_{(3)}} = \frac{P_{s(2)}}{P_{s(3)}} = \frac{\frac{P_{s(3)}}{P_{(3)}}}{\frac{P_{s(2)}}{P_{(2)}}} = 0.982 \, \frac{4.35}{3.05} = 1.400 \quad ,$$

or $P_{(2)} > P_{(3)}$. Hence, $P_{(1)} > P_{(2)} > P_{(3)}$.

The second region lies between the 5-degree and 10-degree characteristics. A balancing pattern is required, similar to that of region 1. This pattern is assumed to be the result of 7.5-degree conditions, or mid-region conditions in region 2. The method used in the analysis of region 2 is a continuation of that of region 1. Figure 4-20 shows the beginning of the pattern. The shear velocities at the junctures of the segments of the characteristics are decreased by the static-pressure

---

22 Ibid.

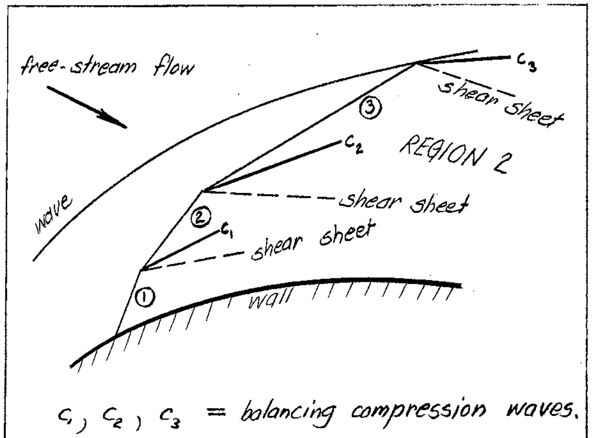

Figure 4-20

Partial Pattern, Region 2

matching process. The effect of the balancing compression waves is to bend the shear sheets away from the wall. Due to the expansion process along the wall, the 10-degree characteristic is bent back more than the 5-degree characteristic, but its curvature is less than that of the 5-degree characteristic because of the decrease in shear velocities. The nature of the matching patterns of successive regions is such that each characteristic is bent back, or downstream, further than its predecessor because of the expansion process along the wall, but the curvature of each successive characteristic becomes less and less until the characteristics become and remain straight. There exists a characteristic, the outer segment of which is parallel to the straight portion of the nose wave. Since this outer segment ceases to touch the wave, its influence on successive outer segments of characteristics remains uniform. The pressure-matching patterns existing between the interior segments decrease shear velocities and force the streamlines away from convergence. A precise drawing of this part of the solution appears in the appendix. The sonic lines on both sides of the nose are shown, but the calculated pattern is drawn for the concave-wall side of the nose only. The pattern of the other side is quite similar, since the nose region is approximately symmetrical about the continuation of the inlet stagnation streamline. No numerical solution of this other side is given, since the downstream pattern may be located without doing so by taking advantage of the near-symmetry.

A stable configuration is reached at and past the first straight characteristic, at which the shear sheets must cease. Supersonic flow tends toward stabilization. Once stabilized, it tends to remain stable. It is safe to assume that all balancing compression waves are weak oblique shocks, none of which changes the stagnation conditions of its particular subregion.

The remainder of the channel remains to be analyzed. The pattern is constructed in the neighborhood of each wall, after which intersections between members of opposite wave families may be examined.

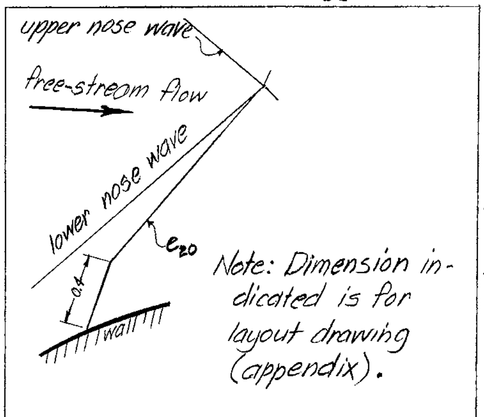

Figure 4-21

e_{20} of Concave Wall

The pattern along the concave wall is examined next. A Prandtl-Meyer expansion takes place close to the wall, beginning at the sonic point, and continuing along the convex portion of the nose zone. The wall curvature then changes to concave, but the Prandtl-Meyer relations still apply to the slow compression along this portion of the wall. Expansion characteristics corresponding to a given value of ϕ are labeled e_ϕ and c_ϕ respectively. The previous analysis permits the assumption that e_{20} is bent. In addition, it is assumed that e_{20} is constructed in two segments, such that the outer segment meets the two oblique waves at their point of intersection.

The tangent line at the wall sonic point corresponds to the $\phi = 0$ reference direction. Wall origin points of characteristics have tangents making the angle of the local value of ϕ with the reference direction. All characteristics past e_{20} are c_ϕ , with the exception of portions past "intersections" with other waves. The wave e_{20} is constructed in accordance with Figures 4-21 and 4-22, and the c_ϕ with the use of Table 4-3. The resulting pattern is shown in Figure 4-23. Waves originating from a single wall are said to belong to the same family. The meeting of such waves with each other is not a proper intersection, and it becomes necessary to analyze all possible types of meeting patterns.

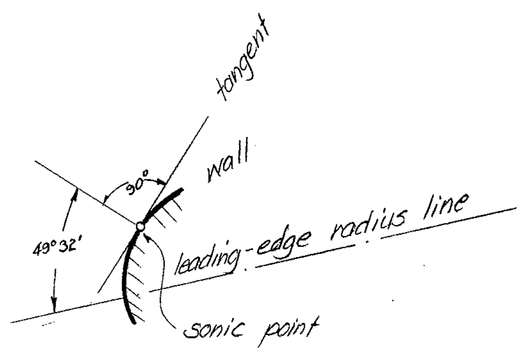

Figure 4-22

Reference Direction, Concave Wall

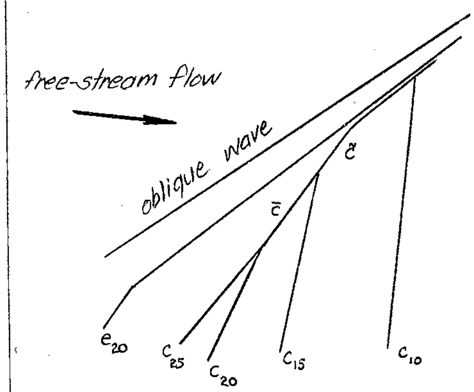

Figure 4-23

Concave-Wall Pattern

Table 4-3

Characteristics Along Concave Wall, Chart 2-11[23]

ϕ degrees	θ_w degrees	M	$\tan \phi$	$\tan \theta_w$	
20	34.3	1.775	0.364	0.682	c_ϕ
25	30.7	1.950	0.466	0.594	e_ϕ
20	34.3	1.775	0.364	0.682	
15	38.6	1.605	0.268	0.798	
10	44.2	1.435	0.176	0.972	
5	52.7	1.255	0.088	1.313	

23 Ibid.

c_{25} and c_{20} are of the same family. If $\Theta_{s,1-2}$ and $\Theta_{s,2-3}$ are sufficiently small, a single wave $\bar{c}$ may be assumed to result past the point of intersection. This compression characteristic is such that

$$\Theta_{s,1-3} = \Theta_{s,1-2} + \Theta_{s,2-3} \quad , \text{ and}$$
$$\Theta_{w,\bar{c}} = \tfrac{1}{2}(\Theta_{w,c_{25}} + \Theta_{w,c_{20}}) \quad .$$

The behavior of $\bar{c}$ is not in full agreement with the method of characteristics; that is, ϕ preceding $\bar{c}$ does not correspond to Θ_w of $\bar{c}$. However, the flow is fixed completely by the equations given. For the sake of agreement, it is assumed that $\phi_{\bar{c}} = 22.5°$, and that the flow in a small region immediately preceding $\bar{c}$ corresponds to $\phi_{\bar{c}}$. $\bar{c}$ is assigned $\Theta_{s,\bar{c}} = 7.5°$ under this assumption. The pattern appears in Figure 4-24. An analogous pattern is formed by $\bar{c}$ and c_{15} , resulting in $\tilde{c}$, as is shown in Figure 4-25. The conditions on $\tilde{c}$ are:

$$\Theta_{s,1-4} = \Theta_{s,1-2} + \Theta_{s,2-3} + \Theta_{s,3-4}$$
and $\Theta_{w,\tilde{c}} = \tfrac{1}{2}(\Theta_{w,\bar{c}} + \Theta_{w,c_{15}})$.

Again, the behavior of $\tilde{c}$ is not in full agreement with the modified method of characteristics; that is, ϕ preceding $\tilde{c}$ does not correspond to Θ_w of $\tilde{c}$. As before, however, the flow is fixed completely by the conditions given. For the sake of

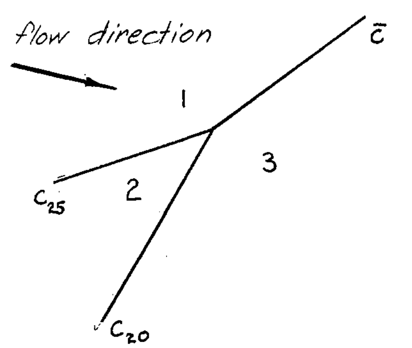

Figure 4-24

Intersection of c_{25} and c_{20}

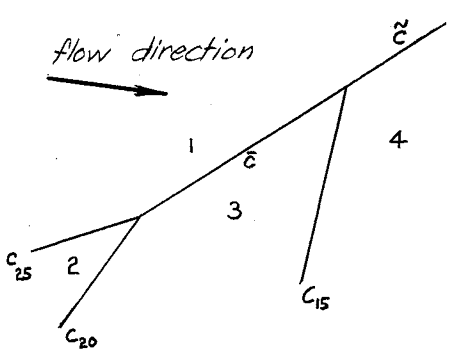

Figure 4-25

Intersection of $\bar{c}$ and c_{15}

agreement, it is assumed that $\phi_{\tilde{c}} = 18^\circ\ 45'$. $\tilde{c}$ is assigned $\theta_{s,\tilde{c}} = 8^\circ\ 45'$.

The expansion characteristic cannot be crossed by a compression characteristic of the same family, since the disturbance cannot communicate itself upstream. Hence, the pattern of Figure 4-26 is formed. The portion of $\tilde{c}$ bent away from e_{20} is assumed to have the same turning power as the other section of the compression wave, but the angular relation of flow direction to wave position is not preserved, unless for purposes of visualization, a "step-wave" is assumed. The "steps" are parallel to

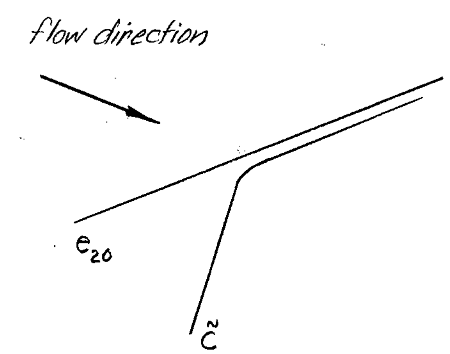

Figure 4-26

Meeting of $\tilde{c}$ and e_{20}

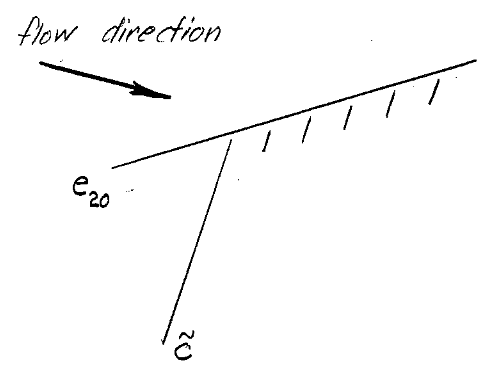

Figure 4-27

Compression "Step-Wave"

the initial section of the characteristic, as shown in Figure 4-27. The "step-wave" segment of $\tilde{c}$ is intersected by c_{10}, forming $\sum c$, a reinforced continuation of the "step-wave." A straight line is substituted for both segments of the "step-wave," as shown in Figure 4-28 (B). The layout drawing, given in the appendix, shows pattern (C), but for purposes of later analysis, (B) is used. $\sum c$ is such that the flow behind it corresponds to that behind c_{10}, which corresponds to the flow preceding c_5 (not shown). c_5 is of indeterminate length, since it is not yet known where it is intersected by a member of the opposite family of characteristics.

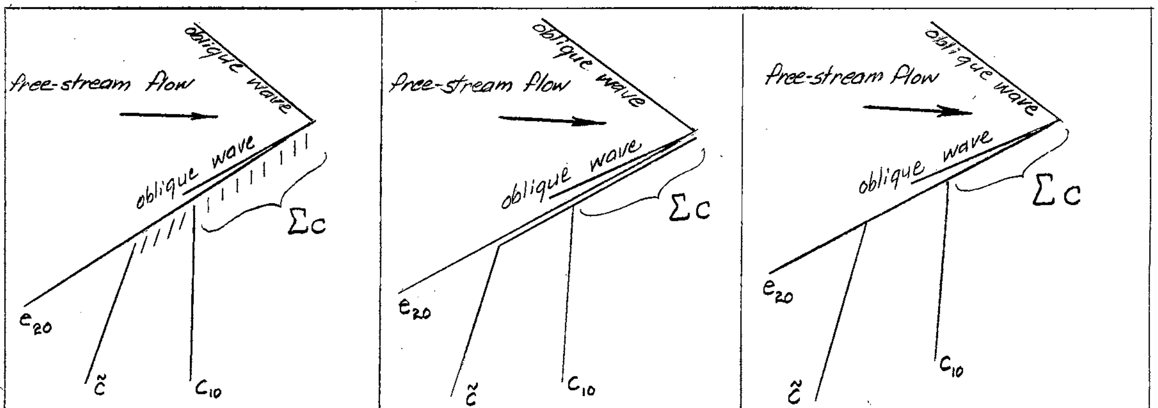

Physical Equivalent (A) | Center Pattern Substitute (B) | Layout Pattern (C)

Figure 4-28 Formation of Σc

The other influence on the center pattern is due to the flow along the convex wall, which is examined next. Since the curvature is always convex, a Prandtl-Meyer expansion takes place in the neighborhood of the wall, beginning at the wall sonic point. All characteristics are expansions waves, and are labeled e_ϕ, where the subscript is the value of ϕ in the subregion preceding each wave. It is assumed that both e_{20} and e_{25} are bent. Each is constructed of two segments, such that the outer segment of each meets the oblique waves at their point of intersection.

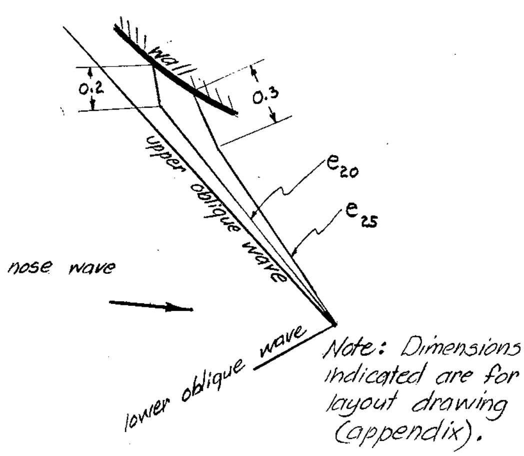

Figure 4-29

e_{20} and e_{25}, Convex Wall

The tangent line at the wall sonic point corresponds to the $\phi = 0$ reference direction. As with the other wall, wall origin points of characteristics have tangents making the angle of the local value of ϕ with the reference direction.

e_{20} and e_{25} are constructed in accordance with Figure 4-29, and the remaining e_ϕ with the use of Table 4-4. Table 4-4 is constructed with values obtained from Chart 2-11[24] for $20^\circ \leq \phi \leq 70^\circ$, and with values obtained by the modified method of characteristics for $\phi = 75^\circ$ and 80°.

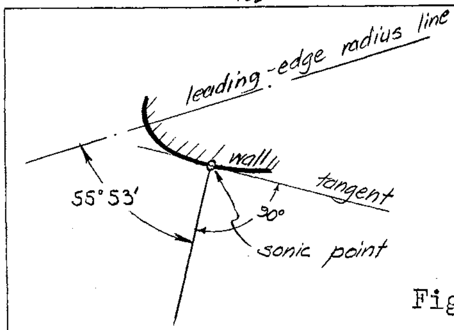

Figure 4-30

Angle between leading-edge radius line and sonic-point tangent $= 90^\circ - 55^\circ 53' = 34^\circ 07'$.

Reference Direction, Convex Wall

Table 4-4

Characteristics Along Convex Wall			
ϕ degrees	θ_w degrees	$\tan\phi$	$\tan\theta_w$
20	34.3	0.364	0.682
25	30.7	0.466	0.594
30	27.8	0.577	0.527
35	25.3	0.700	0.473
40	23.2	0.839	0.429
45	21.2	1.000	0.388
50	19.4	1.192	0.352
55	17.7	1.428	0.319
60	16.2	1.732	0.291
65	14.75	2.145	0.263
70	13.3	2.748	0.236
75	11.86	3.732	0.210
80	10.65	5.671	0.188

The flow configuration in the small neighborhood of the intersection of the two oblique nose waves is called the center pattern, and is to be analyzed next. e_{30}, originating at the convex wall and c_{25}, originating at the concave wall are straight waves. The outer portion of c_{25} is

---

24 Ibid.

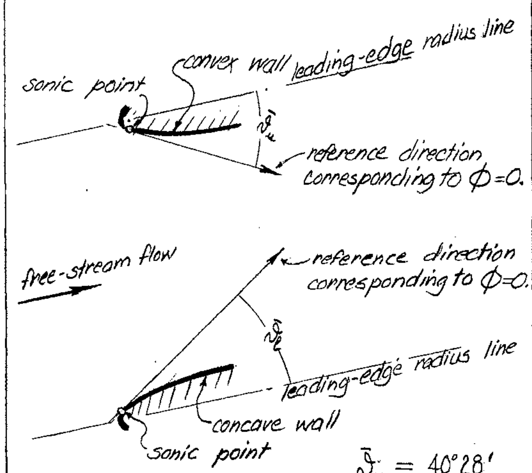

Figure 4-31

Reference Directions

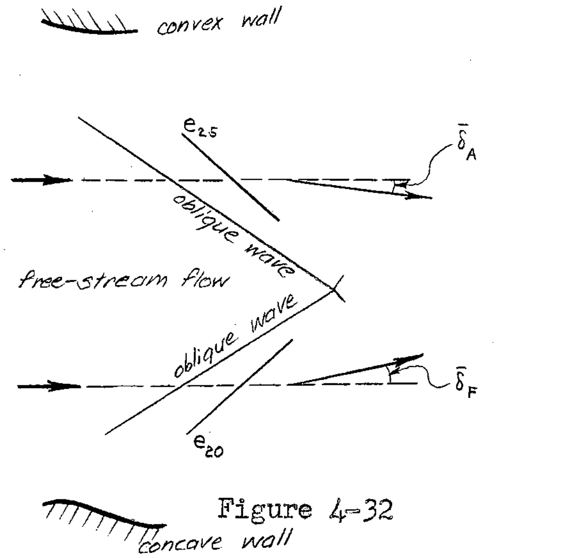

Figure 4-32

Flow Directions Past Last Bent e_ϕ

composed of segments reinforced by successive c_ϕ , and of the special segment Σc. However, the flow preceding this outer portion has the same ϕ as the flow preceding the straight portion of c_{25} . e_{25} , originating at the convex wall and e_{20} , originating at the concave wall are bent in two segments. e_{25} precedes e_{30} , and e_{20} precedes c_{25} . Hence, all conditions past e_{25} must be the same as those preceding e_{30} . Similarly, all conditions past e_{20} must be the same as those preceding c_{25} . Therefore, past e_{25} (convex) the flow direction is $30°$ from $\bar{\vartheta}_u$; past e_{20} (concave) the flow direction is $25°$ from $\bar{\vartheta}_l$. $\bar{\delta}_A$ and $\bar{\delta}_F$ are the flow directions with respect to the free-stream flow direction, past e_{25} and e_{20} , respectively. From Figures 4-31 and 4-32,

$$\bar{\delta}_A = \bar{\vartheta}_u - 30° = 40°\ 28' - 30° = 10°\ 28' ,$$
$$\bar{\delta}_F = \bar{\vartheta}_l - 25° - 34°\ 07' - 25° = 9°\ 07' .$$

The pattern of Figure 4-33 is assumed in the center region. Let

$\mathcal{R}$ = subregion, as labeled, A, B, . . . ,

owc_u = continuation of upper oblique wave,

owc_l = continuation of lower oblique wave,

Σc_c = continuation of Σc,

e_{25c} = continuation of e_{25} ,

e_{20c} = continuation of e_{20} ,

δ = flow deflection through wave, degrees,

$\bar{\delta}$ = local flow direction with respect to free-stream direction, degrees.

The symbols $\uparrow$ and $\downarrow$ following δ and $\bar{\delta}$ specify direction tendencies. Five identities must hold in the $\mathcal{R}$'s:

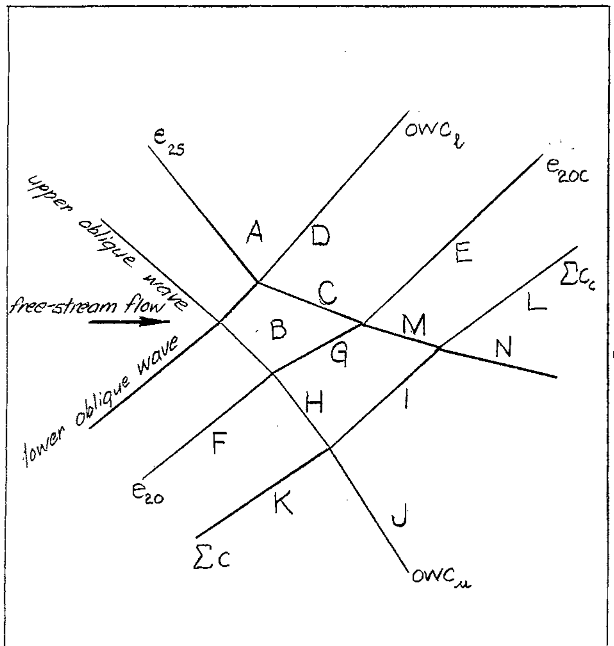

Figure 4-33

Center Pattern

1) $\bar{\delta}_C \equiv \bar{\delta}_D$,

2) $\bar{\delta}_E \equiv \bar{\delta}_M$,

3) $\bar{\delta}_G \equiv \bar{\delta}_H$,

4) $\bar{\delta}_I \equiv \bar{\delta}_J$,

5) $\bar{\delta}_L \equiv \bar{\delta}_N$.

The turning powers of the waves are:

$\delta_{owc_u} = 1^\circ \downarrow$,

$\delta_{owc_\ell} = 1^\circ \uparrow$,

$\delta_{e_{25}} = \delta_{e_{25c}} = 9^\circ\ 28' \downarrow$,

$\delta_{e_{20}} = \delta_{e_{20c}} = 8^\circ\ 07' \uparrow$,

$\delta_{\Sigma c} = \delta_{\Sigma c_c} = 20^\circ \uparrow$.

Table 4-5 shows the result of applying these relations to the pattern of Figure 4-33, with the exception of $\delta_{e_{25}} = \delta_{e_{25c}}$ and $\delta_{e_{20}} = \delta_{e_{20c}}$. These quantities are found by locating all possible $\bar{\delta}$'s with the aid of the known δ 's, from which the unknown δ 's may be derived. When these are known, the remaining unknown $\bar{\delta}$'s may be computed. It is seen that $\bar{\delta}_L \equiv \bar{\delta}_N = 18^\circ\ 39' \uparrow$ is the flow direction immediately downstream of the center pattern. Neither the e_ϕ , nor the c_ϕ , nor their combinations make the proper Θ_W's with their respective flow directions for

Table 4-5

Center Pattern Flow Directions					
$\mathcal{R}$	$\bar{\delta}$		$\mathcal{R}$	$\bar{\delta}$	
A	10° 28'	↓	H	8° 07'	↑
B	0°	—	I	28° 07'	↑
C	9° 28'	↓	J	28° 07'	↑
D	9° 28'	↓	K	29° 07'	↑
E	1° 21'	↓	L	18° 39'	↑
F	9° 07'	↑	M	1° 21'	↓
G	8° 07'	↑	N	18° 39'	↑

reasons given previously. The analysis is made on the assumption of correct flow deflections and other flow conditions.

A simplification is introduced to reduce the work required to analyze the interference pattern of the waves issuing from the center region with the downstream members of both families of characteristics. The single wave λ is substituted for the three waves owc_{ℓ} , e_{20c} and Σc_c . Similarly, ν is the substitution wave for the two waves owc_{μ} and e_{25_c} . The modified center pattern appears in Figure 4-34. Since λ is a single

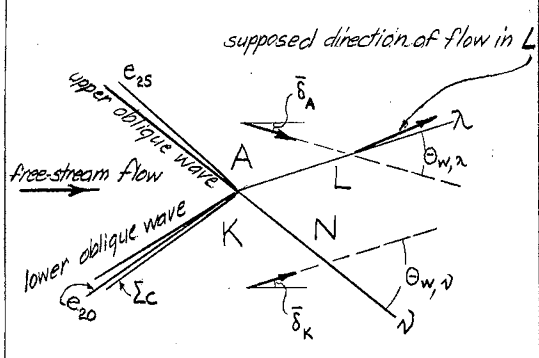

Figure 4-34

Modified Center Pattern

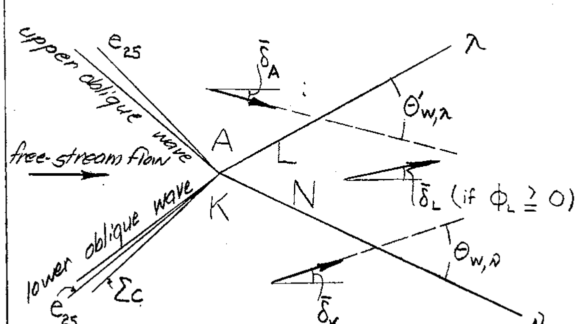

Figure 4-35

Corrected Modified Center Pattern

wave, a contradiction is reached because $\Theta_{W,\lambda} < \delta_\lambda$, which means that the flow does not cross the wave. λ must be modified to satisfy the necessary condition that $\Theta_W > \delta$. Therefore, it is assumed that in a small region immediately preceding λ, $\phi = \phi_A - \frac{1}{2}\Delta\phi_\lambda$, where $\Delta\phi_\lambda = \phi_A - \phi_L$. $\theta'_{w,\lambda}$ corresponding to this assumption satisfies the necessary condition that $\theta'_{w,\lambda} > \delta_\lambda$. δ_ν of the lower substitute wave ν is not excessively large, and the necessary condition, $\theta_{w,\nu} > \delta_\nu$, is not violated. Figure 4-35 shows the corrected pattern.

The waves λ and ν are not fully established, since it is necessary to check that $\phi_L = \phi_N \geq 0$. $\delta_\lambda = \delta_{A-L} = 29^\circ\ 07' \uparrow$,

$$\phi_L = \phi_A - \delta_{A-L} = 30^\circ - 29^\circ\ 07' = 0^\circ\ 53' .$$

Hence, the wave λ is established, provided that $\phi_L = \phi_N$. The value of ϕ past the wave ν is checked next.

$$\delta_\nu = \delta_{K-N} = 10^\circ\ 28' \downarrow ,$$
$$\phi_N = \phi_K - \delta_{K-N} = 5^\circ - 10^\circ\ 28' = -4^\circ\ 32' .$$

Hence, the wave ν cannot be established, since ϕ cannot be less than zero for a Prandtl-Meyer compression. The flow in subregion N is subsonic. Let ν' by substituted for ν, with $\delta_{\nu'}$ just sufficient to produce $M = 1$ past the wave. The lower pattern still contains sufficient energy to compress the flow by an amount equal to the subsonic equivalent of a decrease in ϕ of $4^\circ\ 32'$, if such an equivalent exists. No such equivalent is known to exist, and the condition of flow in subregion N remains indeterminate. In subregion L, the flow is supersonic, but in N the flow is subsonic. If the pressures in L and N are matched, a shear sheet forms their common interface. No information is available on what occurs at a shear sheet which has a subsonic zone on one side, and expansion characteristics "crossing" into it from the supersonic zone on the other side. Therefore, no solution of the mixed-flow region can be found.

The previous portion of this analysis is based on the assumption that the change in Φ across each substitute wave is a function of δ across each substitute wave. Another assumption is possible. It is only stated here, and requires further investigation. Let $\Delta\Phi$ equal the change in Φ across the wave denoted by the subscript attached. Let

$$\Delta\Phi_{\lambda} = \Delta\Phi_{owc_{l}} + \Delta\Phi_{e_{20c}} + \Delta\Phi_{\Sigma c_{c}} \quad ,$$

$$\text{and } \Delta\Phi_{\nu} = \Delta\Phi_{owc_{\nu}} + \Delta\Phi_{e_{25c}} \quad .$$

Then it can be shown that

$$\Phi_{L} > 0 \; , \qquad \Phi_{N} > 0 \quad ,$$

$$\text{and} \qquad \Phi_{L} \neq \Phi_{N} \quad .$$

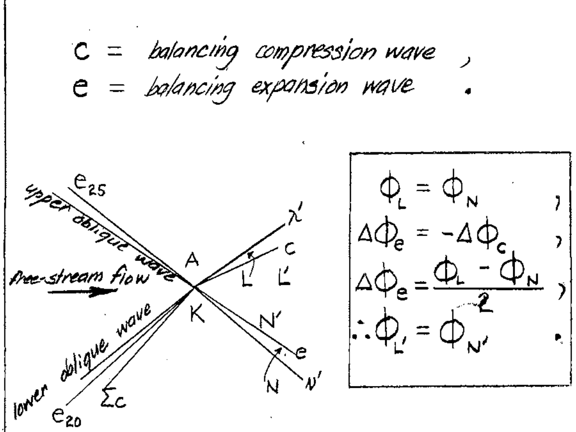

Figure 4-36

Alternate Matching Pattern

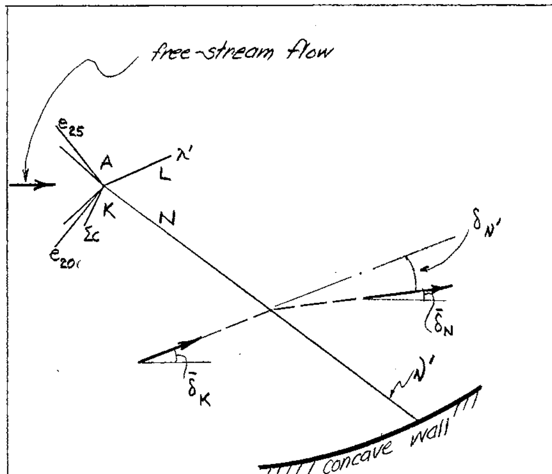

Figure 4-37

Changed Behavior of Wave

It is possible to match static pressures past subregions L and N, such that in a subsequent pair of subregions L' and N', $\Phi_{L'} = \Phi_{N'}$. This pattern is shown in Figure 4-36. These conditions are sufficient to establish both λ and ν , but they change the character of ν to that of an expansion wave with the extraordinary property that δ_{ν} is directed in a manner opposite to that associated with ordinary expansion waves. This behavior is shown in Figure 4-37. No proper explanation can be found, and, as stated above, further investigation is necessary. Hence, the first set of assumptions is used. This conclusion demonstrates that the second assumption is also of no help toward a solution.

It is desirable to avoid mixed flow in the channel, since this type of flow cannot be solved by any known or attempted means. The only alternative which will produce a result is an alteration of the profiles such that no mixed flow occurs for both the blunt-nosed and the sharp-nosed cascade channels.

B Cascade of Second Modification of Blunt-Nosed Profiles

1 Profile and Channel Layout

In the alteration of the blunt-nosed profile, as much of the old construction as is possible should be retained. In accordance with Chapter III, a sharp-nosed profile is associated with the blunt-nosed one. Both must be considered simultaneously, since their shape limits must be established such that all mixed flows in their respective channels are eliminated.

To establish the required limits, the construction of the sharp-nosed profile channel wall which replaces the concave wall of the original channel is considered first. A straight wall is selected, since concave curvature causes excessive compression, which is to be avoided. If the semi-wedge angle associated with this wall is chosen too large, the reflection of the attached oblique shock from the opposite channel wall will cause the flow to be subsonic. Hence, it is desirable to select a small semi-wedge angle to insure supersonic flow in the sharp-nosed profile channel.

Consider next the wall of the blunt-nosed profile channel replacing the original concave wall. Compression at the original wall begins past the inflection point on the wall. If all compression is avoided, the reflection of the straight continuation of the detached nose wave will not be strong enough to cause compression to subsonic flow either at the convex wall or at the lower wall, if the direction of the reflection is such that it strikes the lower wall.

These limits determine the new lower walls for both required channels. Since both walls must be nearly the same, let the lower wall of the sharp-nosed profile channel be a semi-wedge, with the associated angle $\delta = 9^\circ\ 07'$, which corresponds to the slope angle of the original lower wall at the point of inflection. The lower wall of the new blunt-nosed profile channel consists of half of the nose region of the original profile superimposed on the lower wall of the sharp-nosed profile channel, with a fillet drawn from the point of inflection to the semi-wedge wall. Figure 4-38 shows the configuration of both new lower walls.

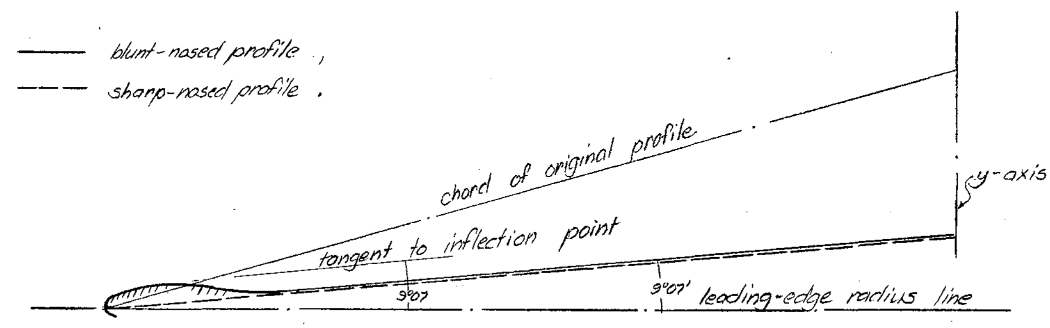

Figure 4-38

New Lower Walls of Sharp-Nosed and Blunt-Nosed Profile Channels

The upper wall of the new blunt-nosed profile channel now can be established completely. Figure 4-39 illustrates how this is accomplished.

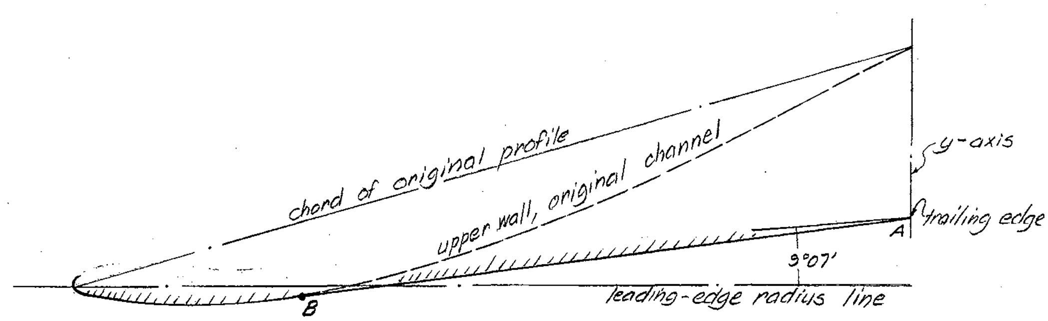

Figure 4-39

Upper Wall of New Blunt-Nosed Profile Channel

AB is a straight line from A, drawn tangent to the original profile at B.

2 Nose Region

The nose region, including the subsonic zone behind the nose wave, the sonic line, and the detached shock wave, is preserved in the alteration of the channel.

3 Supersonic Downstream Region

The nose portion of the new profile coincides with that of the original one to the point corresponding to $\phi = 25^\circ$ along the lower channel wall, and up to the point corresponding to $\phi = 51^\circ\ 46'$ along the upper channel wall. The flow along the lower wall is identical to the original flow from the sonic line to the subregion immediately past e_{20}. Along the upper wall, the flow remains unaltered from the sonic line to and including the subregion immediately past e_{45}.

The patterns in the neighborhood of each wall are constructed next, after which the intersections of members of opposite wave families may be examined.

The remainder of the pattern along the lower wall is examined next with the use of the modified method of characteristics and the terminology of the first channel analysis. e_{25} is the last bent e_ϕ. Its construction is shown in Figure 4-40. e_{30} is the last e_ϕ. The next two waves are c_ϕ, and are the last waves along the lower wall. Through each of these, c_{35} and c_{30}, the flow is deflected through 5 degrees, so that the flow past c_{30} corresponds to $\phi = 25^\circ$. c_{35} and c_{30} are of the

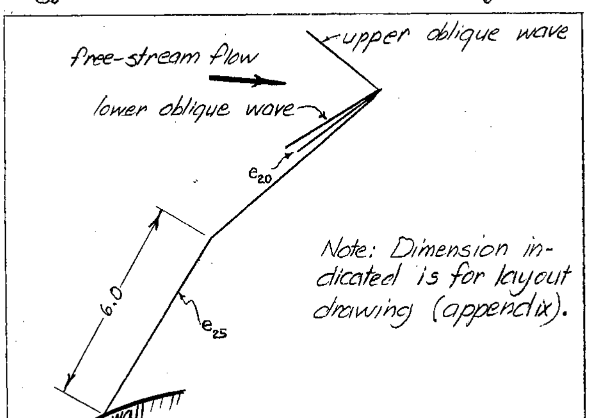

Figure 4-40

Construction of e_{25}, Lower Wall

same family. If $\Theta_{s,1-2}$ and $\Theta_{s,2-3}$ are sufficiently small, a single wave $\check{c}$ may be assumed to result past the point of intersection. $\check{c}$ is such that

$$\Theta_{s,1-3} = \Theta_{s,1-2} + \Theta_{s,2-3} \quad ,$$

and $$\Theta_{w,\check{c}} = \Theta_{w,c_{30}} \quad .$$

The pattern appears in Figure 4-41. The behavior of $\check{c}$ is not in agreement with the modified method of characteristics; that is, ϕ preceding $\check{c}$ does not correspond to Θ_w of $\check{c}$. However, the flow is fixed completely by the equations given. For the sake of agreement, it is assumed that $\phi_{\check{c}} = 30^\circ$, and that the flow in a small region immediately preceding $\check{c}$ corresponds to $\phi_{\check{c}}$.

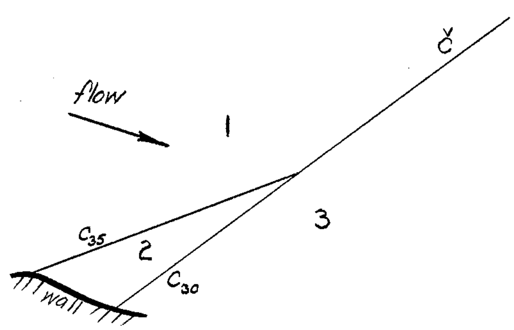

Figure 4-41

Remainder of Pattern, Lower Wall

$\Theta_{s,\check{c}} = 5^\circ$ under this assumption. e_{30} and $\check{c}$ are of indeterminate length.

Next to be examined is the remainder of the pattern along the upper wall. e_{50} is the last upper-wall characteristic. Instead of the standard turning of 5 degrees through each of the e_ϕ , $\Theta_{s,e_{50}} = 1^\circ\ 46'$, since $\phi = 51^\circ\ 46'$ past e_{50} . This configuration is shown in Figure 4-42.

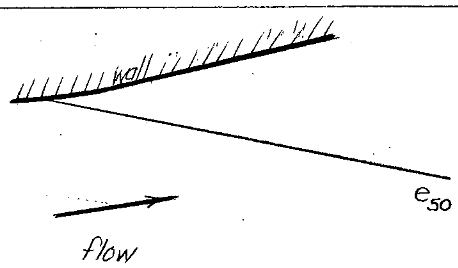

Figure 4-42

e_{50} , Upper Wall

The new center pattern may be examined now. The method and terminology are nearly identical to those used for the analysis of the first channel. The pattern of Figure 4-43 is

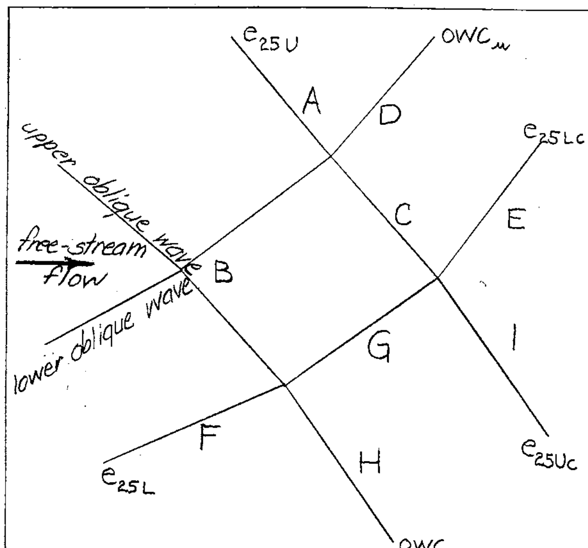

Figure 4-43

Center Pattern

assumed in the center region. Three identities must hold in the $\mathcal{R}$'s:

1) $\overline{\delta}_C \equiv \overline{\delta}_D$,

2) $\overline{\delta}_G \equiv \overline{\delta}_H$,

3) $\overline{\delta}_E \equiv \overline{\delta}_I$.

The turning powers of the waves are:

$\delta_{owc_u} = 1^\circ \downarrow$,

$\delta_{owc_\ell} = 1^\circ \uparrow$,

$\delta_{e_{25U}} = \delta_{e_{25Uc}} = 9^\circ\ 28' \downarrow$,

$\delta_{e_{25L}} = \delta_{e_{25Lc}} = 3^\circ\ 07' \uparrow$.

Table 4-6 shows the results of applying these relations to the pattern of Figure 4-43, with the exception of $\delta_{e_{25U}} = \delta_{e_{25Uc}}$ and $\delta_{e_{25L}} = \delta_{e_{25Lc}}$. These quantities are found by locating all possible $\overline{\delta}$'s with the aid of

Table 4-6

Center Pattern Flow Directions			
$\mathcal{R}$	$\overline{\delta}$	$\mathcal{R}$	$\overline{\delta}$
A	$10^\circ\ 28'$ $\downarrow$	F	$4^\circ\ 07'$ $\uparrow$
B	0° —	G	$3^\circ\ 07'$ $\uparrow$
C	$9^\circ\ 28'$ $\downarrow$	H	$3^\circ\ 07'$ $\uparrow$
D	$9^\circ\ 28'$ $\downarrow$	I	$6^\circ\ 21'$ $\downarrow$
E	$6^\circ\ 21'$ $\downarrow$		

the known δ's, from which the unknown δ's may be derived. When these are known, the remaining unknown $\overline{\delta}$'s may be computed. Immediately downstream of the center pattern, the flow direction is equal to $\overline{\delta}_E \equiv \overline{\delta}_I = 6^\circ\ 21' \downarrow$. For reasons given previously, neither the e_ϕ , nor the c_ϕ , nor their combinations make the proper θ_w's with their respective flow directions. All other flow quantities are assumed correctly.

To reduce the work required to analyze the interference pattern of the waves issuing from the center region with the downstream members of both families of characteristics, a simplification is introduced. The single wave ζ is substituted for the two waves owc_{l} and e_{25Lc}. Similarly, ξ is the substitution wave for the two waves owc_{u} and e_{25Uc}. The modified center pattern appears in Figure 4-44. A necessary condition for establishing the two substitute waves is that $\Theta_{W} > \delta$. Both ζ and ξ fulfill this requirement. Then, the sufficient condition for the establishment of the waves is that $\phi_{E} \geq 0$, and $\phi_{I} \geq 0$. This condition must be checked for each wave.

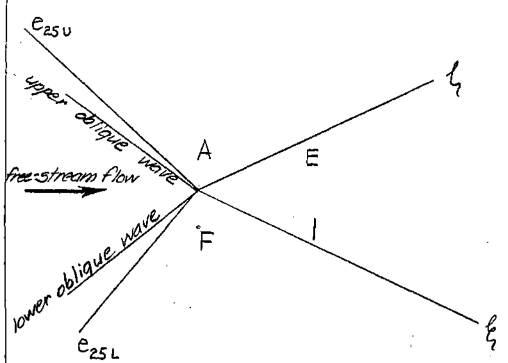

Figure 4-44

Modified Center Pattern

$$\phi_{E} = \phi_{A} - \delta_{\zeta} = 30^{\circ} - 4^{\circ}\ 07' = 25^{\circ}\ 53' \quad .$$

Hence, the wave ζ is established.

$$\phi_{I} = \phi_{F} - \delta_{\xi} = 30^{\circ} - 10^{\circ}\ 28' = 19^{\circ}\ 32' \quad .$$

Hence, the wave ξ is established.

The flow past the center region must be such that the flow directions and static pressures are matched. Let

$$\Delta\phi_{E-I} = \phi_{E} - \phi_{I} = 25^{\circ}\ 53' - 19^{\circ}\ 32' = 6^{\circ}\ 21' \quad .$$

The existence of a pair of waves, $\check{c}$ and $\check{e}$, is assumed, as shown in Figure 4-45. Each is assigned a turning power equal to $\frac{1}{2}\Delta\phi_{E-I}$; that is,

$$\delta_{\check{c}} = 3^{\circ}\ 10.5' \uparrow \ ,$$

$$\delta_{\check{e}} = 3^{\circ}\ 10.5' \uparrow \ .$$

δ_{ζ} and δ_{ξ} do not change value. Then,

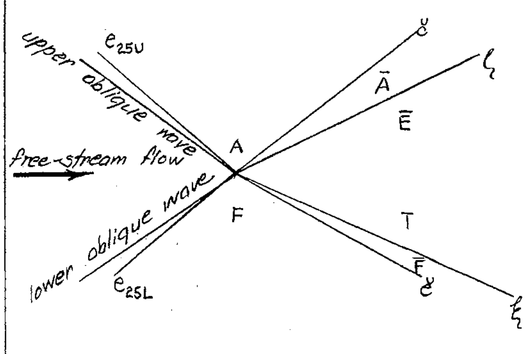

Figure 4-45

Corrected Modified Center Pattern

$$\Phi_{\bar{E}} = \Phi_A - \delta_{\check{c}} - \delta_{\zeta} \quad ,$$
$$\Phi_{\bar{E}} = 30^\circ - 3^\circ\ 10.5' - 4^\circ\ 07' \quad ,$$
$$\Phi_{\bar{E}} = 22^\circ\ 42.5' \quad ;$$
$$\Phi_{\bar{I}} = \Phi_F + \delta_{\check{c}} - \delta_{\xi} \quad ,$$
$$\Phi_{\bar{I}} = 30^\circ + 3^\circ\ 10.5' - 10^\circ\ 28.5' ,$$
$$\Phi_{\bar{I}} = 22^\circ\ 42.5' \quad .$$

Since $\Phi_{\bar{E}} = \Phi_{\bar{I}}$, static pressures past the center pattern are matched, as required. The new $\bar{\delta}$'s are found with the use of the computed values of δ , and are given in Table 4-7.

Table 4-7

Center Pattern Flow Directions (Pressures matched)		
$\mathcal{R}$	$\bar{\delta}$	
A	$10^\circ\ 28'$	↓
$\bar{A}$	$7^\circ\ 17.5'$	↓
F	$4^\circ\ 07'$	↑
$\bar{F}$	$7^\circ\ 17.5'$	↑
$\bar{E}$	$3^\circ\ 10.5'$	↓
$\bar{I}$	$3^\circ\ 10.5'$	↓

For further simplification, a wave χ is substituted for the two waves $\check{c}$ and ζ . The final center pattern is shown in Figure 4-46. The flow directions of Table 4-7 remain unchanged. For the purpose of visualization, subregion $\bar{A}$ becomes infinitesimally small.

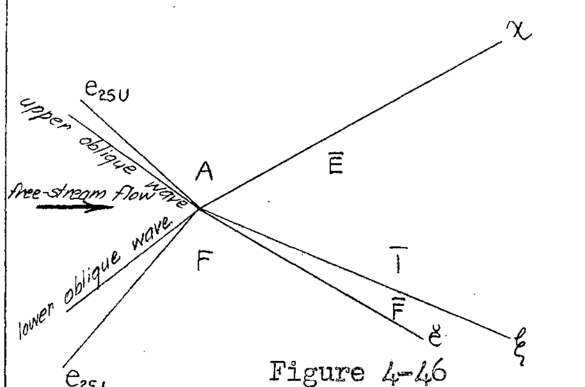

Figure 4-46

Final Center Pattern

The intersection pattern of the e_ϕ originating from the upper wall and the wave χ is located next. For each of these e_ϕ , $\delta = 5^\circ$, from which the flow directions are obtained, as shown in Figure 4-47. Let $\bar{\theta}_{w,(\ )}$ be the angle between the wave segment indicated by the second subscript and the free-stream flow direction. Values of $\bar{\Theta}_{w,(\ )}$ are obtained by adding or subtracting the value of $\bar{\delta}$ preceding each wave

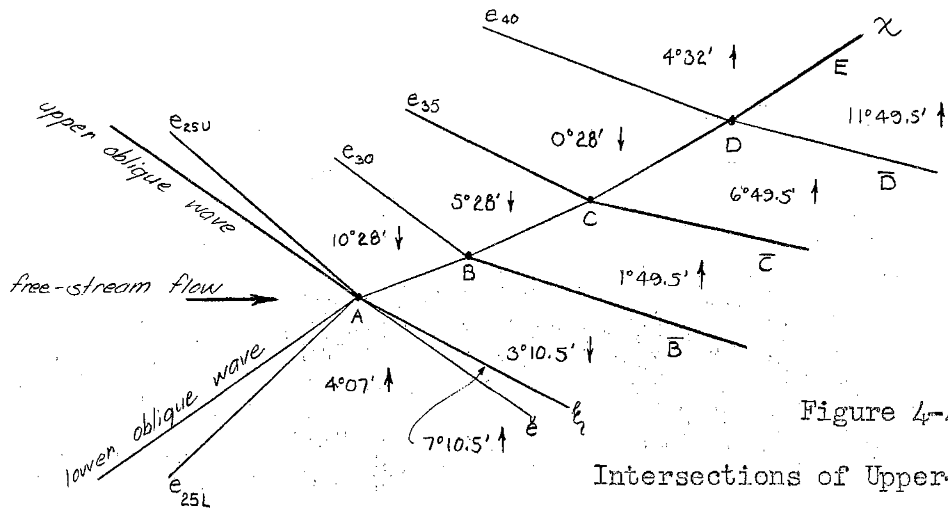

Figure 4-47

Intersections of Upper-Wall e_ϕ and the Wave χ

segment, as necessary. The results appear in Table 4-8.

Table 4-8

Values of $\bar{\Theta}_{w,(\ )}$ for Wave Segments of Figure 4-47					
Wave Segment	ϕ	$\Theta_{w,(\ )}$ Chart 2-11[25]	$\bar{\delta}$	$\bar{\Theta}_{w,(\ )}$	tan $\bar{\Theta}_{w,(\ )}$
AB	30°	27° 48'	10° 28' ↓	17° 20'	0.312
BC	35°	25° 18'	5° 28' ↓	19° 50'	0.361
CD	40°	23° 12'	0° 28' ↓	22° 44'	0.419
DE	45°	21° 12'	4° 32' ↑	25° 44'	0.482
$\breve{\xi}$	30°	27° 48'	4° 07' ↑	23° 41'	0.439
ξ	33° 10.5'	26° 18'	7° 10.5' ↑	19° 00.5'	0.344
$B\bar{B}$	22° 42.5'	32° 20'	3° 10.5' ↓	35° 30.5'	0.714
$C\bar{C}$	27° 42.5'	29° 15'	1° 49.5' ↑	27° 25.5'	0.519
$D\bar{D}$	32° 42.5'	26° 30'	6° 49.5' ↑	19° 40.5'	0.358

A similar analysis is made for the pattern of Figure 4-48. The results appear in Table 4-9. It is necessary to check for agreement between the local values of $\bar{\delta}$ and ϕ. e_{30} cannot cross ξ, since the

---

25 Ibid.

nose wave of the upper wall is a component of ξ , and the disturbance of e_{30} cannot communicate itself upstream across the nose wave. The pro-

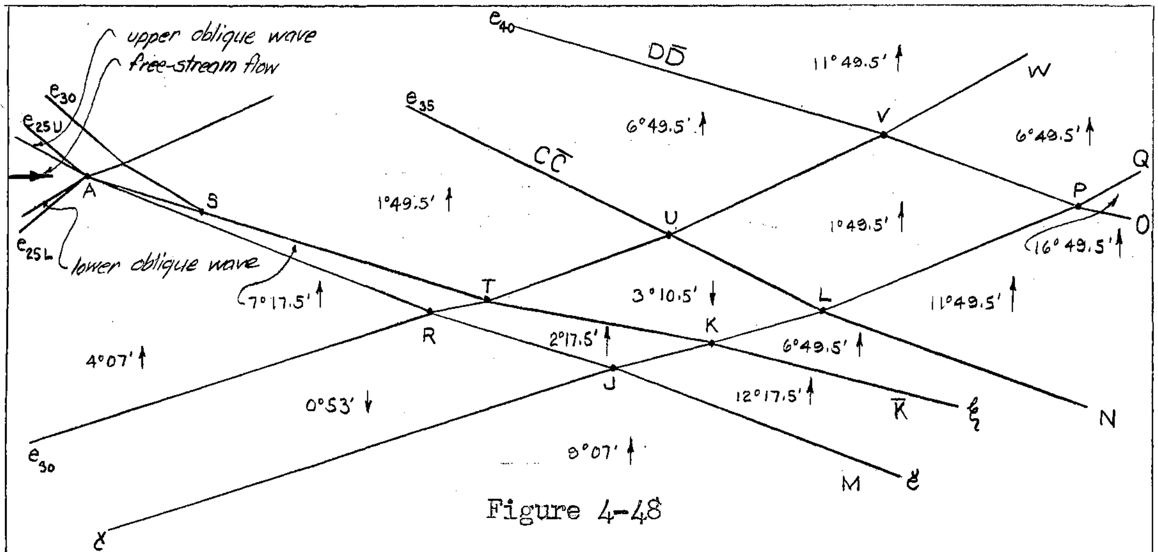

Figure 4-48

Lower Portion of Downstream Wave Pattern

Table 4-9

Values of $\bar{\theta}_{w,(\ )}$ for Wave Segments of Figure 4-48

Wave Segment	ϕ	$\theta_{w,(\ )}$ Chart 2-11[26]	$\bar{\delta}$	$\bar{\theta}_{w,(\ )}$	tan $\bar{\theta}_{w,(\ )}$
RJ	35°	25° 18'	0° 53' ↓	26° 11'	0.492
JM	25°	30° 42'	9° 07' ↑	21° 35'	0.396
T$\bar{K}$	38° 10.5'	24°	2° 17.5' ↑	21° 42.5'	0.398
KK	28° 10.5'	28° 48'	12° 17.5' ↑	16° 30.5'	0.296
RT	33° 10.5'	26° 18'	7° 17.5' ↑	33° 35.5'	0.664
TU	27° 42.5'	29° 15'	1° 49.5' ↑	31° 04.5'	0.603
UV	32° 42.5'	26° 30'	6° 49.5' ↑	33° 19.5'	0.658
VW	37° 42.5'	24° 12'	11° 49.5' ↑	36° 01.5'	0.727
JK	38° 10.5'	24°	2° 17.5' ↑	26° 17.5'	0.494
KL	32° 42.5'	26° 30'	3° 10.5' ↓	23° 19.5'	0.431
LP	37° 42.5'	24° 12'	1° 49.5' ↑	26° 01.5'	0.488
PQ	42° 42.5'	22° 10'	6° 49.5' ↑	28° 59.5'	0.554
UL	32° 42.5'	26° 30'	3° 10.5' ↓	29° 40.5'	0.570
LN	22° 42.5'	32° 20'	6° 49.5' ↑	25° 30.5'	0.477
VP	37° 42.5'	24° 12'	1° 49.5' ↑	22° 22.5'	0.412
PO	27° 42.5'	29° 15'	11° 49.5' ↑	17° 25.5'	0.314

26 Ibid.

cess of checking the matching of the $\bar{\delta}$'s is identical to that using the $\bar{\delta}$ identities in the analyses of the center patterns. For the dummy pattern of Figure 4-49, the following relations must hold:

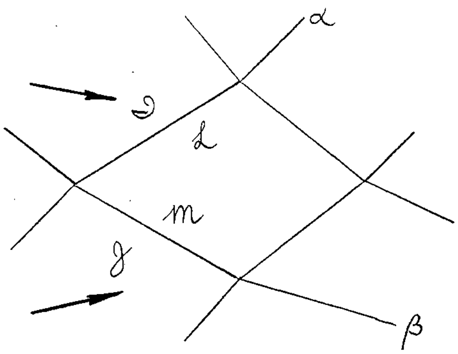

Figure 4-49

Typical Subregion of Figure 4-48

1) $\bar{\delta}_{\ell} \equiv \bar{\delta}_{m}$,

2) $\phi_{\ell} \equiv \phi_{m}$, where

$\phi_{\ell} = \phi_{\vartheta} \pm \delta_{\alpha}$,

and $\phi_{m} = \phi_{\gamma} \pm \delta_{\beta}$,

where the sign is + when the wave is an e_{ϕ} , and - when the wave is a c_{ϕ} . It is not necessary to reproduce the substitution computations for the subregions which are in agreement with these relations.

The three subregions downstream of the segment of ξ beginning at S, however, do not at first satisfy the relations. $\delta = 10^{\circ}\ 28' \downarrow$ holds for the segment AS of ξ . The continuation of ξ past S is assigned the turning $\delta = 5^{\circ}\ 28' \downarrow$. The slopes of the segments ST, TK, and $K\bar{K}$ of the continuation are unchanged, since they are fixed by their respective upstream flows. The continuation $STK\bar{K}$ is a substitute wave for two waves; ξ and an expansion wave originating at S which has the effect of making $\delta_{\xi} > \delta_{STK\bar{K}} = 5^{\circ}\ 28' \downarrow$. The assumption of the substitute wave produces the desired holding of the relations for the three subregions downstream of the segment of ξ beginning at S. In the computation of the quantities of Table 4-9, the matching of $\bar{\delta}$'s and ϕ 's in each subregion was assumed. The assumption of the substitute wave $STK\bar{K}$ serves as a physical explanation which justifies the first assumption for the three subregions examined last. Hence, all waves necessary for the computation of the flow at channel exit are located.

4 Channel-Exit Region

The exit pattern appears in Figure 4-50. The dashed line represents the exit control surface, which passes through the trailing edges of the profiles. The upstream control surface is parallel to the exit surface, and is drawn between stagnation streamlines (which coincide with respective leading-edge radius lines) an arbitrarily small distance ahead of the detached shock. The interior stagnation streamlines between upstream and exit control surfaces define the lateral control surfaces of the channel.

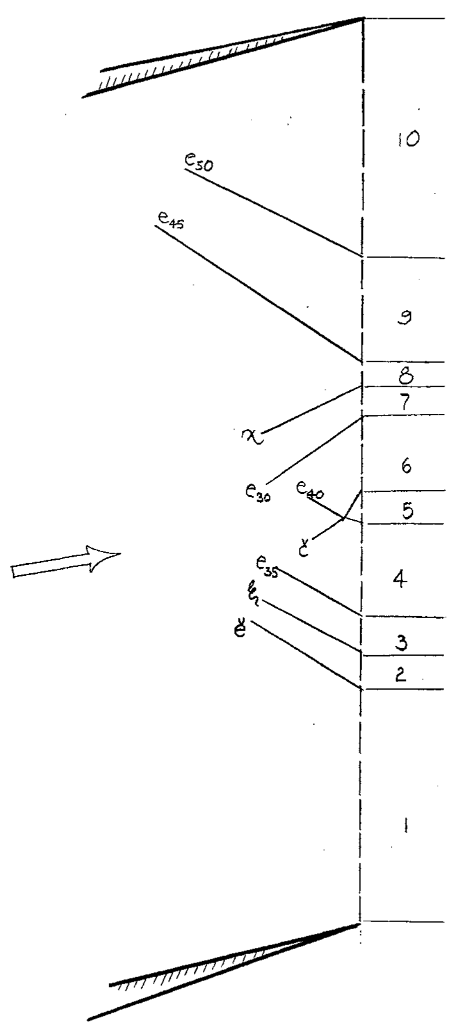

Figure 4-50

Channel-Exit Pattern

All flow quantities at the entrance of the channel are known. It is necessary to compute the distribution of static pressures and momenta at channel exit in order to find the forces which the flow exerts upon the channel walls. Pertinent quantities which have been computed already are assembled conveniently in Table 4-10.

At Standard Sea Level, the mass density, ρ_{s0}, of air is 0.002378 slugs /cf, and the corresponding weight density, γ_{s0}, equals 0.07651 lbs/cf. Since the free-stream Mach number is rather high, channel entrance conditions corresponding to an altitude of

Table 4-10

Flow Direction, Expansion Angle, and Mach Number at Channel Exit			
Station	$\bar{\delta}$	ϕ	M Chart 2-11[27]
1	9° 07'	25°	1.950
2	12° 17.5'	28° 10.5'	2.067
3	6° 49.5'	22° 42.5'	1.870
4	11° 49.5'	27° 42.5'	2.055
5	16° 49.5'	32° 42.5'	2.246
6	6° 49.5'	42° 42.5'	2.660
7	11° 49.5'	37° 42.5'	2.445
8	4° 32'	45°	2.765
9	9° 32'	50°	3.014
10	11° 18'	51° 46'	3.109

20,000 ft, Standard Atmosphere are selected. The subscript 0 refers to Standard Sea Level conditions, and the subscript s to stagnation conditions. Let a_s equal the local acoustic velocity, fps, and T_s equal the absolute temperature, degrees R. At channel entrance,

$$\frac{\rho_s}{\rho_{s0}} = 0.5327 \quad ,$$

$$\frac{P_s}{P_{s0}} = 0.4593 \quad ,$$

$$T_s = 447.7° \text{ R},$$

$$a_s = 1040 \text{ fps.}$$ [28]

$$\rho_s = \rho_{s0} \frac{\rho_s}{\rho_{s0}} = 0.002378(0.5327) = 0.001268 \text{ slugs/cf} \quad ,$$

27 Ibid.

28 M. J. Zucrow, Principles of Jet Propulsion and Gas Turbines, p. 34.

$$P_s = P_{s0}\frac{P_s}{P_{s0}} = 14.7(0.4593) = 6.75 \text{ psia} \quad .$$

Tables 4-11 and 4-12 contain the flow conditions at channel entrance and at the ten stations of the channel exit. The columns of figures are numbered continuously throughout the two tables. Let

ρ = local mass density, slugs/cf;

a = local acoustic velocity, fps;

$V = Ma$ = local flow velocity, fps;

A = local station area, sq. in. = (station width, in.)(1 in.), since blade height = 1 in.;

α = angle between local flow direction and outward normal to control surface, degrees;

$V_n = V \cos\alpha$ = velocity component normal to control surface, fps;

$V_x = V_n$ = velocity component along x-axis, fps, since x-axis is parallel to normal to control surface;

$V_y = V \sin\alpha$ = velocity component along y-axis, fps, since y-axis is parallel to control surface;

$A_x = 0$ sq. in., by choice of axes, = component of control surface segment A parallel to x-axis, sq. in.;

$A_y = A$ = component of control surface segment A parallel to y-axis, sq. in., since control surface is parallel to y-axis.

Then, the values of the entries for a given station are obtained by the scheme which follows on the next two pages.

The data of Tables 4-11 and 4-12 permit the computation of the forces which the flow exerts upon the walls of the channel. The channel configuration has been described already, and is shown in Figure 4-51.

	(A)	(B)	(C)	(D)
Entry in Column	Obtained by Reading	At Value of	(And) Multi-plying	By
1	Chart 1-1[29]	M, Table 4-10[30]	———	———
2	Column 1	———	$P_s = 6.75$	1/(A)
3	Chart 1-2[29]	M, Table 4-10[30]	———	———
4	Column 3	———	$\rho_s = 0.001268$	1/(A)
5	Chart 1-4[29]	M, Table 4-10[30]	———	———
6	Column 5	———	$a_s = 1040$	1/(A)
7	Column 6	———	M, Table 4-10[30]	(A)
8	Station Length on Scale D'wng.	———	———	———
9	Angle between $\bar{\delta}$, Table 4-10[30] and outw. normal to contr. surface	———	———	———
10	Trig. Tables	Column 9	———	———
11	Trig. Tables	Column 9	———	———
12	———	———	Column 7	Column 10
13	———	———	Column 12	Itself

---

29 C. L. Dailey and F. C. Wood, <u>ibid</u>.

30 P. 51.

Entry in Column	(A) Obtained by Reading	(B) At Value of	(C) (And) Multiplying	(D) By
14	----	----	Column 7	Column 11
15	----	----	Column 4	Column 8
16	----	----	Column 15	Column 13
17	----	----	Product of Col. 15 and Col. 12	Column 14
18	----	----	Column 2	Column 8

The y-axis coincides with the exit control surface, and the origin with the trailing edge of the lower profile. The results sought are the components of the forces along the axes. Let n_1 be the outward normal to the entrance control surface, and n_2 the outward normal to the exit control surface. Then, the acute angle between n_1 and the free-stream velocity upstream equals $3^\circ\ 50'$. Since all $\overline{\delta}$'s are referred to the direction of the free-stream velocity upstream, the entries of column 9 may be obtained by computation.

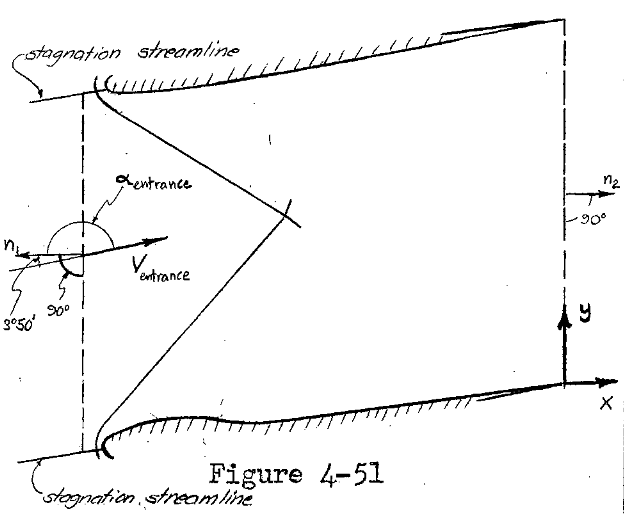

Figure 4-51

Location of Axes of Modified Blunt-Nosed Profile Channel

$\alpha_{entrance}$ equals $180^\circ - 3^\circ\ 50'$. Since the $\overline{\delta}$'s of the exit stations all have the postscript $\uparrow$, the value of α for any exit station equals $\overline{\delta}_i + 3^\circ\ 50'$, where i = exit station number. Let Σ indicate a summation

Table 4-11

Channel-Entrance and -Exit Distributions, Part 1 of 2 Parts									
	1	2	3	4	5	6	7	8	9
Station	P_s/P	P	ρ_s/ρ	ρ $\times 10^4$	$\sqrt{T_s/T}$	a	V	$A = A_y$	α
Entrance	4.94	1.367	3.125	4.060	1.257	828	1408	1.6000	176° 10'
1	7.27	0.928	4.1	3.095	1.327	784	1530	0.2750	12° 57'
2	8.70	0.776	4.67	2.717	1.362	764	1580	0.0670	16° 07.5'
3	6.40	1.056	3.76	3.375	1.304	797	1490	0.0404	10° 39.5'
4	8.55	0.790	4.625	2.742	1.358	766	1573	0.2490	15° 39.5'
5	11.50	0.587	5.72	2.217	1.417	734	1649	0.0096	20° 39.5'
6	21.8	0.3097	9.05	1.402	1.555	668	1778	0.1452	10° 39.5'
7	15.6	0.433	7.14	1.776	1.482	702	1718	0.0788	15° 39.5'
8	25.7	0.2625	10.16	1.250	1.591	654	1810	0.0260	8° 22'
9	37.5	0.180	13.23	0.958	1.678	620	1869	0.1970	13° 22'
10	43.2	0.1563	14.70	0.863	1.712	607	1888	0.5120	15° 08'

Table 4-12

Channel-Entrance and -Exit Distributions, Part 2 of 2 Parts

Station	10	11	12	13	14	15	16	17	18
	$\cos\alpha$	$\sin\alpha$	$V_n = V_x$	V_n^2 $\times 10^{-6}$	V_y	ρA_y $\times 10^4$	ρAV_n^2 $= \rho A_y V_n V_x$	ρAV_nV_y	PA_y
Entrance	-0.998	0.067	-1405	1.975	94.4	6.49	-1283.	-86.1	2.185
1	0.975	0.224	1492	2.224	342.8	0.851	189.3	43.5	0.255
2	0.961	0.278	1518	2.304	439.	0.182	42.0	12.14	0.052
3	0.983	0.185	1465	2.146	275.7	0.1363	29.28	5.51	0.04265
4	0.963	0.270	1516	2.297	425.	0.683	156.8	44.0	0.1942
5	0.936	0.353	1543	2.383	582.	0.02125	5.08	1.912	0.00564
6	0.983	0.185	1748	3.057	329.	0.2036	62.2	11.71	0.0449
7	0.963	0.270	1655	2.740	464.	0.1399	38.32	10.76	0.0341
8	0.989	0.146	1791	3.205	264.2	0.0325	10.43	1.538	0.00683
9	0.973	0.231	1819	3.305	431.5	0.1888	62.4	14.82	0.03545
10	0.965	0.261	1822	3.320	493.	0.442	146.7	39.67	0.0801

of terms, and let

$\mathcal{M}_{x,entrance}$ = x-component of momentum at entrance, lbs(114);

$\mathcal{M}_{x,exit}$ = x-component of momentum at exit, lbs(114);

$\Delta\mathcal{M}_x$ = x-component of change of momentum, lbs(144).

The analogous terms along the y-axis are obtained by substituting y for x in the subscripts and definitions.

$$\mathcal{M}_{x,entrance} = \left[\rho A_y V_n V_x\right]_{entrance} \quad ,$$

$$\mathcal{M}_{x,exit} = \sum_{i=1}^{10} \left[\rho A_y V_n V_x\right]_i \quad , \text{ i = exit station number,}$$

$$\Delta\mathcal{M}_x = \mathcal{M}_{x,entrance} - \mathcal{M}_{x,exit} \quad .$$

Let $F_{\Delta\mathcal{M}_x}$ force due to $\Delta\mathcal{M}_x$, lbs. Then,

$$\Delta\mathcal{M}_x = 1283 - 742.5 = 540.5 \text{ lbs(114)} \quad ,$$

$$F_{\Delta\mathcal{M}_x} = \frac{1}{144}(540.5) = 3.75 \text{ lbs} \quad .$$

Let $\mathcal{P}_{x,entrance}$ = x-component of force due to static pressure at entrance, lbs;

$\mathcal{P}_{x,exit}$ = x-component of force due to static pressure at exit, lbs;

$F_{\mathcal{P}_x}$ = x-component of net force due to static pressure, lbs;

F_x = x-component of total force, lbs.

$$\mathcal{P}_{x,entrance} = \left[PA_y\right]_{entrance} = 2.185 \text{ lbs} \quad ,$$

$$\mathcal{P}_{x,exit} = \sum_{i=1}^{10}\left[PA_y\right]_i = 0.751 \text{ lbs, i = exit station number,}$$

$$F_{\mathcal{P}_x} = \mathcal{P}_{x,entrance} - \mathcal{P}_{x,exit} = 2.185 - 0.751 \quad ,$$

$$F_{\mathcal{P}_x} = 1.434 \text{ lbs} \quad ,$$

$$F_x = F_{\Delta\mathcal{M}_x} - F_{\mathcal{P}_x} = 3.75 - 1.434 = 2.316 \text{ lbs} \quad .$$

$$\mathcal{M}_{y,\text{entrance}} = \left[\rho A V_n V_y\right]_{\text{entrance}} = 86.1 \text{ lbs}(144) \quad ,$$

$$\mathcal{M}_{y,\text{exit}} = \sum_{i=1}^{10} \left[\rho A V_n V_y\right]_i = 185.6 \text{ lbs}(144) \quad ,$$

$$\Delta\mathcal{M}_y = \mathcal{M}_{y,\text{exit}} - \mathcal{M}_{y,\text{entrance}} = 185.6 - 86.1 \quad ,$$

$$\Delta\mathcal{M}_y = 99.5 \text{ lbs}(144) \quad ,$$

$$F_{\Delta\mathcal{M}_y} = \frac{1}{144}\Delta\mathcal{M}_y = \frac{1}{144} 99.5 = 0.691 \text{ lbs} \quad ;$$

$$F_y = F_{\Delta\mathcal{M}_y} = 0.691 \text{ lbs} \quad ,$$

since the choice of axes forces the x-components of the entrance and exit control surface areas to be zero, which forces the y-components of forces due to static pressures to be zero. F_x is the axial thrust per channel, and F_y the torque-force per channel of the cascade. Figure 4-52 shows the directions of all forces with respect to the axes.

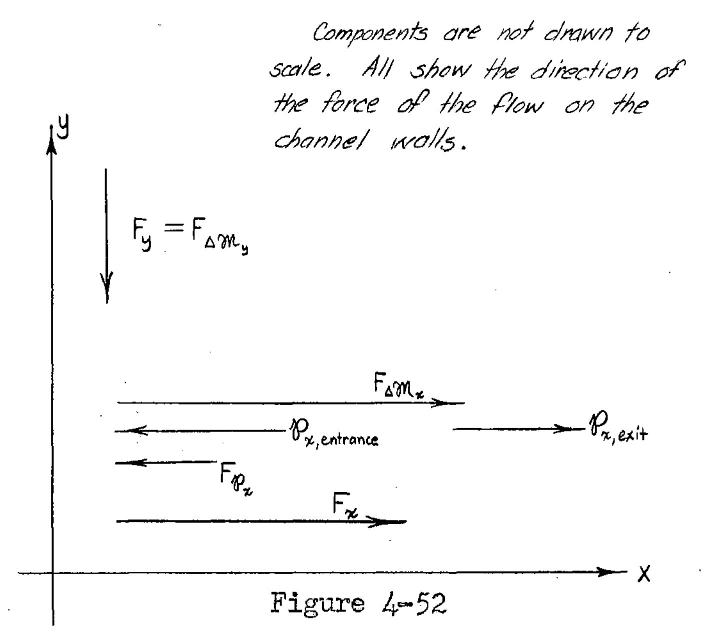

Figure 4-52

Force Components for Channel in Cascade of Second Modification of Blunt-Nosed Profiles

C Cascade of Sharp-Nosed Profiles

1 Profile and Channel Layout

Most of the profile has been designed already in part B of this chapter. For the sake of convenience, the parts already selected are shown in Figure 4-53. The portion left incomplete is the semi-ogive on the lower nose arc of the profile. A semi-wedge angle of 14 degrees is selected for the initial section of the semi-ogive. A smooth connection curve is drawn, replacing the corner made by the intersection of the semi-wedge line and the original nose outline. The layout is complete now, and the new nose, or leading edge appears as shown in Figure 4-54.

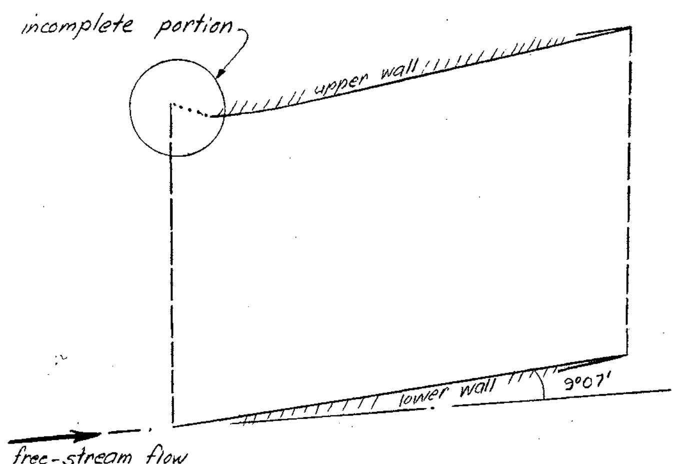

Figure 4-53

Layout of Channel of Sharp-Nosed Profiles (Incomplete)

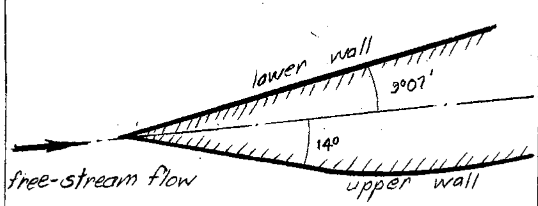

Figure 4-54

Nose Region of Sharp-Nosed Profile

2 Nose Region

The nose portion of the lower channel wall is a semi-wedge. The initial flow preceding the leading edge is identical to that of the first two profiles analyzed. Hence, at the lower wall, $\bar{\delta} = \delta = 9^\circ\ 07'$. A weak oblique shock wave is caused by the semi-wedge. The shock is a straight wave, originating at the wedge point, and intersecting the attached nose wave originating at the entrance point of the upper channel wall.

Most of the symbols used in the remainder of this chapter already have been defined. Additional quantities shall be introduced and defined as needed. Let

OWL = oblique wave originating at lower channel wall entrance,

OWU = oblique wave originating at upper channel wall entrance.

For the wave OWL, $\theta_w = 46^\circ$, Chart 2-1[31].

Past the wave, $M = 1.376$, Chart 2-7[31];

$\phi = 8^\circ\ 15'$, Chart 2-11[31].

For the wave OWU, $\theta_w = 53^\circ\ 50'$, Chart 2-1[31].

Immediately past the wave, $M = 1.175$, Chart 2-7[31];

$\phi = 3^\circ$, Chart 2-11[31].

Figure 4-55 shows the initial segments of both OWL and OWU. Following

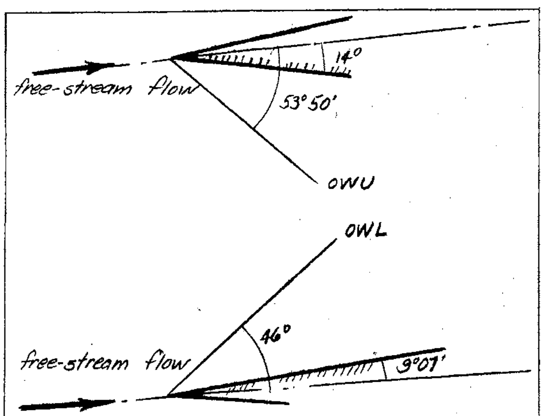

Figure 4-55

Initial Segments of OWL and OWU

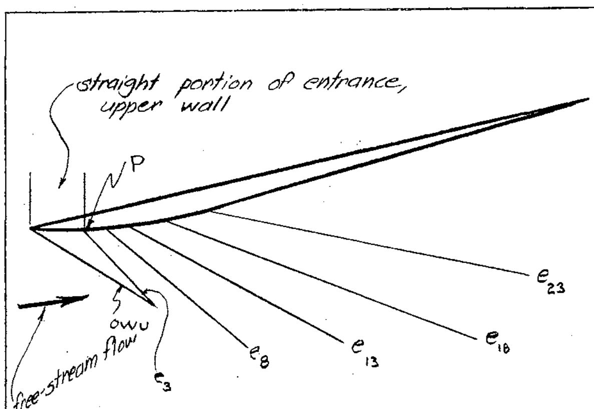

Figure 4-56

Flow Along Upper Wall

the straight portion of the initial segment of the upper channel wall is a circular-arc convex transition section, which is in turn followed by

31 C. L. Dailey and F. C. Wood, <u>ibid</u>.

a long portion of straight wall. This appears in Figure 4-56.

The turning along the convex portion of the upper wall is from $14^\circ\downarrow$ to $11^\circ\ 18'\uparrow$, with respect to the free-stream flow direction. Hence, the turning equals $25^\circ\ 18'$. At P, $\phi = 3^\circ$. Therefore, ϕ corresponding to the turning past the curved portion equals $3^\circ + 25^\circ\ 18' = 28^\circ\ 18'$. Since the wall remains straight, this is also ϕ_{exit} at the wall, unless a wave from the opposite wall is reflected at the upper wall.

Five expansion characteristics are used, with the first one originating at P. The first four of these e_ϕ are assigned respective $\Delta\phi = \delta = 5^\circ$. The last e_ϕ is assigned $\Delta\phi = \delta = 5^\circ\ 18'$. Table 4-13 presents the layout quantities for the upper-wall characteristics.

Table 4-13

e_ϕ Along Upper Wall of Sharp-Nosed Profile Channel							
Char.	ϕ	$\Delta\phi$	θ_w	$\bar{\delta}$	tan $\bar{\delta}$	$\bar{\theta}_w$	tan $\bar{\theta}_w$
			Chart 2-11[32]				
e_3	3°	5°	$58^\circ\ 24'$	$14^\circ\downarrow$	0.249	$72^\circ\ 24'$	3.152
e_8	8°	5°	$47^\circ\ 12'$	$9^\circ\downarrow$	0.158	$56^\circ\ 12'$	1.494
e_{13}	13°	5°	$40^\circ\ 40'$	$4^\circ\downarrow$	0.070	$44^\circ\ 40'$	0.988
e_{18}	18°	5°	$35^\circ\ 50'$	$1^\circ\uparrow$	0.017	$34^\circ\ 50'$	0.696
e_{23}	23°	$5^\circ\ 18'$	$32^\circ\ 10'$	$6^\circ\uparrow$	0.105	$26^\circ\ 10'$	0.491

The shape of the remainder of OWU remains to be determined. Let

R_w = radius of curvature of the ogive portion of the wall, in.;

$K_w = \frac{1}{R_w}$ = curvature of ogive portion of wall, $\frac{1}{\text{in.}}$;

32 Ibid.

R_s = radius of curvature of attached nose shock, in.;

$K_s = \frac{1}{R_s}$ = curvature of attached nose shock, $\frac{1}{\text{in.}}$.

The distances are measured on the layout pattern (see appendix), which has a scale ratio of 10 to 1.

At a free-stream M of 1.7, and with a semi-wedge angle of 14 degrees,

$$\frac{K_s}{K_w} = 1.00\text{, by interpolation.}[33]$$

Hence,

$$R_s = R_w = 3.296 \text{ in.}$$

The curved portion of the nose shock begins at the point of intersection of e_3 and the initial segment of OWU, and ends when the local $\theta_w = 36°$. From this point, OWU continues as a straight line, with $\theta_w = 36°$, until it intersects OWL. The straight outer portion of OWU is a Mach wave of zero turning power. The construction of the curved portion of OWU appears in Figure 4-57. It is reasonable to assume that the central angle of the circle arc which matches the ogive wall arc is approximately equal to the central angle of the circle arc forming the curved portion of OWU. By measurement,

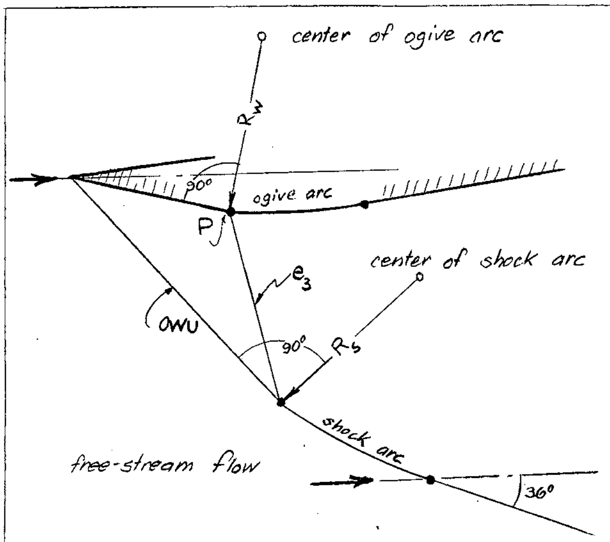

Figure 4-57

Construction of Curved Portion of OWU

(central angle, wall arc)

= 16° 42', and

---

33 M. M. Munk and R. C. Prim, "Surface-Pressure Gradient and Shock-Front Curvature at the Edge of a Plane Ogive with Attached Shock Front," Journal of the Aeronautical Sciences, XV (November, 1948), Fig. 4, 693.

(central angle, arc of curved portion of OWU) $= 17^\circ 50'$, which satisfies the assumption. If the angles are too greatly different, the cause-and-effect relation between the ogive wall and the curved portion of the shock fails.

The first three of the five e_ϕ are straight, and cease at their respective points of intersection with OWU. This behavior is confirmed by actual pictures of patterns of flow about lenticular airfoils.[34]

3 Downstream Region

The center pattern must be examined next. Again, the method and the terminology are nearly identical to those used for the analyses of the two previous channels. The pattern, as shown in Figure 4-58, is simpler than before. Past AB, the flow corresponds to $M = 1.7$, and $\phi = 17^\circ 45'$, Chart 2-11[35], Past e_{13}, $\phi = 18^\circ$, according to Table 4-13[36]. The two flows should match, and it is assumed that the flow past AB is identical to that behind e_{13}. The error due to this assumption is practically zero. The flow directions, or $\bar{\delta}$'s, are inscribed in each subregion. The computation of the quantities

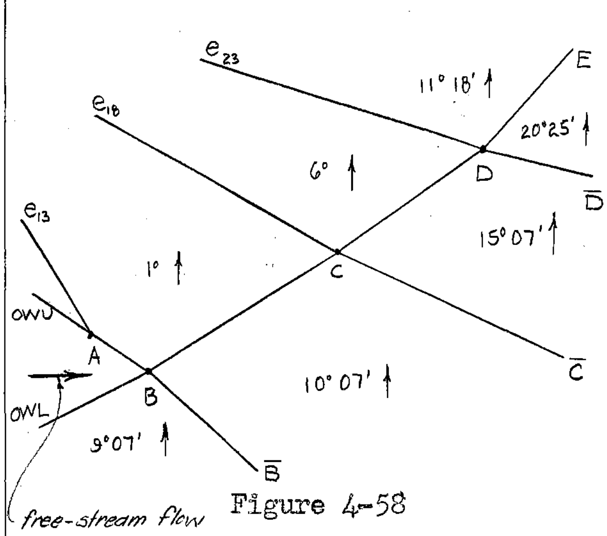

Figure 4-58

Center Pattern

34 Antonio Ferri, Elements of Aerodynamics of Supersonic Flows, Fig. 104, p. 152 and Fig. 105, p. 153.

35 C. L. Dailey and F. C. Wood, ibid.

36 P. 61.

required for the layout of the continuation of OWL is given in Table

Table 4-14

Continuation of OWL, Center Pattern, Sharp-Nosed Profile Channel						
Segment	ϕ	M Chart 2-11[37]	θ_w Chart 2-1[37]	$\bar{\delta}$	$\bar{\theta}_w$	$\tan \bar{\theta}_w$
BC	18°	1.705	$45^\circ\ 45'$	1° ↑	$46^\circ\ 45'$	1.063
CD	23°	1.88	41°	6° ↑	47°	1.072
DE	$28^\circ\ 18'$	2.072	37°	$11^\circ\ 18'$ ↑	$48^\circ\ 18'$	1.122

4-14. $\overline{BB}$ is the continuation of the Mach wave portion of OWU. $\overline{CC}$ and $\overline{DD}$ are continuations of e_{18} and e_{23}, respectively. The quantities required for the layout of these segments are computed and presented in Table 4-15.

Table 4-15

Continuations of OWU, e_{18}, and e_{23}; Center Pattern, Sharp-Nosed Profile Channel						
Segment	M	ϕ	θ_w	$\bar{\delta}$	$\bar{\theta}_w$	$\tan \bar{\theta}_w$
		← Chart 2-11[37] →				
$\overline{BB}$	1.376	$8^\circ\ 45'$	$46^\circ\ 45'$	$9^\circ\ 07'$ ↑	$37^\circ\ 38'$	0.771
$\overline{CC}$	1.376	$8^\circ\ 15'$	$46^\circ\ 45'$	$10^\circ\ 07'$ ↑	$36^\circ\ 38'$	0.744
$\overline{DD}$	not req.	$13^\circ\ 15'$	$40^\circ\ 20'$	$15^\circ\ 07'$ ↑	$25^\circ\ 13'$	0.471

The remainder of the channel pattern may be analyzed now. The continuation of the weak oblique shock OWL is reflected from the upper channel wall, as shown in Figure 4-59. The flow directions are noted in each subregion. EF is the reflected wave. The location of the wave segment DE, the flow direction, $\bar{\delta}$, preceding DE, and $\bar{\delta}$ past DE have been deter-

37 C. L. Dailey and F. C. Wood, *ibid*.

mined in the analysis of the center pattern. $\bar{\delta}$ past EF is prescribed by the wall direction; that is, the flow past EF must be parallel to the wall.

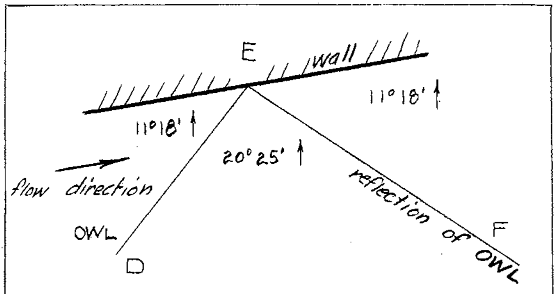

Figure 4-59

Reflection of OWL

$$\Phi_{EF} = \Phi_{D\bar{D}} + \delta_{\Theta_{23}} \quad ,$$
$$\Phi_{EF} = 13^\circ\ 15' + 5^\circ\ 18' = 18^\circ\ 33' ;$$
$$M_{EF} = 1.723, \text{ Chart 2-11}^{38} ;$$
$$\delta_{EF} = 9^\circ\ 07' ;$$
$$\Theta_{w,EF} = 45^\circ\ 15', \text{ Chart 2-1}^{38} ;$$
$$\bar{\Theta}_{w,EF} = \Theta_{w,EF} - \bar{\delta}_{EF} \quad ,$$
$$\bar{\Theta}_{w,EF} = 45^\circ\ 15' - 20^\circ\ 25' \quad ,$$
$$\bar{\Theta}_{w,EF} = 24^\circ\ 50' \quad ,$$
$$\tan \bar{\Theta}_{w,EF} = 0.463 \quad .$$

Past EF, $M = M_{II,EF}$.

$$M_{II,EF} = 1.405, \text{ Chart 2-7}^{38} \quad ,$$
$$\Phi_{II,EF} = 9^\circ\ 10', \text{ Chart 2-11}^{38} \quad .$$

The continuation of OWU, labeled $B\bar{B}$, is reflected from the lower wall. At the center pattern, the flow behind $B\bar{B}$, has $\bar{\delta} = 10^\circ\ 07' \uparrow$, but at the lower wall, $\bar{\delta}$ must equal $9^\circ\ 07' \uparrow$. An adjustment is necessary, and it is assumed that the transition between the two directions is smooth, takes place close to the center, and leaves most of the flow past $B\bar{B}$ at $\bar{\delta} = 9^\circ\ 07' \uparrow$. The reflection pattern appears in Figure 4-60. The flow

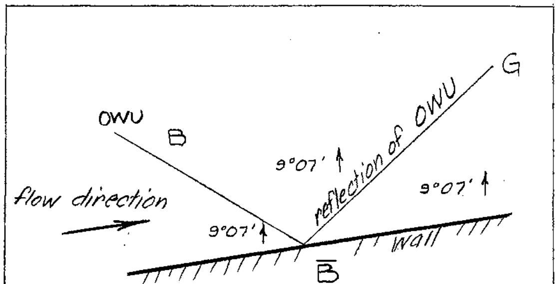

Figure 4-60

Reflection of OWU

through $B\bar{B}$ and the reflected wave $\bar{B}G$ does not change direction of condi-

---

38 Ibid.

tion.

$$M_{\overline{BG}} = M_{\overline{BB}} = 1.376, \text{ Table 4-15}^{39} ,$$
$$\phi_{\overline{BG}} = 8^{\circ}\ 15', \text{ Chart 2-11}^{40} ;$$

$$\underline{\theta}_{w,\overline{BG}} = 46^{\circ}\ 45', \text{ Chart 2·11}^{40} ,$$
$$\overline{\theta}_{w,\overline{BG}} = \underline{\theta}_{w,\overline{BG}} + \overline{\delta}_{\overline{BG}} = 46^{\circ}\ 45' + 9^{\circ}\ 07' = 55^{\circ}\ 52' ,$$
$$\cot \overline{\theta}_{w,\overline{BG}} = 0.678 .$$

As stated previously, ϕ, M, and other flow quantities past $\overline{BG}$ are the same as ahead of $\overline{BG}$.

4 Channel-Exit Region

The analysis of this section closely parallels that of Section 4, Part B of this chapter. Figure 4-61 displays the exit pattern. The exit control surface, indicated by the dashed line, passes between the trailing edges of the two adjacent profiles. The inlet control surface is parallel to the exit surface, and passes between the leading edges of the two adjacent profiles. The lateral control surfaces of the channel are formed by the interior stagnation streamlines between the inlet and the exit control surfaces.

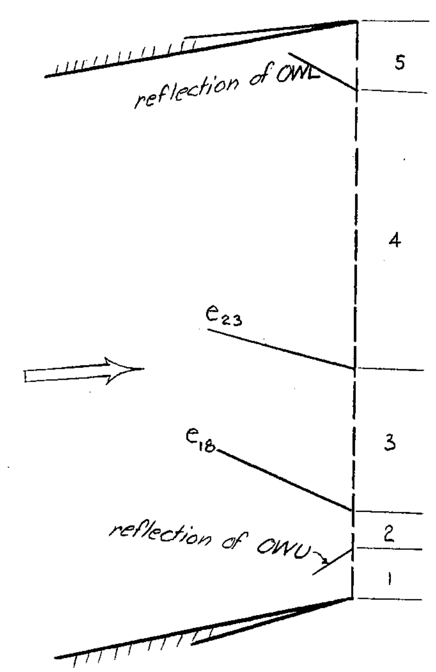

Figure 4-61

Channel-Exit Pattern

All flow quantities at channel entrance are known. In order to find the

---

39 P. 64.

40 C. L. Dailey and F. C. Wood, <u>ibid</u>.

forces which the flow exerts upon the channel walls, it is necessary to compute the distribution of static pressures and momenta at channel exit. For convenience, pertinent quantities which have been computed already are assembled in Table 4-16. The flow conditions at channel inlet and

Table 4-16

Flow Direction, Expansion Angle, and Mach Number at Channel Exit			
Station	$\bar{\delta}$	ϕ	M Chart 2-11[41]
1	$9^\circ\ 07'$ ↑	$8^\circ\ 15'$	1.376
2	$9^\circ\ 07'$ ↑	$8^\circ\ 15'$	1.376
3	$15^\circ\ 07'$ ↑	$13^\circ\ 15'$	1.545
4	$20^\circ\ 25'$ ↑	$18^\circ\ 33'$	1.723
5	$11^\circ\ 18'$ ↑	$9^\circ\ 10'$	1.405

at the five stations of the channel exit are contained in Tables 4-17 and 4-18. The values of the entries for a given station are obtained by the scheme produced in Section 4, Part B of this chapter.

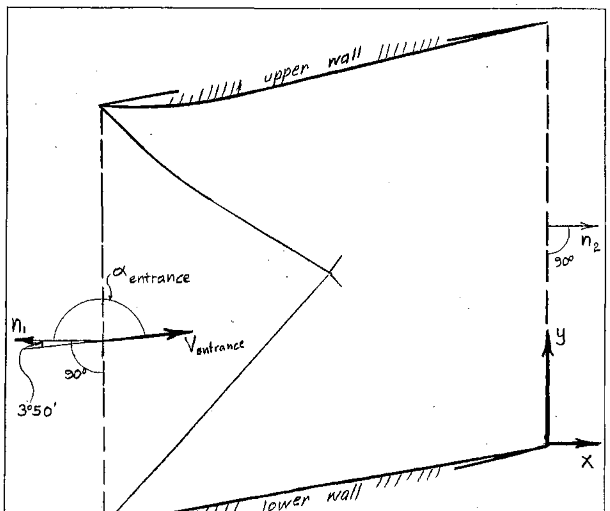

Figure 4-62

Axes and Outward Normals of Sharp-Nosed Profile Channel

Sufficient data are available now for the computation of the forces which the flow exerts upon the walls of the channel. The channel configuration, along with the outward normals n_1 and n_2, are shown in Figure 4-62. As before, the acute angle between n_1 and the direction of the free-stream velocity at inlet equals

41 Ibid.

Table 4-17

Channel-Entrance and -Exit Distributions, Part 1 of 2 Parts									
	1	2	3	4	5	6	7	8	9
Station	P_s/P	P	ρ_s/ρ	ρ $\times 10^4$	$\sqrt{T_s/T}$	a	V	$A = A_y$	α
Entrance	4.94	1.367	3.125	4.060	1.257	828	1408	1.6000	176° 10'
1	3.08	2.192	2.23	5.69	1.174	886	1218	0.0364	12° 57'
2	3.08	2.192	2.23	5.69	1.174	886	1218	0.1776	12° 57'
3	3.92	1.722	2.66	4.765	1.216	856	1322	0.3932	18° 57'
4	5.12	1.318	3.22	3.94	1.263	823	1418	0.9136	24° 15'
5	3.21	2.103	2.30	5.515	1.181	881	1238	0.0792	15° 08'

Table 4-18

Channel-Entrance and -Exit Distributions, Part 2 of 2 Parts									
	10	11	12	13	14	15	16	17	18
Station	$\cos\alpha$	$\sin\alpha$	$V_n = V_x$	V_n^2 $\times 10^{-6}$	V_y	ρA_y $\times 10^4$	$\rho A V_n^2 = \rho A_y V_n V_x$	$\rho A V_n V_y$	PA_y
Entrance	-0.998	0.067	-1405	1.975	94.4	6.49	-1283.	-86.1	2.185
1	0.975	0.224	1188	1.413	273.	0.2072	29.25	6.715	0.0798
2	0.975	0.224	1188	1.413	273.	1.012	142.9	32.8	0.389
3	0.946	0.325	1250	1.563	429.5	1.873	293.4	100.7	0.677
4	0.912	0.411	1294	1.677	583.	3.60	603.5	272.	1.204
5	0.965	0.261	1195	1.428	323.	0.437	62.4	16.88	0.1668

$3^\circ\ 50'$.

$$\Delta\mathcal{M}_x = \mathcal{M}_{x,\text{entrance}} - \mathcal{M}_{x,\text{exit}} = 1283. - 1131.5 = 151.5 \text{ lbs}(144),$$

$$F_{\Delta\mathcal{M}_x} = \frac{1}{144}\Delta\mathcal{M}_x = \frac{1}{144}\,151.5 = 1.052 \text{ lbs} \quad .$$

$$\mathcal{P}_{x,\text{entrance}} = \Big[PA_y\Big]_{\text{entrance}} = 2.185 \text{ lbs} \quad ,$$

$$\mathcal{P}_{x,\text{exit}} = \sum_{i=1}^{5}\Big[PA_y\Big]_i = 2.517 \text{ lbs}, \ i = \text{exit station number},$$

$$F_{\mathcal{P}_x} = \mathcal{P}_{x,\text{exit}} - \mathcal{P}_{x,\text{entrance}} = 2.517 - 2.185 \quad ,$$

$$F_{\mathcal{P}_x} = 0.332 \text{ lbs} \quad ,$$

$$F_x = F_{\Delta\mathcal{M}_x} + F_{\mathcal{P}_x} = 1.052 + 0.332 = 1.384 \text{ lbs} \quad .$$

$$\mathcal{M}_{y,\text{exit}} = \sum_{i=1}^{5}\Big[\rho A V_n V_y\Big]_i = 429.1 \text{ lbs}(144) \quad ,$$

$$\mathcal{M}_{y,\text{entrance}} = \Big[\rho A V_n V_y\Big]_{\text{entrance}} = 86.1 \text{ lbs}(144) \quad ,$$

$$\Delta\mathcal{M}_y = \mathcal{M}_{y,\text{exit}} - \mathcal{M}_{y,\text{entrance}} \quad ,$$

$$\Delta\mathcal{M}_y = 429.1 - 86.1 \quad ,$$

$$\Delta\mathcal{M}_y = 343.0 \text{ lbs}(144) \quad ,$$

$$F_{\Delta\mathcal{M}_y} = \frac{1}{144}\Delta\mathcal{M}_y = \frac{1}{144}\,343.0 \quad ,$$

$$F_{\Delta\mathcal{M}_y} = 2.382 \text{ lbs} \quad ,$$

$$F_y = F_{\Delta\mathcal{M}_y} = 2.382 \text{ lbs}.$$

Figure 4-63 shows the directions of all force components with respect to the axes.

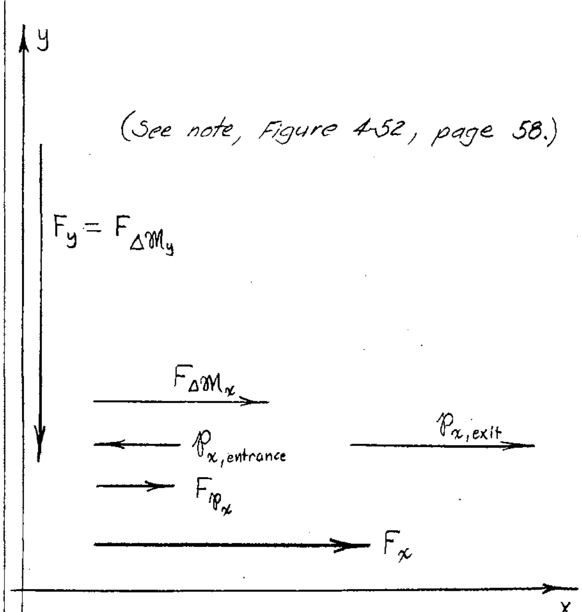

Figure 4-63

Force Components for Channel in Cascade of Sharp-Nosed Profiles

CHAPTER V

FALLACIES AND ERRONEOUS APPROACHES

A Introduction

This chapter may be omitted entirely without disturbing the continuity of the study. It is presented only in order to save other workers the trouble of pursuing certain fruitless paths. The following items are presented in outline form. In each instance, the fallacious assumption is given, and, where necessary, the successful alternative assumption is pointed out.

B Joukowski Profile

After selecting a suitable direction of approach of the incompressible free stream, a Joukowski profile[1] having the same thickness and camber as the original cascade element is constructed, partly by trial-and-error, and the stagnation streamline plotted in the neighborhood ahead of the leading edge. The transformation of the curve to both the supersonic and subsonic regions is quite difficult, and totally unnecessary for the location of the entrance flow direction, as may be seen from the analysis in Chapter IV, Part A, Section 2.

C Analytic Relation Between Nose and Shock Shapes

A search is made for an analytic relation between the shape of the detached wave and the nose region of the original profile on the assumption of the existence of such a relation. The fact that the flow is mixed makes this very difficult. The direction of solution is not re-

---

1 Richard von Mises, Theory of Flight, p. 122 ff.

versible, which makes the direction of procedure unique. The first assumption must be that of the shape of the shock wave. A relation may be written then defining the nose shape in terms of the shock shape with a power series. For each assumption of a shock shape, there exists a unique nose shape. The process of assuming shock shapes until a nose shape approximately equivalent to that of the original profile is found is a long one. In addition, the solution of the power series relation is not straightforward. Hence, this method is not attempted because the amount of work involved is not justified.

Instead, an alternate assumption must be made. It is supposed that the shock shape can be located through the method of isoclines, or that the shock shape is an integral curve of the nose shape.[2] This is a graphical construction. From a shadowgraph,[3] a center of isoclines is located. It is assumed that this point does not shift for a change in Mach number from 1.8 to 1.7. The nose wave found thus is used in the subsequent location of a pair of sonic lines, and for the analysis of the supersonic region downstream. The resulting flows converge very rapidly toward each other and toward the wall. This leads to the physical impossiblity of vanishing flow. Since the analysis is rather straightforward, the failure is due to the wrong assumption of the shape of the nose wave. This conclusion is supported by Busemann, who contradicts the assumption of an analytic relation.[4] The incorporation of his alterna-

---

2 Theodore v. Kármán and Maurice A. Biot, Mathematical Methods in Engineering, p. 7.

3 Hans Wolfgang Liepmann and Allen E. Puckett, op. cit., Fig. 6.13, p. 99.

4 Adolf Busemann, op. cit., p. 11.

tive leads to a successful solution, as presented in Chapter IV, Part A, Section 2.

D Selection of Entrance M in Relation to Nose Pattern Overlap

The problem of detached shock is comparatively old, and the absence of theoretical results implies that it is difficult to solve. Sharp-nosed profiles demand a unique direction of flow approach for optimum performance, and even a small deviation from this produces flow patterns having large entropy jumps, and hence large losses of energy. It is hoped that this property does not pertain to blunt-nosed profiles of sufficiently slim proportions. The free-stream M may be selected slightly larger than 1.0, whereupon the detached shock is very strong, and the region behind the wave is probably entirely subsonic. Behind the intersection of adjacent waves, the flow has an even lower M. The energy losses due to this overlap become prohibitive, and Mach numbers only slightly greater than 1.0 must be avoided. Too high an M should be avoided also, since little is known about the hypersonic region. Hence the next stage of practical research should concern itself with $1.0 < M \leq 2.0$. The selection of $M = 1.7$ at channel entrance is prompted by the availability of a shadowgraph photograph, mentioned in Part C.

E Shear Sheet Energy Dissipation in a Supersonic Region

The assumption that shear sheets die out rapidly in a supersonic flow fails. Supersonic flow is essentially stable, and disturbances tend to persist. Also, the actual channel is extremely short, less than 2 inches long, and the flow time required is insufficient for dissipation in such a brief path.

F Build-Up of Shock Along Concave Wall Due to Wedge Nose on Profile

If it is assumed that the flow in the channel of the original profiles is entirely supersonic past the nose regions, then the comparison channel must have one concave wall, the entrance to which is a semi-wedge. To preserve similarity, the semi-wedge angle is large, and a strong oblique shock is attached to the nose of the profile. The concave form of the downstream wall causes a series of compression characteristics. Immediately past the strong attached shock, the flow is but slightly supersonic, so that the succeeding slow compression results in the building of a shock-wave envelope in the interior of the channel. After sufficient turning of the flow, a portion of the envelope shock becomes normal, and the flow downstream of this portion becomes subsonic. If this had been noticed earlier, it could have been used as a reason for abandoning the original profile, since even the comparison profile results in subsonic conditions in the channel. These are, of course, to be avoided.

G Analysis Downstream of Channel Trailing Edges

It is extremely difficult to locate the portion of the stagnation streamline downstream of each trailing edge. At first, this seems necessary in order to define the channel walls completely for a change-of-momentum analysis. This solution is not required, however, since the channel side walls end at the trailing edges of the profiles, by the definition of the exit control surface.

H Partial Center Pattern Resulting in Void-Wedge Flow

If the assumption is made that the last bent e_ϕ intersects the nose wave ahead of the center point, either above or below, a void wedge of flow results downstream of the intersection, as shown in Figure 5-1. Hence, this partial pattern cannot be used in the solution of the center region. This failure is avoided in Parts B and C of Chapter IV by a different assumption for each of the center patterns.

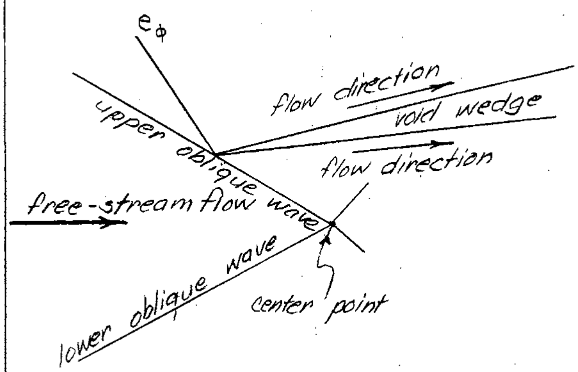

Figure 5-1

Void-Wedge Flow

CHAPTER VI

SUMMARY

A method is developed for computing the axial thrust and tangential force, or torque-force, reactions of a suitabley selected cascade of blunt-nosed profiles to a compressible-fluid flow having a free-stream Mach number arbitrarily set at 1.7. The problem is reduced to the analysis of the two-dimensional channel flow between two adjacent profiles of the cascade. A criterion is found for locating the detach distance, and the shape of the detached nose shock ahead of each profile. The limits of the subsonic region behind the detached shock are defined then, and the subsequent supersonic flow in the channel is computed. It is found that too sharp a curvature of a concave wall causes an indeterminate interior pattern. The only fact evident in this case is that the flow in this interior pattern is strongly subsonic. To avoid excessive turning of the flow, which produces strong shocks in the channel and subsonic flow of indeterminate configuration, the original cascade slement is modified such that the formerly concave channel wall is initially convex, then straight. A valid solution then in obtained and compared to that found for a channel, the bordering elements of which are sharp-nosed profiles, identical to the modified blunt-nosed profiles with the exception of the nose region. The method of analysis for the flow of a compressible fluid about a sharp-nosed profile is already known, and the subsequent channel analysis is straightforward. Since no experimental results are available for comparison to the theoretical values obtained for the channel of blunt-nosed profiles, the results of the sharp-nosed profile channel analysis are the only measure of validity for the original developments of

this work.

A cascade of sharp-nosed profiles in an initially supersonic flow has but one angle of attack for which the performance is at an optimum. If this angle is changed, the shock either detaches itself from the nose of the profile, or a subsonic zone forms on one side of the nose of each cascade element. In either case, cascade performance is very poor, and high energy losses result. A slim blunt-nosed element, however, permits a slight variation of the angle of attack for which useful performance may still be obtained from the cascade. If the blunt nose of the element is sufficiently small, the region of strong shock of the detached shock is quite small, and only small entropy increases occur. In addition, the convex curvature past the subsonic zone behind the strong portion of the detached shock permits a smooth expansion of the flow, and hence a desirable increase in Mach number without increase in entropy. The comparison element, or sharp-nosed profile, has either no, or a very small section of convex surface serving as a guide to smooth supersonic expansion.

The mass flow per inch of blade height at the entrance of each channel equals 0.912 slugs/sec. At the exit control surface of the sharp-nosed profile channel, the mass flow equals 0.8957 slugs/sec. This is sufficiently close to the value of the entrance mass flow to satisfy the mass flow continuity condition for this channel. However, the mass flow across the exit control surface of the blunt-nosed profile channel is found to be equal to 0.4599 slugs/sec. This is only slightly more than 50 per cent of the mass flow at the channel entrance control surface. The neglect of strong flows parallel to the detached wave in the subsonic region is the cause of this violation of the mass flow continuity condition. However, the trend of the given solution relative to the comparison solution is still correct from the standpoint of energy analysis.

It is possible to compute a fictitious set of values for the exit distribution of the blunt-nosed profile channel, such that these values will indicate the upper performance limit of the channel. Let BNC refer to the blunt-nosed profile channel already computed, BNC' to the blunt-nosed profile channel with the fictitious exit distribution, and SNC to the sharp-nosed profile channel. Let ρ_i' designate the mass density in slugs/cf at exit station i, where

$$i = 1, 2, 3, \ldots, 10.$$

The mass flow continuity condition is satisfied approximately if it is assumed that

$$\rho_i' = 2\rho_i \text{ , where } \rho_i \text{ refers to BNC exit stations.}$$

It is known that

$$\frac{P_s}{P} = \left(1 + \frac{\gamma - 1}{2} M^2\right)^{\frac{\gamma}{\gamma-1}} ,$$

and

$$\frac{\rho_s}{\rho} = \left(1 + \frac{\gamma - 1}{2} M^2\right)^{\frac{1}{\gamma-1}} ;$$ [1]

from which it can be seen that

$$\frac{P_s'}{P'} = \left(\frac{\rho_s'}{\rho'}\right)^{\gamma} ,$$

where P' is the static pressure corresponding to ρ'. Corresponding stagnation pressures and densities remain unchanged; that is,

---

1 Hans Wolfgang Liepmann and Allen E. Puckett, op. cit., equations 3·9 and 3·10, p. 26.

$$P_s{}' = P_s \quad , \qquad \text{and} \qquad \rho_s' = \rho_s \quad .$$

With the aid of these relations, the entries of Table 6-1 are computed. The product $P'A_y$ is the static pressure force per inch of blade height for each exit station.

Table 6-1

Modified Exit Static Pressure Force Distribution, Blunt-Nosed Profile Channel

Station	ρ_s/ρ Table 4-11[2]	ρ_s'/ρ'	P_s'/P'	P'	A_y Table 4-11[2]	$P'A_y$
1	4.1	2.05	2.73	2.473	0.2750	0.6800
2	4.67	2.335	3.276	2.062	0.0670	0.1382
3	3.76	1.88	2.42	2.79	0.0404	0.1128
4	4.625	2.313	3.23	2.09	0.2490	0.5210
5	5.72	2.86	4.35	1.552	0.0096	0.0149
6	9.05	4.525	8.27	0.816	0.1452	0.1185
7	7.14	3.57	5.94	1.137	0.0788	0.0896
8	10.16	5.08	9.73	0.694	0.0260	0.01805
9	13.23	6.615	14.10	0.479	0.1970	0.0944
10	14.70	7.35	16.30	0.414	0.5120	0.2120

Using the symbols defined in Chapter IV, the forces of the flow on BNC' now may be computed . Since the channel entrance conditions remain unchanged, $\mathcal{M}_{x,\text{entrance}}$ has the same value as before. However, because of the change in ρ , $\mathcal{M}_{x,\text{exit}}$ of BNC' is double that of BNC. This statement holds if y is substituted for x in the subscripts.

$$\mathcal{M}_{x,\text{entrance}} = 1283.\ \text{lbs}(144) \quad ,$$

$$\mathcal{M}_{x,\text{exit}} = 2(742.5) = 1485.\ \text{lbs}(144) \quad ,$$

$$\Delta\mathcal{M}_x = \mathcal{M}_{x,\text{entrance}} - \mathcal{M}_{x.\text{exit}} \quad ,$$

$$\Delta\mathcal{M}_x = 1283. - 1485. = -202.\ \text{lbs}(144) \quad ,$$

---

2 P. 55.

$$F_{\Delta \mathcal{M}_x} = \frac{1}{144}(-202.) = -1.402 \text{ lbs} \quad .$$

The force due to static pressure at channel entrance remains the same as that for Parts B and C of Chapter IV. Since $P'A_y$ is the static pressure force for each exit station, the summation of the last column of Table 6-1 is equal to the force due to static pressure at channel exit.

$$\mathcal{P}_{x,\text{entrance}} = 2.185 \text{ lbs} \quad ,$$

$$\mathcal{P}_{x,\text{exit}} = \sum_{i=1}^{10} \left[P'A_y\right]_i = 1.999 \text{ lbs} \quad ,$$

$$F_{\mathcal{P}_x} = \mathcal{P}_{x,\text{entrance}} - \mathcal{P}_{x,\text{exit}} \quad ,$$

$$F_{\mathcal{P}_x} = 2.185 - 1.999 = 0.186 \text{ lbs} \quad ,$$

$$F_x = F_{\Delta \mathcal{M}_x} - F_{\mathcal{P}_x} = -1.402 - 0.186 \quad ,$$

$$F_x = -1.588 \text{ lbs} \quad .$$

The minus sign implies that energy is supplied to the flow in the interior of the channel, since the axial drag is negative. This is not possible physically without an exterior energy source, but does not hamper the computation of BNC' values as upper performance limits. From the statement on page 78,

$$\mathcal{M}_{y,\text{entrance}} = 86.1 \text{ lbs}(144) \quad ,$$

$$\mathcal{M}_{y,\text{exit}} = 2(185.6) = 371.2 \text{ lbs}(144) \quad ,$$

$$\Delta \mathcal{M}_y = \mathcal{M}_{y,\text{exit}} - \mathcal{M}_{y,\text{entrance}} \quad ,$$

$$\Delta \mathcal{M}_y = 371.2 - 86.1 = 285.1 \text{ lbs}(144) \quad ,$$

$$F_{\Delta \mathcal{M}_y} = \frac{1}{144}\Delta \mathcal{M}_y = \frac{1}{144} 285.1 = 1.978 \text{ lbs} \quad ,$$

$$F_y = F_{\Delta \mathcal{M}_y} = 1.978 \text{ lbs} \quad .$$

A comparison is made between important values of BNC, SNC, and BNC', and

Table 6-2

Comparison of Constituents of/and Cascade Channel Force Components, Part 1 of 3 Parts					
Quantity, Units	BNC	Rel.	SNC	By ___% SNC	Commentary
$\mathcal{M}_{x,entrance}$, lbs(144)	1283.	$\equiv$	1283.	----	Identical entrance conditions.
$\mathcal{M}_{x,exit}$, lbs(144)	742.5	$<$	1131.5	34.4	Greater loss of energy due to detached shock.
$F_{\Delta\mathcal{M}_x}$, lbs	3.75	$>$	1.052	256.4	Greater loss of energy due to detached shock.
$\mathcal{P}_{x,entrance}$, lbs	2.185	$\equiv$	2.185	----	Identical entrance conditions.
$\mathcal{P}_{x,exit}$, lbs	0.751	$<$	2.517	70.2	Exit velocities of BNC $>$ exit velocities of SNC.
$F_{\mathcal{P}_x}$, lbs	1.434	$>$	0.332	331.8	From the above, since $\mathcal{P}_{x,entrance}$ is constant.
F_x, lbs	2.316	$>$	1.384	67.3	Greater axial drag is due to detached shock.
$\mathcal{M}_{y,entrance}$, lbs(144)	86.1	$\equiv$	86.1	----	Identical entrance conditions.
$\mathcal{M}_{y,exit}$, lbs(144)	185.6	$<$	429.1	56.7	Greater loss of energy due to detached shock.
F_y, lbs	0.691	$<$	2.382	71.0	Greater loss of energy due to detached shock.

Table 6-3

Comparison of Constituents of/and Cascade Channel Force Components, Part 2 of 3 Parts					
Quantity, Units	BNC'	Rel.	BNC	By ___% BNC	Commentary
$\mathcal{M}_{x,entrance}$, lbs(144)	1283.	$\equiv$	1283.	---	Identical entrance conditions.
$\mathcal{M}_{x,exit}$, lbs(144)	1485.	$>$	742.5	100.	Since $\rho'_i = 2\ \rho_i$.
$F_{\Delta\mathcal{M}_x}$, lbs	- 1.402	$<$	3.75	137.3	Energy is supplied in the BNC' channel.
$\mathcal{P}_{x,entrance}$, lbs	2.185	$\equiv$	2.185	---	Identical entrance conditions.
$\mathcal{P}_{x,exit}$, lbs	1.999	$>$	0.751	166.5	Since $\rho'_i = 2\ \rho_i$.
$F_{\mathcal{P}_x}$, lbs	0.186	$<$	1.434	87.1	From the above, since $\mathcal{P}_{x,entrance}$ is constant.
F_x, lbs	- 1.588	$<$	2.316	168.8	Energy is supplied in the BNC' channel.
$\mathcal{M}_{y,entrance}$, lbs(144)	86.1	$\equiv$	86.1	---	Identical entrance conditions.
$\mathcal{M}_{y,exit}$, lbs(144)	371.2	$>$	185.6	100.	Since $\rho'_i = 2\ \rho_i$.
F_y, lbs	1.978	$>$	0.691	186.2	Since $\rho'_i = 2\ \rho_i$.

Table 6-4

Comparison of Constituents of/and Cascade Channel Force Components, Part 3 of 3 Parts					
Quantity, Units	BNC'	Rel.	SNC	By ___% SNC	Commentary
$\mathcal{M}_{x,\text{entrance}}$, lbs(144)	1283.	$\equiv$	1283.	---	Identical entrance conditions.
$\mathcal{M}_{x,\text{exit}}$, lbs(144)	1485.	$>$	1131.5	31.22	Energy is supplied in the BNC' channel.
$F_{\Delta\mathcal{M}_x}$, lbs	$-$ 1.402	$<$	1.052	233.5	Energy is supplied in the BNC' channel.
$\mathcal{R}_{x,\text{entrance}}$, lbs	2.185	$\equiv$	2.185	---	Identical entrance conditions.
$\mathcal{R}_{x,\text{exit}}$, lbs	1.999	$<$	2.517	20.57	Since $\rho'_i = 2\,\rho_i$.
$F_{\mathcal{R}_x}$, lbs	0.186	$<$	0.332	44.0	From the above, since $\mathcal{R}_{x.\text{entrance}}$ is constant.
F_x , lbs	$-$ 1.588	$<$	1.384	214.4	Energy is supplied in the BNC' channel.
$\mathcal{M}_{y,\text{entrance}}$, lbs(144)	86.1	$\equiv$	86.1	---	Identical entrance conditions.
$\mathcal{M}_{y,\text{exit}}$, lbs(144)	371.2	$<$	429.1	13.5	Since $\rho'_i = 2\,\rho_i$.
F_y , lbs	1.978	$<$	2.382	16.97	Since $\rho'_i = 2\,\rho_i$.

presented in Tables 6-2, 6-3, and 6-4. Rel. at the head of each third column stands for relation; that is, respectively, is greater than, is less than, and is identical to.

The five graphs which follow give a clear comparison of the most important exit distribution quantities of the blunt-nosed profile channel of Part B, and the sharp-nosed profile channel of Part C of Chapter IV, The values are extracted from the tables of Section 4 of the respective parts of the same chapter.

Figure 6-1

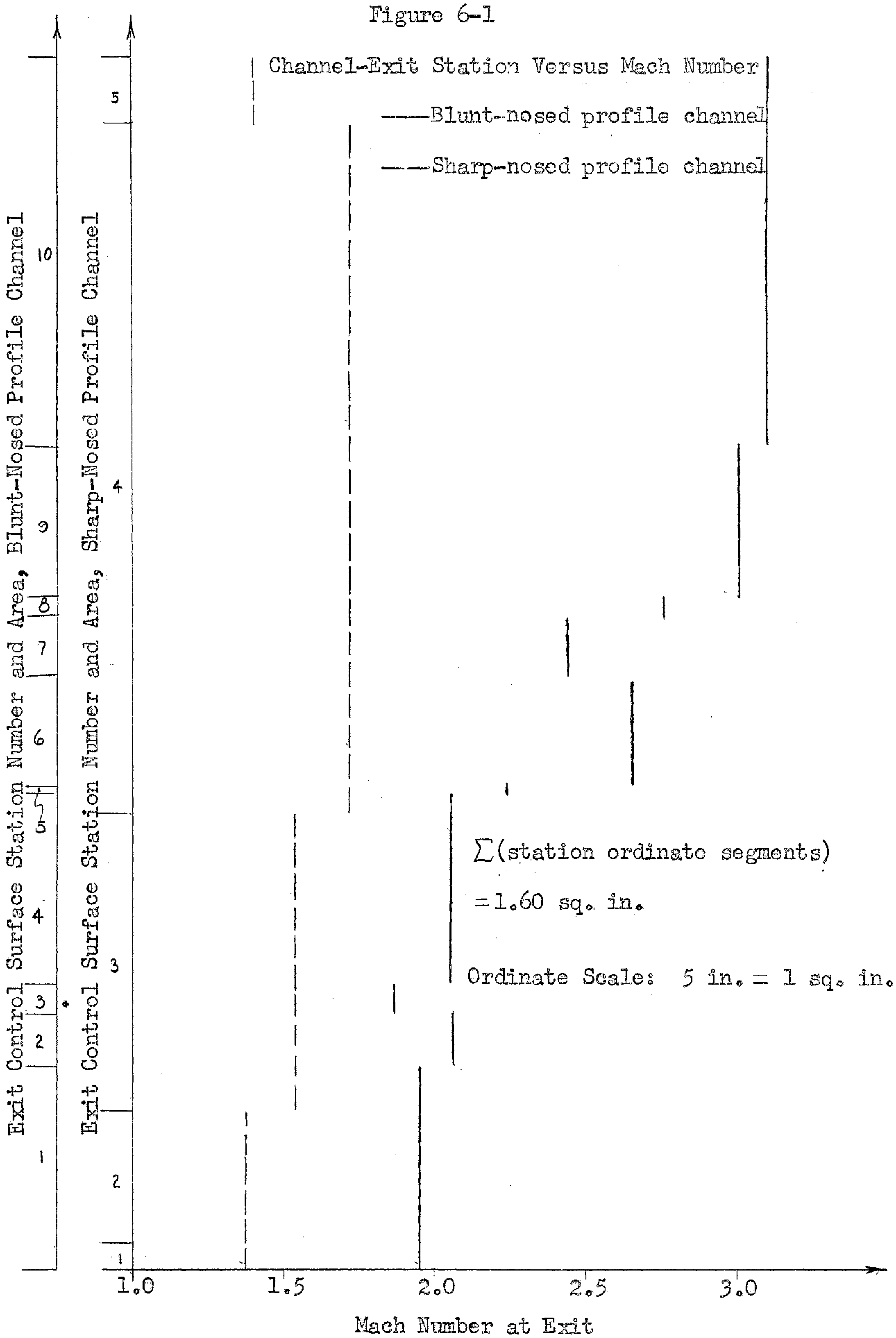

Channel-Exit Station Versus Mach Number
——Blunt-nosed profile channel
– – –Sharp-nosed profile channel
Exit Control Surface Station Number and Area, Blunt-Nosed Profile Channel
Exit Control Surface Station Number and Area, Sharp-Nosed Profile Channel
1
2
3
4
5
6
7
8
9
10
∑(station ordinate segments)
= 1.60 sq. in.
Ordinate Scale: 5 in. = 1 sq. in.
1.0
1.5
2.0
2.5
3.0
Mach Number at Exit

Figure 6-2

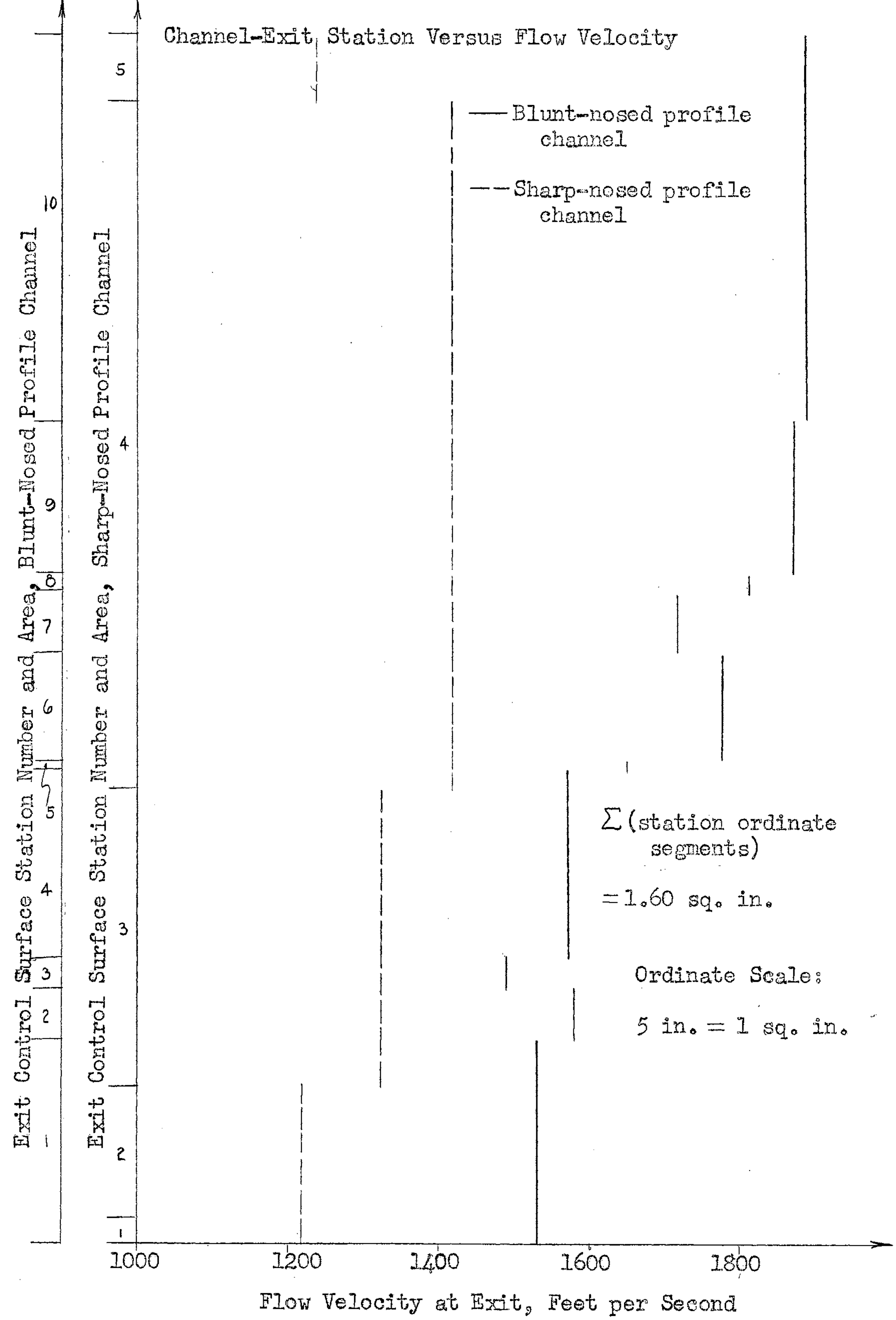
Channel-Exit Station Versus Flow Velocity
Blunt-nosed profile channel
Sharp-nosed profile channel
Σ (station ordinate segments) = 1.60 sq. in.
Ordinate Scale: 5 in. = 1 sq. in.
Exit Control Surface Station Number and Area, Blunt-Nosed Profile Channel
Exit Control Surface Station Number and Area, Sharp-Nosed Profile Channel
1
2
3
4
5
6
7
8
9
10
1
2
3
4
5
1000
1200
1400
1600
1800
Flow Velocity at Exit, Feet per Second

Figure 6-3

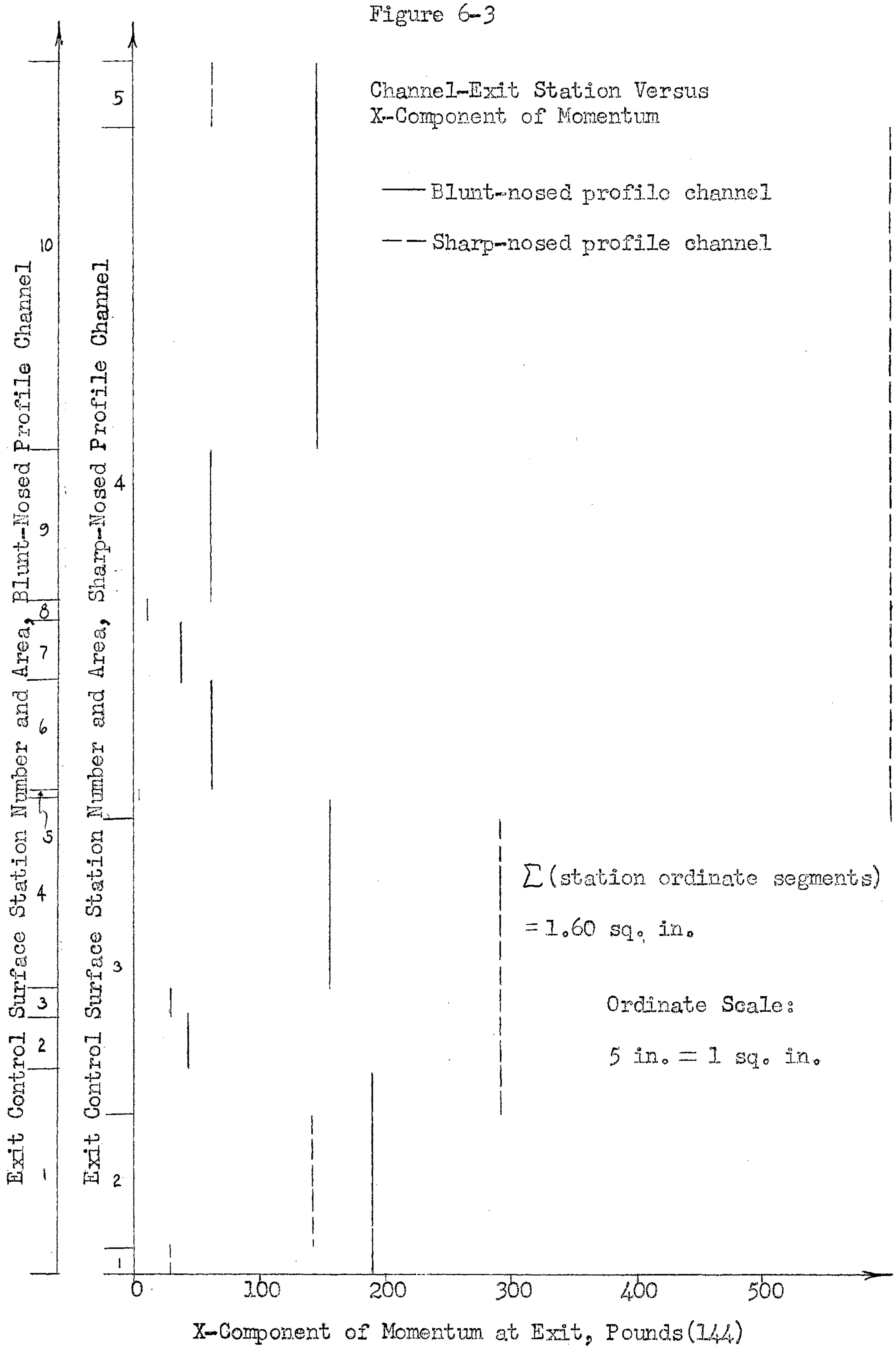
Channel-Exit Station Versus
X-Component of Momentum
Blunt-nosed profile channel
Sharp-nosed profile channel
Σ(station ordinate segments)
= 1.60 sq. in.
Ordinate Scale:
5 in. = 1 sq. in.
Exit Control Surface Station Number and Area, Blunt-Nosed Profile Channel
Exit Control Surface Station Number and Area, Sharp-Nosed Profile Channel
0
100
200
300
400
500
X-Component of Momentum at Exit, Pounds(144)

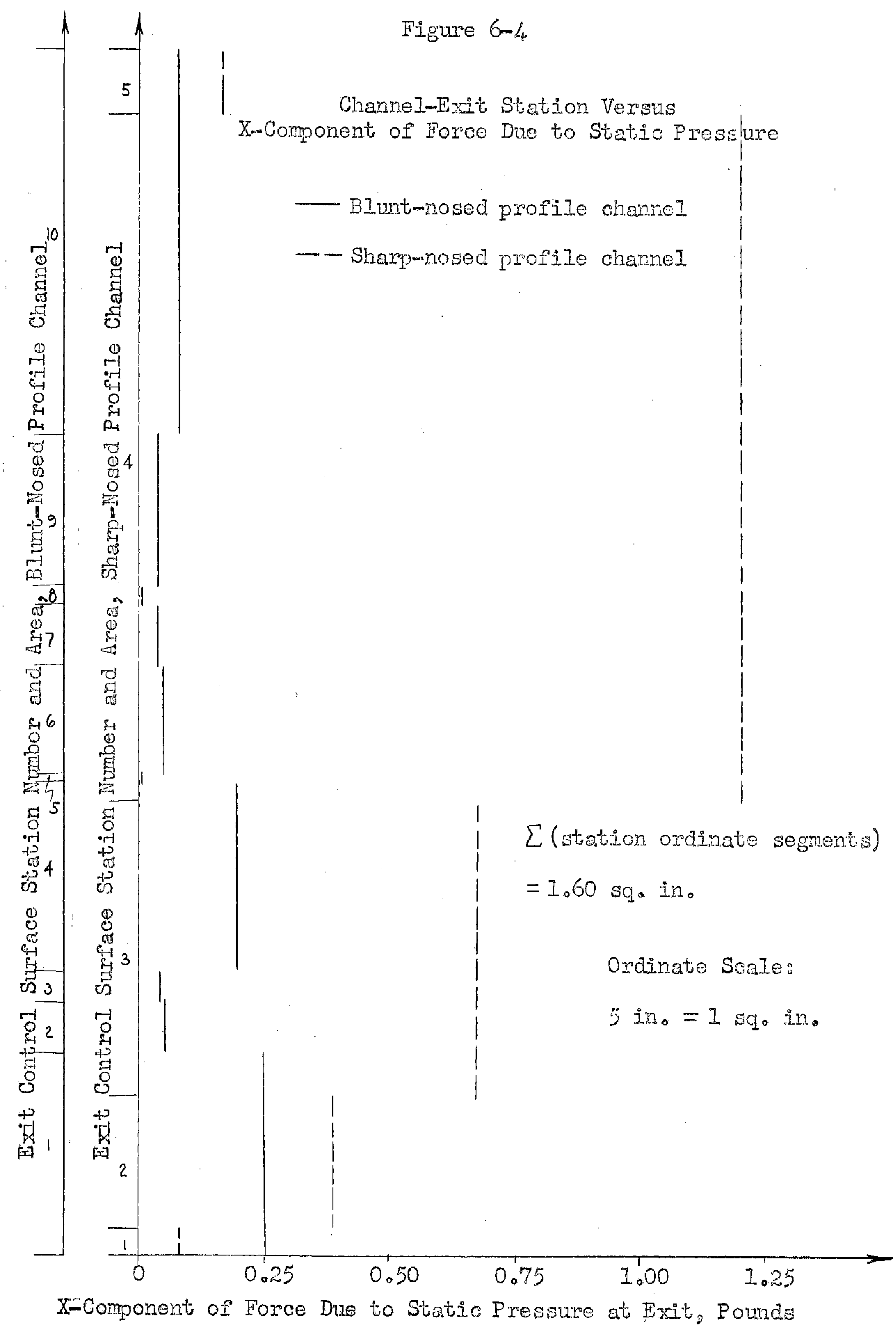
Figure 6-4
Channel-Exit Station Versus
X-Component of Force Due to Static Pressure
Blunt-nosed profile channel
Sharp-nosed profile channel
Σ (station ordinate segments)
= 1.60 sq. in.
Ordinate Scale:
5 in. = 1 sq. in.
Exit Control Surface Station Number and Area, Blunt-Nosed Profile Channel
Exit Control Surface Station Number and Area, Sharp-Nosed Profile Channel
0
0.25
0.50
0.75
1.00
1.25
X-Component of Force Due to Static Pressure at Exit, Pounds

Figure 6-5

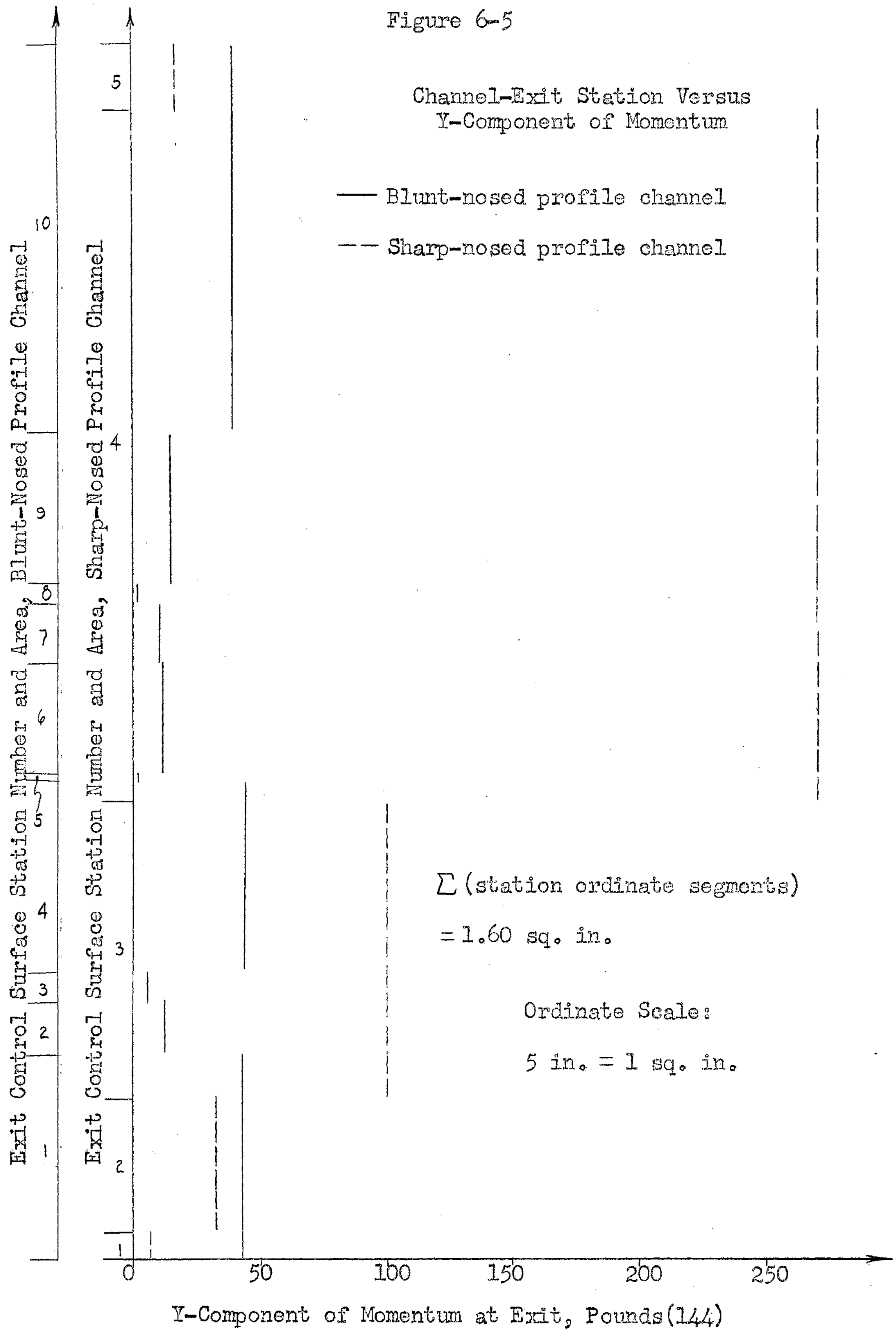

Channel-Exit Station Versus Y-Component of Momentum
Blunt-nosed profile channel
Sharp-nosed profile channel
Σ (station ordinate segments) = 1.60 sq. in.
Ordinate Scale:
5 in. = 1 sq. in.
Exit Control Surface Station Number and Area, Blunt-Nosed Profile Channel
Exit Control Surface Station Number and Area, Sharp-Nosed Profile Channel
1
2
3
4
5
6
7
8
9
10
0
50
100
150
200
250
Y-Component of Momentum at Exit, Pounds(144)

CHAPTER VII

CONCLUSION

The chief purpose of this investigation, the determination of the thrust- and torque-reactions of a straight cascade of blunt-nosed profiles to the flow of air with an entrance Mach number of 1.7, has been achieved. The pattern is shown in Figure A-3 of the Appendix. The axial force, or drag of the flow, per channel, per inch of blade height equals 2.316 lbs. The tangential force, or torque force of the flow on the cascade equals 0.691 lbs per channel, per inch of blade height. In the symbols already developed,

$$F_{x,BNC} = 2.316 \text{ lbs} \quad ,$$
$$F_{y,BNC} = 0.691 \text{ lbs} \quad .$$

For the comparison channel of sharp-nosed profiles, shown in Figure A-4 of the Appendix,

$$F_{x,SNC} = 1.384 \text{ lbs} \quad ,$$
$$F_{y,SNC} = 2.382 \text{ lbs} \quad ,$$

where the terms have definitions corresponding to those of the blunt-nosed profile cascade.

Because of the discrepancy in mass flows in the analysis of the blunt-nosed profile channel, a fictitious set of force values, labeled BNC', for which the mass flow continuity condition holds, was computed in Chapter VI. The most important of these values are

$$F_{x,BNC'} = -1.588 \text{ lbs} \quad ,$$

and $$F_{y,BNC'} = 1.978 \text{ lbs} \quad ,$$

where again the terms have definitons corresponding to those of the blunt-nosed profile cascade. In final summation,

$$F_{x,BNC} > F_{x,SNC} > 0 > F_{x,BNC'} ,$$

and

$$F_{y,SNC} > F_{y,BNC'} > F_{y,BNC} .$$

These inequalities are as expected, and are explained in the commentary columsn of Tables 6-2, 6-3, and 6-4 of Chapter VI.

Since the BNC' quantities represent the upper limit of the performance of BNC, a final estimate can be made of both F_x and F_y of BNC which will be the most plausible solution available at present. Let these final estimates be designated by $\bar{F}_{x,BNC}$ and $\bar{F}_{y,BNC}$, having values which are assumed to lie midway between respective upper and lower performance limits. Hence,

$$\bar{F}_{x,BNC} = \tfrac{1}{2}(F_{x,BNC} + F_{x,SNC}) ,$$
$$\bar{F}_{x,BNC} = \tfrac{1}{2}(2.316 + 1.384) ,$$
$$\boxed{\bar{F}_{x,BNC} = 1.850 \text{ lbs}} ;$$

and

$$\bar{F}_{y,BNC} = \tfrac{1}{2}(F_{y,BNC'} + F_{y,BNC}) ,$$
$$\bar{F}_{y,BNC} = \tfrac{1}{2}(1.978 + 0.691) ,$$
$$\boxed{\bar{F}_{y,BNC} = 1.335 \text{ lbs}} .$$

It is seen that

$$\bar{F}_{x,BNC} > F_{x,SNC} \quad \text{and} \quad \bar{F}_{y,BNC} < F_{y,SNC} ,$$

which is in accordance with the energy analysis result that the losses in a blunt-nosed profile channel are greater than those in a similar sharp-nosed profile channel.

The criteria found for locating the detach distance and the shape of the detached shock wave ahead of each blunt-nosed profile are somewhat crude. Further refinement should lead to a mapping relation in which the shape of the sensitive shoulder arcs and the distance from the shoulder circle center to the normal-shock point on the detached wave are the principal parameters with which the shock-wave shape can be located from the profile nose shape.

Excessive turning of the flow must be avoided in the design of blunt-nosed profile cascades, since it causes strong subsonic flow in the interior of each channel. Further analysis is required to locate conditions of maximum turning without interior subsonic flow.

Figure A-3 of the Appendix shows that the blunt-nosed profiles are too slim to be sufficiently strong. A redesign is necessary. The cascade spacing, or pitch, should not be decreased, but the profiles should be shortened, as shown in Figure 7-1. This assures that no subsonic flow will occur in the interior of the channel. In fact, the exit flow will be more supersonic, and most of the flow will have a greater turning, and hence a greater change of momentum in the tangential, or y, direction. Hence, F_y will be greater than before, and a stronger blade with better performance is the fortunate result. Since strength is no consideration in this solution, the redesign is not given here.

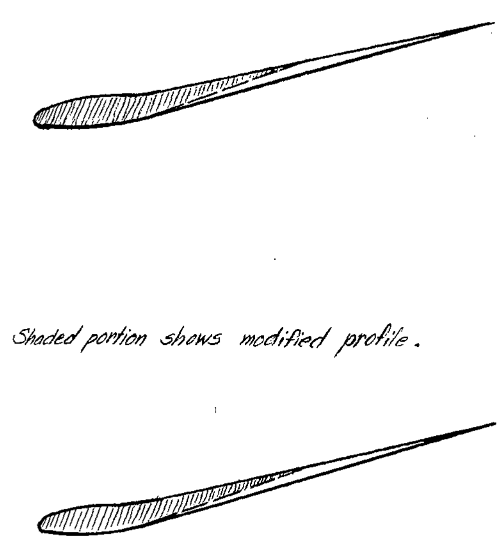

Figure 7-1

Suggested Cascade Design Change

In the development of high-speed aircraft, new designs of axial-flow turbomachines are required. These machines must operate both at supersonic and subsonic flight speeds. The nucleus of these designs is a straight cascade capable of operating in both speed ranges. A blunt-nosed profile is best for subsonic operation, while a sharp-nosed one is preferable for supersonic flight. Until now, it was feared that the blunt-nosed profile was incapable of supersonic operation. Although its performance is inferior to that of a sharp-nosed profile, the results of this work show that it can be used for both speed ranges, while it is already known that a sharp-nosed profile cannot. Of course, a means must be devised for moving from the subsonic range to the supersonic one. The most obvious method is the brief use of booster rockets. No special auxiliary equipment is required for the reverse operation.

It is demonstrated that useful performance may be obtained from a cascade of blunt-nosed profiles, provided that the turning of the flow is not great enough to cause subsonic flow in the interior of each channel. The performance of the blunt-nosed profile cascade is inferior to that of a sharp-nosed profile cascade in a supersonic flow. Although the solution of the problem lacks rigor, it is hoped that it will be a small aid in the development of the general theories of detached-shock flow and mixed-flow cascades, since no experimental results are available at present.

This analysis is but the first small step toward the design of a subsonic-supersonic turbomachine. The results are sufficiently promising to allow the author to recommend that further work should be done.

BIBLIOGRAPHY

Abbott, Ira H. and Doenhoff, Albert E. von. Theory of Wing Sections. New York: McGraw-Hill Book Company, Inc., 1949.

Bergman, Stefan. "On Supersonic and Partially Supersonic Flows." NACA, TN 1096 (December, 1946).

Busemann, Adolf. "A Review of Analytical Methods for the Treatment of Flows with Detached Shocks." NACA, TN 1858 (April, 1949).

Costello, George R. "Method of Designing Cascade Blades with Prescribed Velocity Distributions in Compressible Potential Flows." NACA, R 978. Washington: 1950.

Dailey, C. L. and Wood, F. C. Computation Curves for Compressible Fluid Problems. New York: John Wiley and Sons, Inc., c. 1949.

Dugundji, John. "An Investigation of the Detached Shock in Front of a Body of Revolution." Journal of the Aeronautical Sciences, XV (December, 1948), 699-705.

Ferri, Antonio. Elements of Aerodynamics of Supersonic Flows. New York: The Macmillan Company, 1949.

Frankl, F. "On the Problem of Chaplygin for Mixed Sub- and Supersonic Flows." NACA, TM 1155 (June, 1947).

Kármán, Theodore v. and Biot, Maurice A. Mathematical Methods in Engineering. New York: McGraw-Hill Book Company, Inc., 1940.

Liepmann, Hans Wolfgang and Puckett, Allen E. Introduction to Aerodynamics of a Compressible Fluid. New York: John Wiley and Sons, Inc., c. 1947.

Lin, C. C. "On an Extension of the von Kármán-Tsien Method to Two-Dimensional Subsonic Flows with Circulation Around Closed Profiles." Quarterly of Applied Mathematics, IV(October, 1946), 291-297.

Mises, Richard von. Theory of Flight. New York: McGraw-Hill Book Company, Inc., 1945.

Munk, M. M. and Prim, R. C. "Surface-Pressure Gradient and Shock-Front Curvature at the Edge of a Plane Ogive with Attached Shock Front." Journal of the Aeronautical Sciences, XV (November, 1948), 691-695.

Wang, Chi-Teh. "Variational Method in the Theory of Compressible Fluid." Journal of the Aeronautical Sciences, XV (November, 1948), 675-685; also errata, XVI (February, 1949), 125 f.

Weinig, F. Die Strömung um die Schaufeln von Turbomaschinen. Leipzig: Verlag von Johann Ambrosius Barth, 1935.

Zucrow, M. J. Principles of Jet Propulsion and Gas Turbines. Revised printing. New York: John Wiley and Sons, Inc., c. 1948.

Figure A-1

Nose Region of Blunt-Nosed Profile

Scale: 125 in. = 1 in.

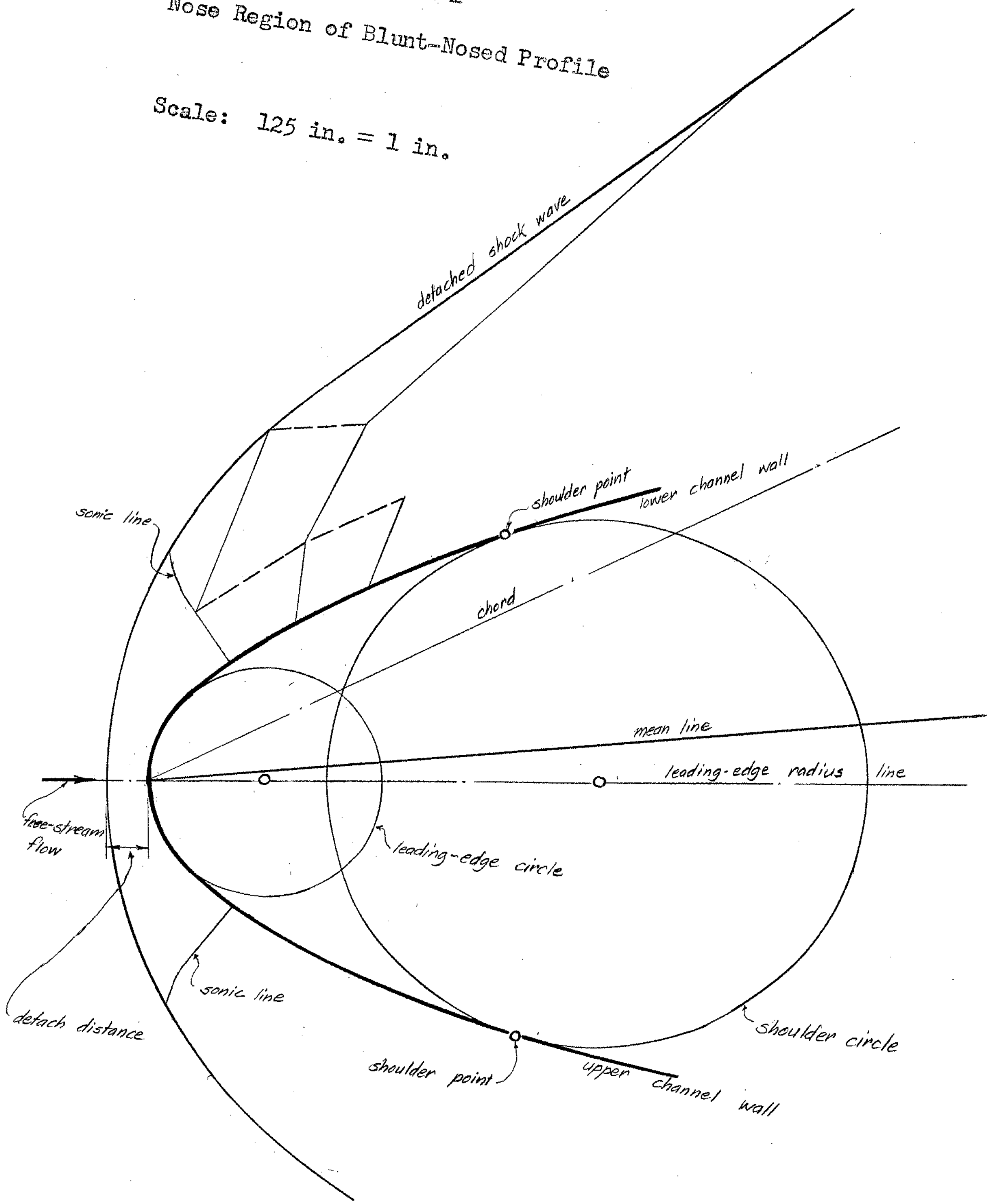

Scale Ratios:
Drawing, 10 : 1 ,
Photographic Reduction, 3 : 1 .

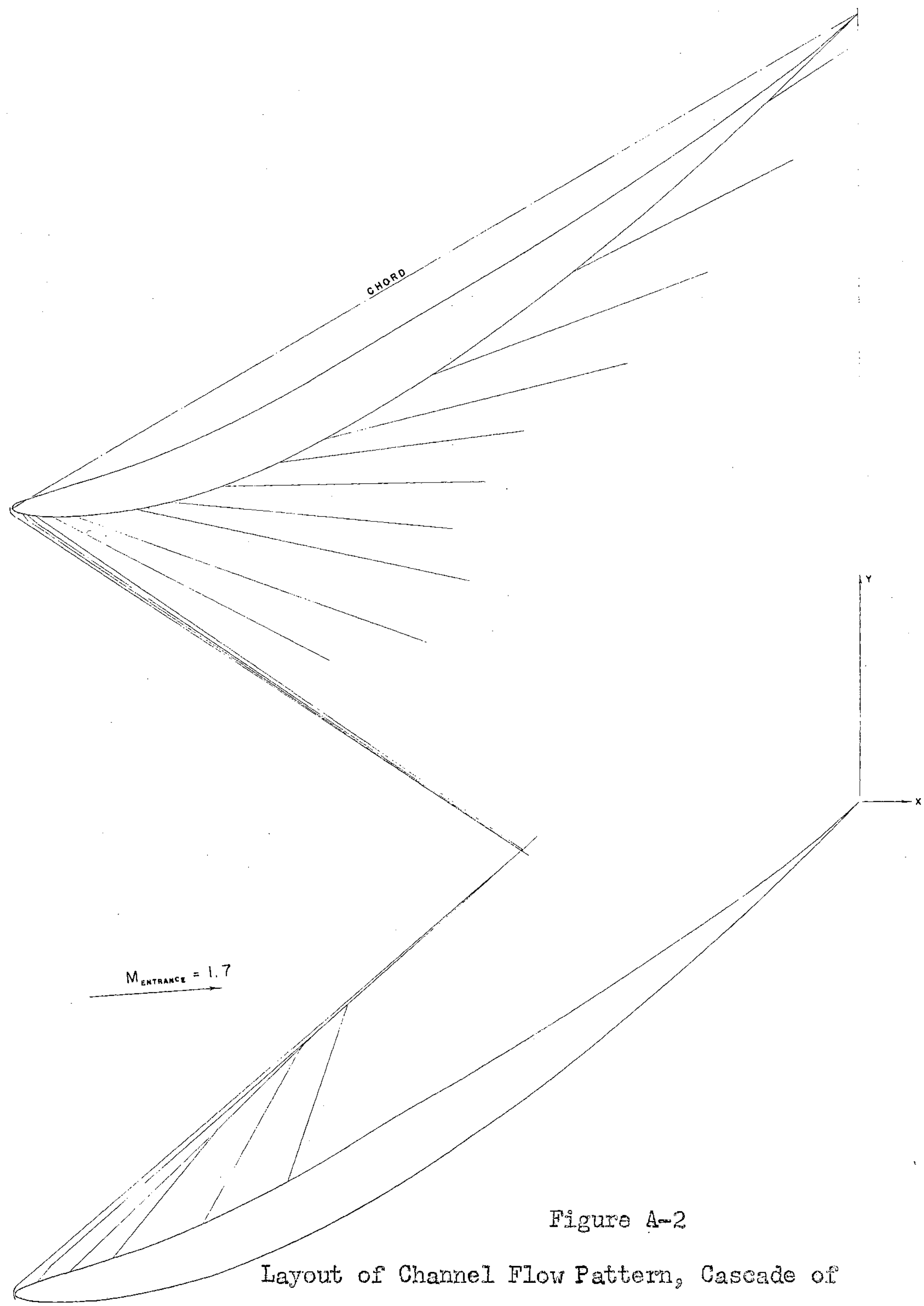

Figure A-2

Layout of Channel Flow Pattern, Cascade of

Modified NACA Blunt-Nosed Profiles (Solution fails)

Scale Ratios:
Drawing, 10 : 1 ,
Photographic Reduction, 3 : 1 .

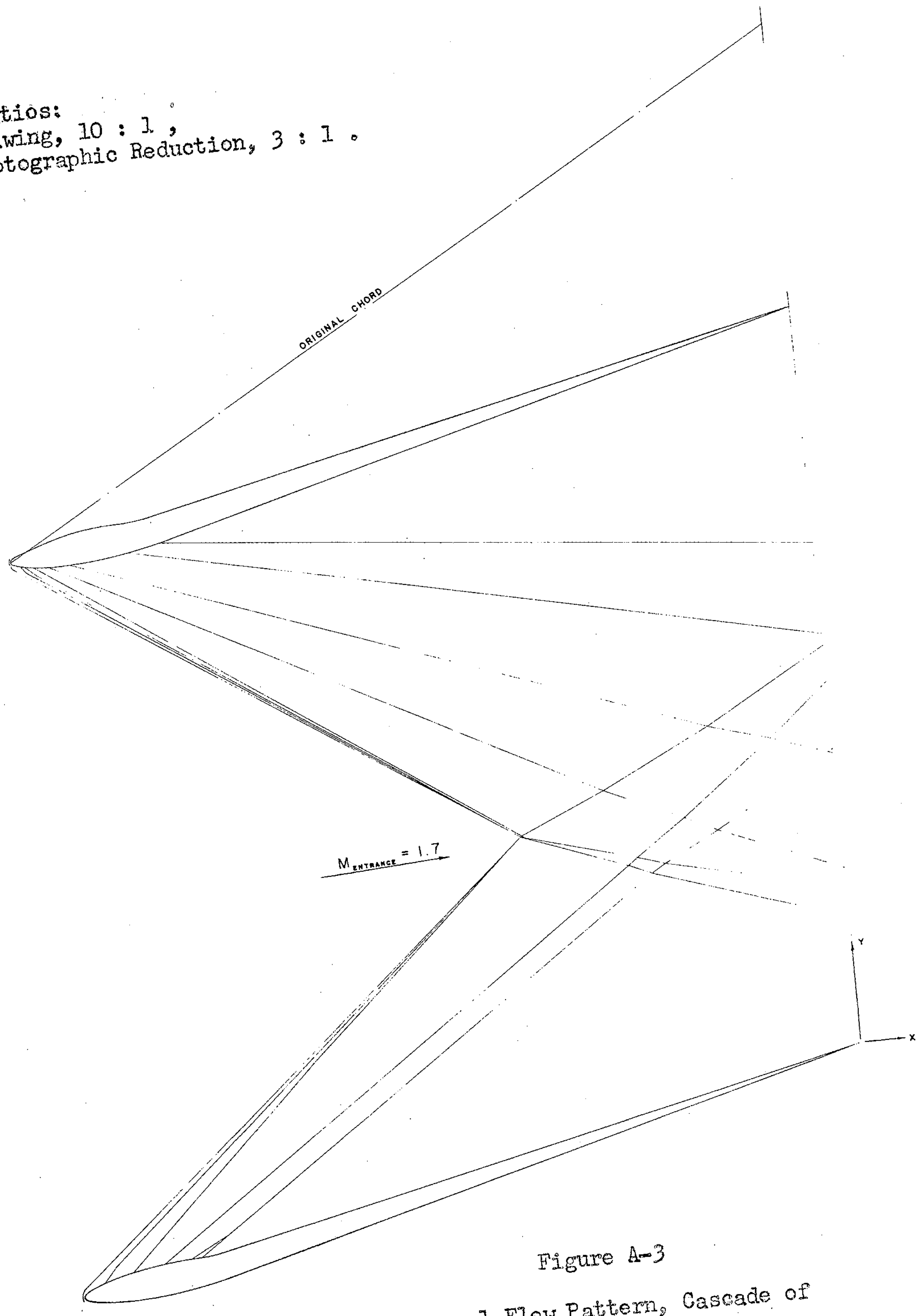

Figure A-3

Layout of Channel Flow Pattern, Cascade of
Second Modification of Blunt-Nosed Profiles

Scale Ratios:
Drawing, 10 : 1 ,
Photographic Reduction, 3 : 1 .

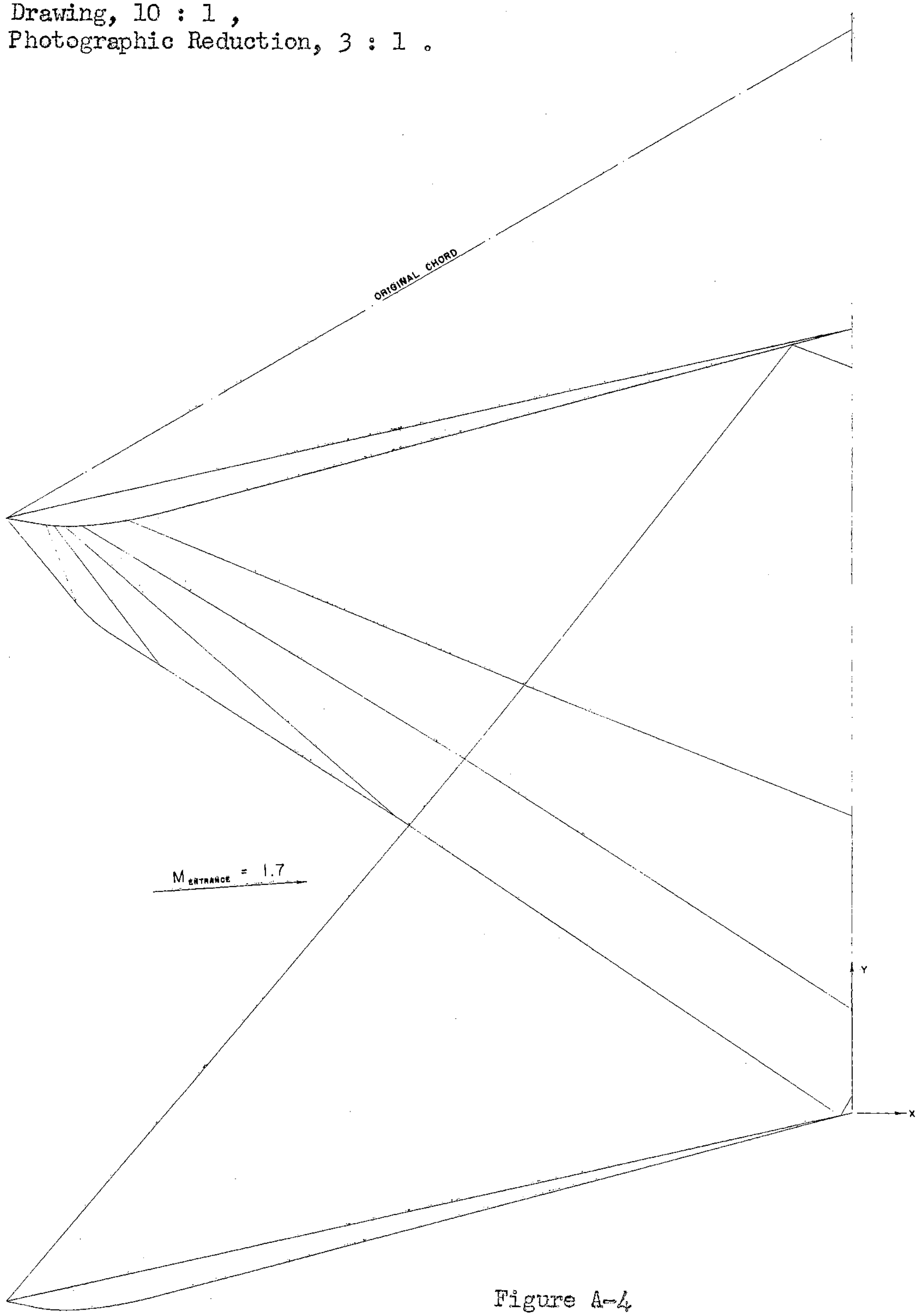

Figure A-4

Layout of Channel Flow Pattern, Cascade of

Sharp-Nosed Profiles

VITA

Walter Ascher
candidate for the degree of
Master of Science

Thesis: INVESTIGATION OF COMPRESSIBLE-FLUID FLOW THROUGH A CASCADE OF BLUNT-NOSED PROFILES

Major: Mechanical Engineering

Minor: None

Biographical and Other Items:

Born: July 3, 1928 at Zürich, Switzerland.
Undergraduate Study: Tulane University, 1945-1949.
Graduate Study: O.A.M.C., 1949-1952.
Experiences: Graduate Fellow, teaching, School of Mechanical Engineering, O.A.M.C., 1949-1951; Test Engineer, General Electric Company, Lockland, Ohio, Fall, 1951.

Member of the American Society of Mechanical Engineers, The Society of Automotive Engineers.

Date of Final Examination: February 27, 1953

THESIS TITLE: Investigation of Compressible-Fluid Flow Through a Cascade of Blunt-Nosed Profiles

AUTHOR: Walter Ascher

THESIS ADVISER: Professor Ladislaus J. Fila

The content and form have been checked and approved by the author and thesis adviser. "Instructions for Typing and Arranging the Thesis" are available in the Graduate School office. Changes or corrections in the thesis are not made by the Graduate School office or by any committee. The copies are sent to the bindery just as they are approved by the author and faculty adviser.

NAME OF TYPIST: Fern B. Hall